arXiv:2503.02607v2 [astro-ph.HE] 5 Mar 2025

Gravitational wave probes of particle dark matter: a review

Andrew L. Miller [1, 2, *]

[1] *Nikhef – National Institute for Subatomic Physics, Science Park 105, 1098 XG Amsterdam, The Netherlands*
[2] *Institute for Gravitational and Subatomic Physics (GRASP), Utrecht University, Princetonplein 1, 3584 CC Utrecht, The Netherlands*

(Dated: March 6, 2025)

Various theories of dark matter predict distinctive astrophysical signatures in gravitational-wave sources that could be observed by ground- and space-based laser interferometers. Different candidates—including axions, dark photons, macroscopic dark matter, WIMPs, and dark-matter spikes—may appear in interferometer data via their coupling to gravity or the Standard Model, altering the measured gravitational-wave strain in distinct ways. Despite their differences, these candidates share two key features: (1) they can be probed through their effects on gravitational waves from inspiraling compact objects, isolated black holes, and neutron stars, or via direct interactions with detectors, and (2) their signatures likely persist far longer than the seconds-long mergers detected today, necessitating new data analysis methods beyond matched filtering. This review outlines these dark matter candidates, their observational signatures, and approaches for their detection.

CONTENTS

I. Introduction 2

II. Ultralight dark matter interacting with the interferometers 3
- A. Generic features of ultralight dark matter signal 3
- B. Axions 5
- C. Dilaton scalar dark matter 5
  1. Changes to size and indices of refraction of solids 7
  2. Changes to neutron-star moment of inertia 7
  3. Changes to atomic clock times 8
- D. Vector dark matter 9
- E. Tensor dark matter 10
- F. Gravitational interactions of dark matter 10

III. Observational constraints on dark matter directly interacting with gravitational-wave interferometers 11
- A. Methods 11
  1. Cross-correlation 11
  2. Excess power time-frequency method 12
  3. Logarithmic power spectral density (LPSD) method 13
  4. Stochastic summing method 13
  5. Distinguishing amongst dark-matter models 14
- B. Ground-based interferometers 14
  1. LIGO, Virgo and GEO600 14
  2. KAGRA 14
- C. Space-based interferometers 15
- D. Pulsar timing arrays 16
  1. Gravitationally-interacting ultralight dark matter 16
  2. Variation of fundamental constants constraints 18
  3. Constraints on vector dark matter 19
  4. Constraints on conformal DM 19
  5. Constraints on axions through polarization measurements 20
- E. Prospects for detecting the coupling of ultralight dark matter to the interferometers 21

IV. Macroscopic dark matter transiting through the interferometers 22
- A. Background 22
- B. Yukawa-like interactions 22
- C. Projected constraints on Yukawa-like interactions 23

V. GWs from ultralight bosonic clouds around rotating BHs 24
- A. Annihilation signal 26
- B. Transition signal 26
- C. Bosenova signal 27
- D. Clouds in binary black hole systems 27
  1. Spin-induced quadrupole moment 28
  2. Tidal disruptions 28
  3. Binary-induced transitions 28
  4. Ionization 28

VI. GW constraints on boson clouds 28
- A. Constraints from the spins of detected binary black holes 29
- B. Search methods 29
  1. Excess power 29
  2. Viterbi 29
  3. Cross-correlation and other methods 29

* andrew.miller@nikhef.nl

C. Recent search results for scalar boson clouds 30
1. All-sky search constraints 30
2. Cygnus X-1 constraints 32
3. Constraints on luminous dark photons clouds 32
4. Stochastic gravitational-wave background constraints 33
D. Prospects for GW probes of boson clouds 33

VII. GW probes of soliton DM 34
A. Impact on phase evolution of binary systems 35
B. Imprint of DM on CW signal from neutron star 35
C. Pulsar-timing constraints on soliton ultralight dark matter 35

VIII. GW probes of WIMP dark matter 36
A. Transmuted black holes in binaries 36
B. GWs to probe the GeV excess 37

IX. GW probes of DM spikes 39
A. Background 39
B. Dephasing due to dynamical friction of IMRI systems 39
C. Upper limits on BH environments 41

X. GW probes of atomic DM 41
A. Background 41
B. Constraints from observations of binary black holes 41
C. Constraints from sub-solar mass binary black hole searches 42

XI. Conclusions 42

Acknowledgments 43

References 44

I. INTRODUCTION

Our knowledge of physics has been incomplete for decades, if not for over a century [1]. Dark energy and dark matter (DM) could comprise 69% and 26% of the universe, and yet we have not been able to directly detect either. The experimental evidence for the existence of some "invisible" or DM is overwhelming: stars orbiting the center of the Milky Way would have flown out of their orbits if DM did not hold them in place [2–5]; anisotropies in the cosmic microwave background could result from DM potential wells in the early universe [6, 7]; DM could seed the formation of large-scale structures visible today, which would have been impossible with ordinary matter alone [8–12]; and gravitational lensing of light by galaxies in between us and the light source could be explained by invisible mass inside the galaxy [13–18].

While the observational evidence indicates that DM may exist, it does not explain what it is made of. Could it be a single new particle, such as the axion [19–21] or dark photon [22–25], a collection of new particles, or macroscopic, in the form of PBHs formed within ~ 1 second of the Big Bang [26]? Or, particle DM may (or may not) exist alongside PBHs, which may comprise a portion or the totality of DM [27–33].

The numerous hypotheses regarding the existence of DM suggest that the mass of its constituents can vary across hundreds of orders of magnitude [34]. Significant time and resources, however, have been spent on searching a somewhat narrow mass range comprising so-called Weakly Interacting Massive Particles (WIMPs) [35]. WIMPs have been probed through collider experiments [36] and DM/ nucleus interactions by experiments such as CDMS [37–39], SuperCDMS [40], XENON [41–45], and LUX [46, 47]. Other experiments have tried to detect annihilating DM *indirectly* through its gamma-ray emission in the Galactic Center, galaxy clusters, or other areas, e.g. MAGIC [48, 49], VERITAS [50], HESS [51] and Fermi [52], or through cosmic rays, e.g. AMS [53–55] or Fermi-LAT [56, 57]. Despite these efforts, however, WIMPS remain undetected[1], and so it is worthwhile to ask whether other models could better explain DM. Thus, the experimental development from the particle physics community has widened to include probing ultralight DM through torsion balance experiments, such as Eöt-Wash [59, 60] and the MICROSCOPE satellite [61, 62], whose results can be interpreted as constraints on DM, and resonant cavity experiments, such as ADMX [63], among others. It is therefore also worth asking whether high-precision GW interferometers, such as LIGO, Virgo and KAGRA [64–66], can be used to search for DM, and in particular, whether continuous gravitational-wave (CWs) can be used as the probe. While not yet as extensive as particle physics experiments, GW probes of DM have already, in many cases, surpassed limits from existing experiments, or *will* beat them as the detectors, both in ground and in space, develop.

CWs are quasi-monochromatic, quasi-infinite-duration signals that canonically arise from asymmetrically rotating, lumpy neutron stars. Over the last few decades, much research has focused on developing ways to probe such neutron stars, both those that are known electromagnetically and those that may only be emitting GWs ("gravitars") [67–72]. Though the signal model is simple, the unknown sky positions and the uncertain neutron-star physics (e.g. the unknown equation of state, "spin wandering" [73, 74], changes in the magnetosphere [75], etc.) complicates these searches, and thus methods that are robust not only to non-Gaussian noise disturbances but also to theoretical uncertainties had to be developed to look for such systems [76–80]. Until now, such searches

[1] DAMA claims to see a periodic oscillation of a DM signal, though this result has not yet been reproduced [58]

have only yielded constraints on the maximum possible deformation of the size of known [81–85] and unknown neutron stars [86, 87].

It turns out that with CWs, we can not only probe neutron stars, but also a wide range of DM models. If DM particles couple to standard model ones, we could see them in GW data via their interactions with detector components, which would give rise to a narrow-band, stochastic "correlated-noise" signal [24, 88–90]. Separately, if a new boson that may or may not be DM exists and couples to gravity, and is of *just* the right mass, it will form clouds around rotating BHs, extracting mass and spin from them as they grow, and emitting CWs as the DM particles annihilate [91]. Heavy, strongly-interacting DM could induce collapses of stars that form in binaries, and as these objects orbit each other, they will emit GWs at particular frequencies distinct from if they were ordinary stars of the same mass [92, 93]. Such ultralight particles could also interact with the material inside neutron stars, changing their moments of inertia and thus their CW emission [94]. CWs can be used to probe the millisecond pulsar hypothesis to the GeV excess, which, as it is more constrained, lends more strength to the WIMP DM annihilation hypothesis for the GeV excess [95–97]. Finally, axions can be constrained using the very slow orbit of the Hulse-Taylor binary and other known binaries to be below to be $f_a < \mathcal{O}(10^{11})$ GeV, depending on the system [98, 99].

In Fig. 1, we show a landscape of the kinds of particle DM that could be probed with current and future interferometers, both by using GWs and and through direct detection of particles interacting with the instruments. There are thus so many different kinds of DM that can be searched for by using instruments that were not strictly designed to probe the existence of DM.

This review article is broken into different parts depending both on the type of DM considered and constraints on DM interactions with gravity or standard model particles. In Section II , we describe different ways that ultralight dark matter could couple to standard model particles in GW interferometers. Section III details the constraints that have been derived from searches of recent LIGO, Virgo and KAGRA data on the different ways that DM could couple to the interferometers. Section IV focuses on how macroscopic DM could transit through the interferometers, giving rise to a measurable differential acceleration of the mirrors. In Section V, we describe how scalar and vector bosons (that could be DM) form around rotating BHs, and the types of GW signals that could be emitted if these BHs are isolated or are in binary systems. Search results for annihilating scalar and vector boson cloud systems are explained in Section VI. Next, we discuss how soliton DM would impact GW signals from binary systems and neutron stars in Section VII. The collection of infamous WIMPs around BHs and in the Galactic Center are discussed in Section VIII in the context of how they can be probed with GWs. We explain how DM spikes around rotating BHs could alter GW signals in Section IX. In Section X, we describe a model of atomic DM that would give rise to "dark atoms" and "dark BHs", and how it can be constrained with GW observations and non-observations of merging compact objects. We conclude in Section XI about the future for the burgeoning field of GW probes of particle DM.

II. ULTRALIGHT DARK MATTER INTERACTING WITH THE INTERFEROMETERS

A. Generic features of ultralight dark matter signal

If it exists, cold, ultralight DM could interact with standard-model particles in model-dependent ways. Such interactions would cause macroscopic differences in the materials, and, depending on the type of DM, would lead to an observable signal in different components of GW interferometers. While the physics behind each type of DM is different, there are some characteristics that are model-independent. First, the number of ultralight DM particles in a given region in space is gigantic, and can be calculated by attributing the DM energy density $\rho_{\rm DM}$ to result from ultralight DM:

$$\begin{aligned} N_0 &= \lambda_{\rm C}^3 \frac{\rho_{\rm DM}}{m_{\rm DM} c^2} = \left(\frac{2\pi\hbar}{m_{\rm DM} v_0}\right)^3 \frac{\rho_{\rm DM}}{m_{\rm DM} c^2}, \\ &\approx 1.69 \times 10^{54} \left(\frac{10^{-12}\ \text{eV}}{m_{\rm DM}}\right)^4, \end{aligned} \tag{1}$$

where $v_0 \simeq 220$ km/s is the virial velocity [100], $\hbar$ is Planck's reduced constant, c is the speed of light, $m_{\rm DM}$ is the mass of the ultralight dark matter particle, $\lambda_{\rm C}$ is the Compton wavelength of DM, and $\rho_{\rm DM} = 0.3\,\text{GeV/m}^3$ is the DM energy density [101] (unless otherwise noted). The large occupation number N_0 implies that ultralight DM can be treated as a coherent region, where within that region, DM can be approximated as a plane wave that oscillates at a fixed frequency f_0, which is given by the DM mass:

$$f_0 = \frac{m_{\rm DM} c^2}{2\pi\hbar} \simeq 241\ \text{Hz} \left(\frac{m_{\rm DM}}{10^{-12}\ \text{eV}/c^2}\right), \tag{2}$$

In other words, the observable effect is that the interferometer components will forever oscillate at a fixed frequency since they always sit in the DM field [102]. The DM wave also has a finite coherence time $T_{\rm coh}$ that relates to the virial velocity of DM:

$$T_{\rm coh} = \frac{4\pi\hbar}{m_{\rm DM} v_0^2} = 1.4 \times 10^4\ \text{s} \left(\frac{10^{-12}\ \text{eV}}{m_{\rm DM}}\right), \tag{3}$$

If we observe for a duration longer than the coherence time, the signal will no longer be monochromatic but

(a)

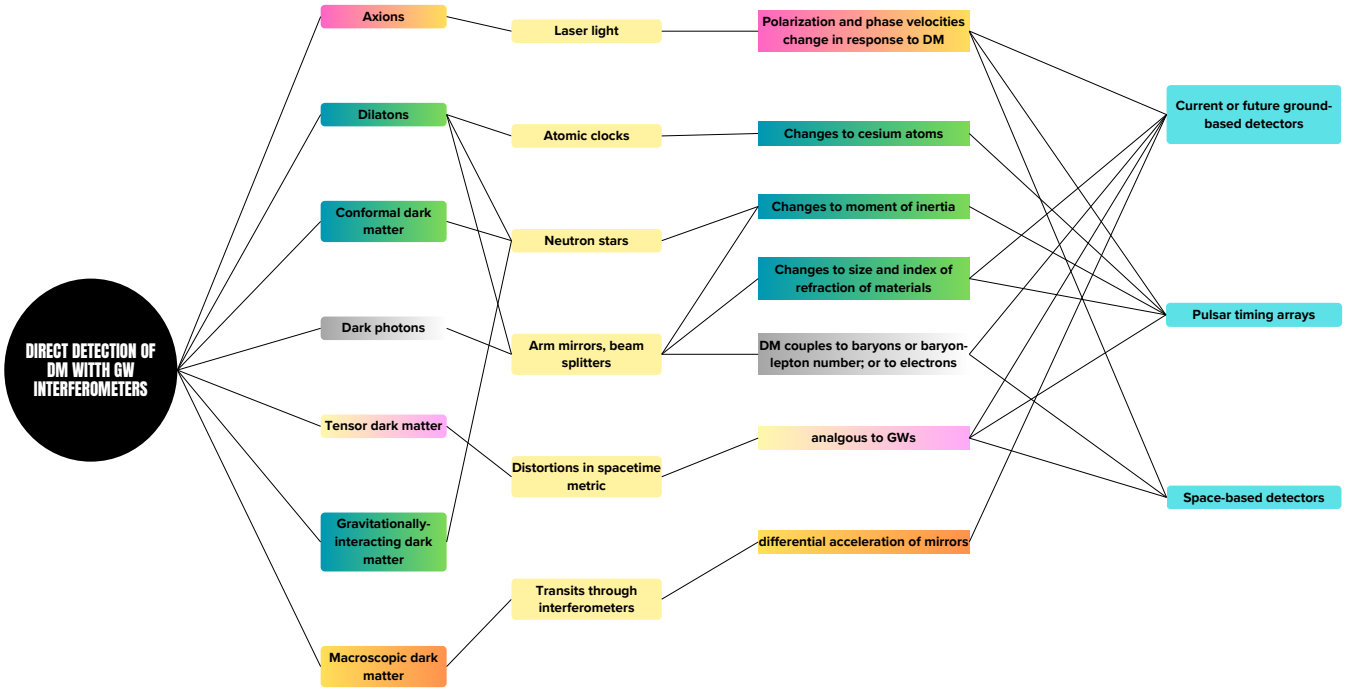

(b)

FIG. 1: Landscape plot of all the kinds of DM that can be probed with GW interferometers, both now and in the future. The logic is as follows, moving from left to right: type of DM → astrophysical source or detector component affected → observable → which detector(s) the signal could be seen in. We note that the mass range of particle DM probed here ranges many orders of magnitude, from $\sim 10^{-23}$ eV with pulsar timing arrays to 10^{-16} eV with space-based detectors to 10^{-12} eV with ground-based detectors to 10^{-9} eV with HFGW detectors, and includes $[10^3, 10^9]$ GeV WIMP DM, [1,10^9] kg macroscopic DM, probes of large-scale DM structure via solitons and DM spikes, and finally atomic DM. Matching colors imply that the source would induce those physical signatures.

have its power stochastically distributed at frequencies slightly higher than the characteristic frequency of the DM particle:

$$\Delta f_v = \frac{1}{2}\left(\frac{v_0}{c}\right)^2 f_0 \approx 2.94\times10^{-7} f_0. \quad (4)$$

This frequency shift arises because in a given coherent region, the number of DM particles is huge, and all are traveling at different velocities that are Maxwell-Boltzmann distributed around the virial velocity. Furthermore, the DM signal has an associated coherence length $L_{\rm coh}$:

$$L_{\rm coh} = \frac{2\pi\hbar}{m_{\rm DM} v_0} = 1.6\times10^9 \text{ m}\left(\frac{10^{-12}\text{ eV}/c^2}{m_{\rm DM}}\right). \quad (5)$$

If observing the interaction of DM with standard-model model particles in detectors separated by distances less than $L_{\rm coh}$, which is the case for ground-based detectors, we expect to observe a correlated signal, again at an almost fixed frequency. In Fig. 2, we show an example of what a simulated vector DM signal interacting with one of the LIGO detectors looks like.

We will now describe different ways in which DM could interact with particles in the interferometers. We will assume that we are working within $T_{\rm coh}$, in order to avoid technical difficulties from working with particles of slightly different frequencies. However, we note that in practice, this consideration is necessary when modelling the signal and assessing the sensitivity of GW interferometers to DM/standard-model interactions.

B. Axions

Axions could couple to photons, given by the following Chern-Simons interaction Lagrangian:

$$\begin{aligned}\mathcal{L}_I &= \frac{g_{a\gamma}}{4} a(t) F_{\mu\nu}\tilde{F}^{\mu\nu} \\ &= g_{a\gamma}\dot{a}(t)\epsilon_{ijk}A_i\partial_j A_k + (\text{total derivative}), \end{aligned} \quad (6)$$

where $a(t)$ is the axion field, $g_{a\gamma}$ is the axion-photon coupling constant, $F_{\mu\nu}$ is field strength of electromagnetic field, $\tilde{F}^{\mu\nu}\equiv\epsilon^{\mu\nu\rho\sigma}F_{\rho\sigma}/2$ is its Hodge dual with the Levi-Civita anti-symmetric tensor $\epsilon^{\mu\nu\rho\sigma}$, the dot denotes the time derivative, and A_μ is the electromagnetic vector potential. $F_{\mu\nu}\equiv\partial_\mu A_\nu - \partial_\nu A_\mu$. All spatial derivatives here are being neglected.

In Fourier space, we can write A_i in terms of two circular polarization modes:

$$A_i(t,\boldsymbol{x}) = \sum_{\lambda=\rm L,R}\int \frac{{\rm d}^3k}{(2\pi)^3} A_\lambda(t,\boldsymbol{k})\, e_i^\lambda(\hat{\boldsymbol{k}})\, e^{i\boldsymbol{k}\cdot\boldsymbol{x}}\ , \quad (7)$$

where $\boldsymbol{k}$ is the wave number vector, and "L" and "R" denote the left- and right-hand polarizations, and $\boldsymbol{x}$ is a spatial point at which the DM field is measured. By completely fixing gauge degrees of freedom ($\partial_i A_i = 0$ and $A_0 = 0$, respectively), and noting how the polarization vectors $e_i^\lambda(\hat{\boldsymbol{k}})$ in different directions relate to each other [104], the equations of motion for $A_{\rm L/R}(t,\boldsymbol{k})$ can be derived:

$$\ddot{A}_{\rm L/R} + \omega_{\rm L/R}^2 A_{\rm L/R} = 0 \quad (8)$$

$$\omega_{\rm L/R}^2 = k^2\left(1 \mp g_{a\gamma}\dot{a}/k\right), \quad (9)$$

where k is the momentum and $\omega_{\rm L/R}$ is the angular frequency of the light. Here, we can see a modified dispersion relationship based on the strength of the axion-photon coupling.

Noting that the axion field can be written as (assuming to work within one $T_{\rm coh}$:

$$a(t) = a_0\cos(m_{\rm DM}t) = \left(\frac{\hbar\sqrt{2\rho_{\rm DM}}}{m_{\rm DM}c}\right)\cos(m_{\rm DM}t) \quad (10)$$

where a_0 is the axion field amplitude normalized by the DM energy density, and t is time. Using the ordinary photon dispersion relationship is $c_0 = \frac{\omega}{k}$, we can derive how the velocities of different polarizations of light will differ:

$$\frac{c_{\rm L/R}(t)}{c} \simeq 1 \pm \delta c(t) \equiv 1 \pm \delta c_0 \sin(m_{\rm DM}t), \quad (11)$$

where $\delta c_0 = g_{a\gamma}a_0 m/(2k)$ is the maximum change in the phase velocity of light induced by the axion, and $\delta c_0 \ll 1$ is assumed. In physical quantities, δc_0 is the amplitude of the signal we expect, and is equal to:

$$\delta c_0 \simeq 1.3\times10^{-24}\left(\frac{\lambda}{1550\text{ nm}}\right)\left(\frac{g_{a\gamma}}{10^{-12}\text{ GeV}^{-1}}\right), \quad (12)$$

in which the laser light is assumed to have a wavelength that relates to k as: $\lambda = 2\pi/k$.

For our purposes, in the presence of an axion field, the phase velocities of circularly polarized photons in the interferometers are modulated [104]. This signal can only be seen if additional but simplistic optical components are added to measure the optical path difference between two orthogonal polarizations of light (p- and s-) [105]. In practice, GW detectors work with linearly polarized light (p-) that will be modulated by axions, making s- polarized light. Furthermore, such deviations in polarizations can also be measured in pulsar timing arrays [106, 107].

C. Dilaton scalar dark matter

Dilaton-like DM [108–116] could cause the rest mass of the electron and other physical constants to oscillate with time. In other words, atoms' Bohr radii of different interferometer components would be modulated at the dilaton

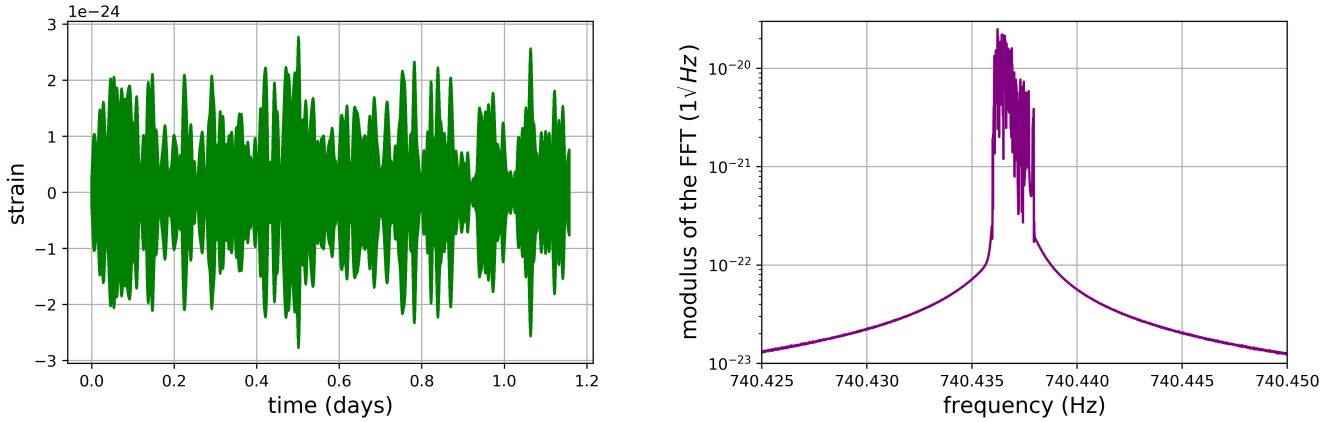

(a) (b)

FIG. 2: Taken from [103]. We show the strain time series $h(t)$ (left) and the Fourier transform of it (right) of a simulated dark photon DM signal. The structure in the amplitude spectrum density in the right-hand plot arises because we have taken the length of the Fourier transform to exceed that of the coherence time of the signal, and the signal is a superposition of 1000 dark photons traveling with distinct Maxwell-Boltzmann-distributed velocities, which cause small frequency deviations away from the minimal frequency $f_0 = 740.436$ Hz ($m_A = 3.06 \times 10^{-12}$ eV/c^2). This plot shows why it is important to choose $T_{\rm FFT} \sim T_{\rm coh}$ for the analysis of DM signals. Though we have simulated a dark photon signal, the power spectrum will appear similarly for the other kinds of DM interaction signals. Here, $T_{\rm obs} \sim 10^5$ s, meaning the frequency resolution is $\delta f = 10^{-5}$ Hz. The coherence time and length of this signal are: $T_{\rm coh} = 4595$ s and $L_{\rm coh} = 5.28 \times 10^8$ m; the coupling strength is $\epsilon = 3 \times 10^{-21}$. The signal is actually simulated for ~ 233 days, though we only show the first day of its time evolution.

frequency [89], and would induce changes in the size and index of refraction of the beam splitter [117] and the arm mirrors [118]. Since beam-splitter size oscillations would asymmetrically affect both rays, DM effects would lead to a differential phase shift (i.e. a measurable signal). In fact, at first the beam splitter effect was assumed to be the only one that mattered, but recently, the finite differences between the thicknesses of the mirrors in each arm of the interferometer lead to non-negligible differences in the path lengths of the light in the interferometer [118].

Similarly to the axion, the scalar ultralight dark-matter field ϕ can be written as [113, 117, 119]:

$$\phi(t, \vec{r}) = \left(\frac{\hbar\sqrt{2\rho_{\rm DM}}}{m_{\rm DM} c} \right) \cos\left(\omega t - \vec{k} \cdot \vec{r} + \Psi \right), \tag{13}$$

where $\vec{r}$ is a position vector, $\omega = (m_{\rm DM} c^2)/\hbar$ is the angular Compton frequency, $\vec{k} = (m_{\rm DM} \vec{v}_{\rm obs})/\hbar$ is the wave vector,Ψ is a phase factor, and $\vec{v}_{\rm obs}$ is the velocity of the DM relative to the observer.

The Lagrangian $\mathcal{L}_{\rm int}$ for this scalar field ϕ is [117]:

$$\mathcal{L}_{\rm int} \supset \frac{\phi}{\Lambda_\gamma} \frac{F_{\mu\nu} F^{\mu\nu}}{4} - \frac{\phi}{\Lambda_e} m_e \bar{\psi}_e \psi_e, \tag{14}$$

where ψ_e and $\bar{\psi}_e$ are the standard-model electron field and its Dirac conjugate, m_e is the mass of the electron, and Λ_γ and Λ_e denote the scalar DM coupling parameters to the photon and electron, respectively.

For comparison, we write a part of the standard model Lagrangian as:

$$\mathcal{L}_{\rm SM} \supset -\frac{F_{\mu\nu} F^{\mu\nu}}{4} - m_e \bar{\psi}_e \psi_e - e J_\mu A^\mu \tag{15}$$

and we can see that the rest mass of the electron effectively changes in the presence of DM:

$$m_e' = m_e \left(1 + \frac{\phi}{\Lambda_e} \right) \tag{16}$$

Additionally, the four-vector potential must be canonically normalized to reproduce Maxwell's equations, so:

$$A_\mu' = A_\mu \sqrt{1 - \frac{\phi}{\Lambda_\gamma}}, \tag{17}$$

which further implies that the charge of the electron e changes as:

$$e' = \frac{e}{\sqrt{1 - \frac{\phi}{\Lambda_\gamma}}} \tag{18}$$

and thus the fine structure constant changes as:

$$\alpha' = \frac{e'^2}{4\pi} = \alpha\left(1 - \frac{\phi}{\Lambda_\gamma}\right)^{-1} \simeq \alpha\left(1 + \frac{\phi}{\Lambda_\gamma}\right) \tag{19}$$

1. Changes to size and indices of refraction of solids

The changes in fundamental constants will lead to a change in length of, or strain on, solid bodies. Noting that the length l of an object is roughly $l \sim N_A a_B$, where N_A is the number of atoms in the body and $a_B = (m_e\alpha)^{-1}$ is the Bohr radius, we can obtain the strain on a solid body in general:

$$\delta l = -N_A(m_e\alpha)^{-2}(m_e\delta\alpha + \alpha\delta m_e) \tag{20}$$

$$\frac{\delta l}{l} = -\left(\frac{\delta\alpha(t)}{\alpha} + \frac{\delta m_e(t)}{m_e}\right) \tag{21}$$

$$\delta l = l\phi\left(\frac{1}{\Lambda_\gamma} + \frac{1}{\Lambda_e}\right) \tag{22}$$

where δ refers to the change in each parameter:

$$\delta m_e = m_e' - m_e = m_e\frac{\phi}{\Lambda_e} \tag{23}$$

$$\delta\alpha = \alpha' - \alpha = \alpha\frac{\phi}{\Lambda_\gamma} \tag{24}$$

Then, the differential displacement $\delta(L_x - L_y)$ on the beam splitter in GW interferometers can be derived [89]. Along the x-arm, assuming that light is incident on the beam splitter at 45 degrees, a reflectivity of the mirror of 50%, the change in the x-arm length, δL_x, is calculated as:

$$\delta L_x \approx \delta[\sqrt{2}nl - l/(2\sqrt{2}) - w/2], \tag{25}$$

where w is the thickness of the mirrors. Along the y-arm, the change in arm length is:

$$\delta L_y = -\delta l/(2\sqrt{2}) - \delta w/2, \tag{26}$$

and finally, the differential length change is:

$$\delta(L_x - L_y) \approx \sqrt{2}\left[\left(n - \frac{1}{2}\right)\delta l\right] \tag{27}$$

$$\approx \left(\frac{1}{\Lambda_\gamma} + \frac{1}{\Lambda_e}\right)\left(\frac{n\,l\,\hbar\sqrt{2\,\rho_{\rm DM}}}{m_{\rm DM}\,c}\right)\cos(\omega t)\,, \tag{28}$$

where n and l are the index of refraction and length of the beam splitter, respectively. We only consider the δl contribution, not one from δn, because it is much larger than than the δn one.

Additionally, dilatons could be visible in a different part of the interferometers, that is, in the reference cavity. Laser light locked to an optical cavity made out of a solid material will have its frequency modulated due to the presence of a dilaton DM field, compared to light locked to a free-space suspended cavity, whose frequency would remain stable [119–121]. The strain amplitude of such a signal can be written as:

$$h_{\rm DM}(t) = \left[\frac{\hbar}{m_{\rm DM}c^3}\sqrt{8\pi\rho_{\rm DM}G}(d_e + d_{m_e})\right]\cos\omega t \tag{29}$$

where d_e and d_{m_e} relate to the other couplings as:

$$d_{e,m_e} = \frac{M_{\rm Pl}}{(\sqrt{4\pi}\Lambda_{\gamma,e})}, \tag{30}$$

where $M_{\rm Pl}$ is the Planck mass, and m_e is the electron mass.

2. Changes to neutron-star moment of inertia

Fluctuations in fundamental constants could also cause other effects, such as changing the moment of inertia of neutron stars [122], or changing the times measured cesium clocks [122]. These effects will be relevant when we describe how ultralight dark matter could be detected in pulsar timing arrays. To study the former, we must also consider interactions in QCD [122, 123]:

$$\mathcal{L}_{\phi,\rm QCD} \supset \frac{\phi}{\Lambda}\left(\frac{d_g\beta_3}{2g_3}G^A_{\mu\nu}G_A^{\mu\nu} - \sum_{q=u,d}(d_q + \gamma_q d_g)m_q\bar{q}q\right) \tag{31}$$

where β_3 is the QCD beta function, g_3 is the QCD gauge coupling, $G^A_{\mu\nu}$ is the gluon field strength tensor, γ_q are the light quark anomalous dimensions, $\Lambda = M_{\rm Pl}/\sqrt{4\pi}$, and d_g, and d_q are the dilaton coupling constants to the gluon and the quarks, respectively. Reading off the Lagrangian, and noting the difference from the standard model, the change in masses of quarks is:

$$\frac{\delta m_q}{m_q} = \frac{d_q}{\Lambda}\phi\,, \tag{32}$$

while in nucleon masses:

$$\frac{\delta m_{p,n}}{m_{p,n}} \simeq \frac{1}{\Lambda}\Big(d_g + C_n\,d_{\hat{m}}\Big)\phi\,, \tag{33}$$

where $C_n = 0.048$ [123], m_p is proton mass, m_n is the neutron mass, and the symmetric combination of the quark mass couplings has been defined to be:

$$d_{\hat{m}} \equiv \frac{d_u m_u + d_d m_d}{m_u + m_d}\,. \tag{34}$$

Moving back to the neutron star, conservation of angular momentum requires that the fluctuations in the spin frequency $\delta\omega$ relate to changes in the pulsar's moment of inertia δI as:

$$\frac{\delta\omega}{\omega_0} = -\frac{\delta I}{I_0}\,. \tag{35}$$

where I_0 is the unperturbed moment of inertia and ω_0 is the unperturbed angular frequency of the neutron star. Based on the above discussion, DM interactions can cause changes in the masses of fundamental particles, which, in turn, cause time-dependent oscillations in the moment of inertia. In the case of neutron stars, the mass of the neutron will oscillate, and thus, indirectly, the mass of the neutron star itself will change as well.

Assuming a simplistic model of a non-rotating, spherically symmetric neutron star composed only of neutrons with a polytropic equation-of-state, the radius and moment of inertia can be written as [124]:

$$R \propto M_0^{-1/3} m_n^{-8/3} \tag{36}$$

$$I_0 \propto M_0 R^2 = M^{1/3} m_n^{-16/3}, \tag{37}$$

where R and M_0 are the radius and unperturbed mass of the neutron star. Solving explicitly the Tolman–Oppenheimer–Volkoff (TOV) equations for a realistic equation-of-state would cause $\mathcal{O}(1)$ deviations from the simple scalings. These "unknown" scalings can be parameterized in terms of η and $\delta\eta$

$$\frac{\delta I}{I_0} = \eta\frac{\delta M}{M_0} + \delta\eta\frac{\delta m_n}{m_n}\,. \tag{38}$$

which are set to $\eta = 1/3$ and $\delta\eta = -16/3$ in line with the simplistic model, and to illustrate the concept.

Because of the changes in the pulsar's moment of inertia, the pulsar's spin frequency will change. For pulsar timing array experiments, the measured quantities are the times of arrivals of pulses from each pulsar, which will change in response to the oscillating moment of inertia. In practice, the observable here is the residual h of the times of arrivals of pulses from the neutron star, which is given by:

$$h = -\int \frac{\delta\omega}{\omega_0} dt = \int \frac{\delta I}{I_0} dt\,. \tag{39}$$

Now, the changes in the particle mass must be related to the macroscopic change in the pulsar mass

$$\frac{\delta M}{M_0} = \sum_{f\in\{e,\mu,p,n\}} Y_f \frac{m_f}{m_n}\frac{\delta m_f}{m_f}\,, \tag{40}$$

where δM is the change in the pulsar's mass. The sum is over the different types of particles present in the pulsar: electrons, muons, protons and neutrons, $Y_f \equiv N_f/(N_n + N_p)$ is a weighting function that gives the number of f particles relative to the sum of protons and neutrons (which dominate the pulsar's mass). For neutron star observed by pulsar timing arrays, the following is assumed for Y_f: $Y_n = 0.9$, $Y_p = Y_e = 0.1$ and $Y_\mu = 0.05$ [122, 125].

By plugging in the relations in Eq. (19) and Eq. (16) to Eq. (40), and subsequently integrating over time in Eq. (39), the changes in the timing residuals due to the ultralight dark-matter particles can be obtained:

$$h(t) = \frac{\sqrt{2\rho_\phi}}{m_{\rm DM}^2\Lambda}\left(\vec{y}\cdot\vec{d}\right)\hat{\phi}_P \sin\left(m_{\rm DM}t + \gamma(\vec{x}_P)\right), \tag{41}$$

where $\vec{x}_P$ is the location of the pulsar, $\hat{\phi}_P$ is the pulsar normalized signal amplitude, γ is a phase, and $\vec{y}\cdot\vec{d} \equiv \sum_i y_i d_i$ where $i \in \{m_e, m_\mu, g, \hat{m}\}$ and:

$$\begin{aligned}\{y_g,\, y_{\hat{m}},\, y_\mu,\, y_e\} =& \eta\left\{1,\, C_n,\, 6\times10^{-3},\, 5\times10^{-5}\right\} \\ &+\delta\eta\left\{1,\, C_n,\, 0,\, 0\right\}\,.\end{aligned} \tag{42}$$

This type of DM interaction would leave imprints on pulsar timing array experiments [126–128], which will be discussed later.

3. *Changes to atomic clock times*

Changes in fundamental constants would also affect the way in which atomic clocks measure time. Since pulsar timing array experiments reference their measurements of the times of arrivals of pulses to terrestrial time (TT) using atomic clocks composed primarily of cesium, any oscillation of the fundamental constants will affect the atomic clocks, and thus the times measured [129]. Likewise, a shift in the frequency of the atomic clock will give rise to an apparent shift in the measured pulsar spin frequency, given by Eq. (39).

From [122, 129], the frequency of an atomic clock is:

$$f \propto \left(m_e\alpha^2\right)\left[\alpha^2 F_{\rm rel}(Z\alpha)\right]\left(\mu\frac{m_e}{m_p}\right)^\zeta \tag{43}$$

where Z is the nuclear charge, $F_{\rm rel}(Z\alpha)$ is a relativistic correction to an atom's energy levels, μ is the nuclear magnetic moment, and $\zeta = 1$ if the clocks that have hyperfine transitions (the case of cesium), and $\zeta = 0$ for optical transitions[2]. The Casmir effect $F_{\rm rel}(Z\alpha)$ is a correction that comes from solving the relativistic wave equation for an electron near the nucleus

[2] This equation arises from solving the non-relativistic Schrodinger equation for the valence electron wavefunction and evaluating it at the nucleus of the atom.

The fluctuations in fundamental constants will cause fluctuations in the frequencies of atomic clocks composed of atoms A:

$$\frac{\delta f_A}{f_A} \simeq \Bigg[\frac{\delta m_e}{m_e} + (4 + K_A)\frac{\delta \alpha}{\alpha} + \zeta \left(\frac{\delta m_e}{m_e} + C_A \sum_{q=u,d} \frac{\delta m_q}{m_q} - \frac{\delta m_p}{m_p} \right) \Bigg], \tag{44}$$

where the derivative of the Casmir effect term is $\delta F_{\rm rel}/F_{\rm rel} = K_A$, and the derivative of the nuclear magnetic moment is $\delta\mu/\mu = C_A\, \delta m_q/m_q$. For Cesium, $K_A = 0.83$ depends nontrivially on Z and α, and $C_A = 0.110$ [129]. m_q is a quark mass, and the index q runs over up and down quarks.

Finally, by substituting the aforementioned equations for fluctuations of the fundamental constants into Eq. (44), and then further plugging this result into Eq. (39), the timing residuals induced by the ultralight dark-matter are :

$$h(t) = \frac{\sqrt{2\rho_{\rm DM}}}{m_{\rm DM}^2 \Lambda} \left(\vec{y} \cdot \vec{d} \right) \hat{\phi}_E \sin\left(m_{\rm DM} t + \gamma \right). \tag{45}$$

where $\vec{x}_E$ is the position of the Earth, and the sensitivity parameters of this search are given by:

$$\{ y_g,\, y_\gamma,\, y_{\hat{m}},\, y_{m_e} \} \simeq \left\{ \zeta,\, \xi_A,\, \zeta \left(C_n + \hat{C}_A \right),\, 1 + \zeta \right\}, \tag{46}$$

where $\xi_A \equiv 4 + K_A$, and $\hat{C}_A = C_A (m_u + m_d)^2 / 2 m_u m_d$. This type of DM interaction would leave imprints on pulsar timing array experiments [126–128], which will be discussed later.

D. Vector dark matter

DM could be spin-1, i.e. vectors, which we refer to as "dark photons". Dark photons could explain the entirety of the relic abundance of DM, which could arise from the misalignment mechanism [130–132], parametric resonance or the tachyonic instability of a scalar field [133–136], or from cosmic string network decays [137]. They could couple to standard model particles, either to baryon or baryon-lepton number. In the interferometers, these interactions would occur everywhere, but would be detectable in the four interferometer mirrors. The dark photons[3] would cause a "dark" force on the mirrors, causing quasi-sinusoidal oscillations [24, 103].

Dark photons can be described analogously to ordinary photons, i.e. with a four-vector potential, which can be written as:

$$A_\mu(t, \vec{x}) = (A_0)_\mu \sin(\omega t - \vec{k} \cdot \vec{x} + \Upsilon)\ \text{kg} \cdot \text{m}/(\text{s}\cdot\text{C}), \tag{47}$$

where $(A_0)_\mu$ is the four-amplitude of A_μ Υ is a random phase, and $\vec{x}$ is the position at which A_μ is measured. The index $\mu = 0, 1, 2, 3$ refers to both time and spatial components.

As always, we have the freedom to choose a gauge, and usually, the Lorenz gauge is easiest to work in ($\partial^\mu A_\mu = 0$). After making this choice, we can compare the time component to magnitude of the spatial components of the four-potential:

$$\frac{(A_0)_0}{|\vec{A}_0|} = \frac{v_0}{c} \simeq 7.667 \times 10^{-4}, \tag{48}$$

where $|\vec{A}_0| = \left(\frac{\hbar \sqrt{2\rho_{\rm DM}}}{m_{\rm DM} c^2} \frac{1}{\sqrt{\epsilon_0}} \right)$ is the magnitude of the spatial components of A_μ, normalized by the present DM energy density of the universe, and ϵ_0 is the permittivity of vacuum. In Eq. (48), we see that the dark scalar potential is suppressed by about three orders of magnitude compared to the the dark three-vector potential. Therefore, the time-component of the four-vector potential can be safely neglected, leaving only the three-vector potential:

$$\vec{A} = \vec{A}_0 \sin\left(\omega t - \vec{k} \cdot \vec{x} + \Upsilon \right), \tag{49}$$

The Lagrangian $\mathcal{L}$ that characterizes the dark photon coupling to a number current density J^μ of baryons or baryons minus leptons is:

$$\mathcal{L} = -\frac{1}{4\mu_0} F^{\mu\nu} F_{\mu\nu} + \frac{1}{2\mu_0} \left(\frac{m_{\rm DM} c}{\hbar} \right)^2 A^\mu A_\mu - \epsilon e J^\mu A_\mu, \tag{50}$$

where μ_0 is the magnetic permeability in vacuum and ϵ is the strength of the particle/dark photon coupling normalized by the electromagnetic coupling constant.

Using Eq. (47), the "dark" electric and magnetic fields can be derived:

$$\vec{E} = \partial_0 \vec{A} - \vec{\nabla} A_0 \simeq \omega \vec{A}_0 \cos(\omega t - \vec{k} \cdot \vec{x} + \phi), \tag{51}$$

$$\vec{B} = \vec{\nabla} \times \vec{A} = -\vec{k} \times \vec{A}_0 \cos(\omega t - \vec{k} \cdot \vec{x} + \phi), \tag{52}$$

and we note that the electric field is much stronger than the magnetic one:

$$\frac{|\vec{E}|}{|c\vec{B}|} \sim \frac{\omega}{|\vec{k}|} = \frac{c^2}{|\vec{v}|} \sim 10^3 c, \tag{53}$$

which implies that we need to only consider the electric field. This dark electric field causes the test masses to

[3] These are different dark photons than those that kinetically mix with the ordinary photon, which will be discussed later in the context of luminous superradiance [138].

oscillate at a quasi-fixed frequency given by the dark photon mass. The acceleration of a given mirror can thus be derived [24, 88]:

$$\vec{a}_j(t,\vec{x}_j) = \frac{\vec{F}_j(t,\vec{x}_j)}{M_j} \simeq \epsilon e \frac{Q_{D,j}}{M_j}\omega|\vec{A}_0|\hat{A}\cos(\omega t - \vec{k}\cdot\vec{x}_j + \phi), \quad \epsilon^2 = \frac{\alpha_{\rm DP}}{\alpha} \tag{54}$$

where $\alpha_{\rm DP}$ is the dark photon fine structure constant, ϵ^2 is the ratio between the dark photon fine structure constant and the electromagnetic fine structure constant α, and $Q_{D,j}$ is the total charge in the jth mirror of mass M_j. $\hat{A}$ is a unit vector, and ϕ is a function of the spatial coordinates. If dark photons couple to the baryon number, q_j is the number of protons and neutrons in each mirror; if they couple to the difference between the baryon and lepton numbers, q_j is the number of neutrons in each mirror. Each mirror is positioned differently with respect to the incoming dark photon DM field, and thus is accelerated at a slightly different amount over time. Thus, the interferometer experiences a measurable differential acceleration, and thus a differential strain.

Assuming that all mirrors are the same, integrating Eq. (54) twice over time, and averaging over random polarization and propagation directions, the strain on the interferometers caused by a dark photon DM signal is [24]:

$$\sqrt{\langle h_D^2\rangle} = C\frac{Q_D}{M}\frac{\hbar e}{c^4\sqrt{\epsilon_0}}\sqrt{2\rho_{\rm DM}}v_0\frac{\epsilon}{f_0}, \simeq 6.56\times10^{-26}\left(\frac{\epsilon}{10^{-22}}\right)\left(\frac{100\text{ Hz}}{f_0}\right), \tag{55}$$

where $C = \sqrt{2}/3$ (in LIGO) is a geometrical factor obtained by averaging over all possible dark photon propagation and polarization directions, and different detector geometricians (the calculation for C is shown in the appendix of [24] and in [139]).

A second strain results due to the so-called "finite light travel time effect, in which the mirrors in the interferometers have moved in the time that it takes the light to reach them from the beamsplitter. This strain can actually be larger than that given in Eq. (55):

$$\sqrt{\langle h_C^2\rangle} = \frac{\sqrt{3}}{2}\sqrt{\langle h_D^2\rangle}\frac{2\pi f_0 L}{v_0}, \simeq 6.58\times10^{-26}\left(\frac{\epsilon}{10^{-23}}\right). \tag{56}$$

The total strain is: $\langle h^2_{\rm total}\rangle = \langle h_D^2\rangle + \langle h_C^2\rangle$.

E. Tensor dark matter

Modifications to gravity due to an additional spin-2 particle could act as DM. Specifically, bimetric gravity [140, 141], a theory in which a massless and massive spin-2 field interact, provides a plausible candidate for ultralight dark matter [142], produced by the misalignment mechanism [108].

Here, we consider a massive spin-2 field $M_{\mu\nu}$ described by the Fierz-Pauli Lagrangian density [143]:

$$\mathcal{L} := \frac{1}{2}M_{\mu\nu}\mathcal{E}^{\mu\nu\rho\sigma}M_{\rho\sigma} - \frac{1}{4}m_{\rm DM}^2\left(M_{\mu\nu}M^{\mu\nu} - M^2\right), \tag{57}$$

where $M := g^{\mu\nu}M_{\mu\nu}$ and $\mathcal{E}^{\mu\nu\rho\sigma}$ is the Lichnerowicz operator, defined in equation 2.2 of [143].

For the Friedman-Lemaitre-Robertson-Walker (FLRW) background metric, the equations of motion for this field, assuming it is ultralight, can be derived at late times as in [142, 144, 145]. The field spatial component can be written in a similar way as for dark photons and scalar bosons at given position $\mathbf{x}$:

$$M_{ij} = \frac{\sqrt{2\rho_{\rm DM}(\vec{x})}}{m}\cos\left(\frac{mc^2}{\hbar}t + \vec{k}\cdot\vec{x} + \Upsilon(\vec{x})\right)\varepsilon_{ij}(\vec{x}), \tag{58}$$

where Υ is a random phase, and ε_{ij} encodes information about the five polarizations of the massive spin-2 field.

The strain on the GW detectors arises analogously to that from GWs: a stretching of space-time in the presence of the field, since the massive spin-2 metric and its coupling constant can be absorbed into the definition of the massless spin-2 metric in the linear regime of the coupling constant $\alpha_{\rm TB}$[4] [143]; thus, the perturbation h_{ij} is:

$$h_{ij}(t) = \frac{\alpha_{\rm TB}}{M_{\rm Pl}}M_{ij}(t) = \frac{\alpha_{\rm TB}\sqrt{2\rho_{\rm DM}}}{mM_{\rm Pl}}\cos\left(\frac{DMc^2}{\hbar}t + \Upsilon\right)\varepsilon_{ij}(\mathbf{x}), \tag{59}$$

where α is a dimensionless constant that quantifies the difference between the strengths of each of the spin-2 fields, and $M_{\rm Pl}$ is the Planck mass.

Contracting h_{ij} with the GW detector response function D^{ij} in the tensor case, the resulting strain is:

$$h(t) = D^{ij}h_{ij} = \frac{\alpha_{\rm TB}\sqrt{\rho_{\rm DM}}}{\sqrt{2}mM_{\rm Pl}}\cos\left(\frac{m_{\rm DM}c^2}{\hbar}t + \Upsilon\right)\Delta\varepsilon, \tag{60}$$

where $\Delta\varepsilon := \varepsilon_{ij}(n^in^j - m^im^j)$.

F. Gravitational interactions of dark matter

The previous sections assumed a coupling of DM to standard-model particles. However, in principle DM need

[4] In the literature, $\alpha_{\rm TB} = \alpha$ simply, but to disentangle it from the fine structure constants, we rename it. TB is tensor boson.

not interact at all with the standard model; thus, models of DM have been devised in which only a minimal coupling to gravity is assumed. This is, in fact, the simplest assumption that can be made, since we only have evidence for the existence of DM through gravitational interactions.

One such hypothetical scalar DM particle has a Lagrangian of:

$$\mathcal{L} = \sqrt{-g}\left[\frac{1}{2}g^{\mu\nu}\partial_\mu\phi\partial_\nu\phi - \frac{1}{2}m_{\rm DM}^2\phi^2\right]. \tag{61}$$

and [94]:

$$\phi(\vec{x},t) = \frac{\sqrt{2\rho_{\rm DM}}}{m_{\rm DM}}\hat{\phi}(\vec{x})\cos\left(m_{\rm DM}t + \gamma(\vec{x})\right), \tag{62}$$

where $\gamma(\vec{x})$ is a phase that depends on position $\vec{x}$, and $\hat{\phi}(\vec{x})$ describes the interference pattern caused by the ultralight dark matter. As before, the scalar field density is normalized by $\rho_{\rm DM}$.

Scalar DM could cause the arrival times of pulses from millisecond pulsars on earth to change, in an analogous way that GWs do [94]. Such a difference in the arrival times can be written as [94, 126]:

$$\delta t_{\rm DM} = \frac{\Psi_{\rm c}(\vec{x})}{2m_{\rm DM}}[\hat{\phi}_{\rm E}^2\sin\left(2m_{\rm DM}+\gamma_{\rm E}\right) - \hat{\phi}_{\rm P}^2\sin\left(2m_{\rm DM}+\gamma_{\rm P}\right)], \tag{63}$$

where

$$\Psi_{\rm c}(\vec{x}) \approx 6.52\times10^{-18}\left(\frac{10^{-22}\ {\rm eV}}{m_{\rm DM}}\right)^2\left(\frac{\rho_\phi}{0.4\ {\rm GeV/cm^3}}\right), \tag{64}$$

where $\gamma_{\rm P} \equiv 2\gamma(\vec{x}_{\rm p}) - 2m_{\rm DM}d_p/c$ ($\gamma_{\rm E} \equiv 2\gamma(\vec{x}_{\rm e})$) parameterize random phases evaluated at the pulsar (P) or Earth (E), and d_p is the distance between the pulsar and the Earth. The DM energy density background is assumed to be constant when calculating $\Psi_{\rm c}(\vec{x})$, though the possibility of deviations, due to the coherently oscilalting ultralight dark-matter field, are parametrized in terms of two phase factors: one for the pulsar $\hat{\phi}^2(\vec{x}_{\rm p}) \equiv \hat{\phi}_{\rm P}^2$ and one for the Earth ($\hat{\phi}^2(\vec{x}_{\rm e}) \equiv \hat{\phi}_{\rm E}^2$). Since all the pulsars are separated by at least a kpc, assuming a constant DM energy density is valid [126].

III. OBSERVATIONAL CONSTRAINTS ON DARK MATTER DIRECTLY INTERACTING WITH GRAVITATIONAL-WAVE INTERFEROMETERS

Section II focused on the currently-known types of DM that could cause a signal in GW interferometer data. While we have indicated the strain amplitudes of such signals for some of the DM models considered, we have not yet discussed whether the interferometers are actually sensitive to such weak signals. In this section, we will describe how searches for DM interactions with GW detectors are performed, show current constraints on various models, and explain what future constraints will be on others.

Each method discussed below can achieve a certain sensitivity, that is, a minimum detectable strain amplitude on the detector at a given confidence level. This strain amplitude, the left-hand side of many equations in Section II, is then mapped to constraints on the physical coupling constant of DM to the standard model. The methods themselves are agnostic towards the particular model of DM that is being searched for.

A. Methods

As explained in Section II A, the expected signal frequency is fixed by the DM mass, but has some stochastic variations of $\mathcal{O}(10^{-6})$ [146]. Because the interferometers always exist in the DM field, the signal is always present. Thus, we can describe the expected signal as: quasi-monochromatic and quasi-infinite duration. Essentially, we are looking for a resonance at a particular frequency fixed by the DM mass.

If the signal were purely monochromatic, we could simply take a single fast Fourier transform of the data and look for peaks in the power spectrum. However, the stochastic frequency variations prevent us from doing that. If we observe for a duration $T_{\rm obs}$ longer than $T_{\rm coh}$, the signal will not be sinusoidal and thus its power will be spread among different frequency bins, which would inhibit a possible detection. Thus, the following methods have been designed to combine signal power across chunks of data $T_{\rm FFT} \ll T_{\rm obs}$ in a way that optimizes sensitivity towards particle DM interactions with the standard model and gravity.

1. *Cross-correlation*

Cross-correlation [24, 88] requires at least two separate time-domain datasets that are Fourier transformed and multiplied together to compute the cross-power in each frequency bin. The cross power is then divided by the auto-power of each detector, and then summed over all the Fourier transforms to arrive at a measure of power at each frequency. It is then divided by the standard deviation of the noise to compute the signal-to-noise ratio.

The cross-correlated signal strength for detector pair IJ is:

$$S_{IJ,j} = \frac{1}{N_{\rm FFT}}\sum_{i=1}^{N_{\rm FFT}}\frac{z_{I,ij}z_{J,ij}^*}{P_{I,ij}P_{J,ij}}, \tag{65}$$

in the $j^{\rm th}$ frequency bin at the $i^{\rm th}$ time. "$*$" denotes the complex conjugate, and $z_{1,ij}$ and $z_{2,ij}$ is the Fourier transform of the time-domain data from detectors 1 and 2, respectively, and $N_{\rm FFT}$ is the total num-

ber of FFTs taken over the observing run. If the observing run lasts $T_{\rm obs}$ and the FFT length is $T_{\rm FFT}$, then $N_{\rm FFT} = [T_{\rm obs}/T_{\rm FFT}]$. $P_{1,ij}$ and $P_{2,ij}$ are the individual detector power spectral densities, which are typically estimated using a running median of each FFT. Typically $T_{\rm FFT} = 1800$ s, independently of the DM mass, which ensures a relatively easy analysis but implies the sensitivity towards DM interactions is not optimal at each mass analyzed.

To obtain a detection statistic, i.e. the signal-to-noise ratio, we have to divide the signal strength by the variance of the data, which is:

$$\sigma^2_{IJ,j} = \frac{1}{N_{\rm FFT}} \left\langle \frac{1}{2P_{I,ij}P_{J,ij}} \right\rangle_{N_{\rm FFT}}, \tag{66}$$

where $\langle ... \rangle_{N_{\rm FFT}}$ is the average over $N_{\rm FFT}$ time segments. We note that the average is over inverse noise-weighted power spectral densities, (analogous to adding resistors in parallel), which helps to suppress spurious power due to large noise disturbances.

The signal-to-noise ratio (SNR), the dection statistic, is then simply:

$$\mathrm{SNR}_{IJ,j} = \frac{S_{IJ,j}}{\sigma_{IJ,j}}. \tag{67}$$

In the presence of pure Gaussian noise, the SNR will follow a normal distribution, with a mean of 0 and a standard deviation of 1. If the SNR exceeds a certain threshold, which is set both theoretically and by the trials factor, then a particular frequency is classified as being "significant".

Depending on the type of DM searched for, the signal-to-noise ratio for spin-0 (labeled SD), spin-1 (DP) and spin-2 (DG) cross-correlation searches can be written as [147]:

$$\mathrm{SNR}^{\rm SD}_{IJ,j} \approx \left| \frac{2\sqrt{2}\alpha_A^2 f_{\rm SD} T_{\rm eff}(\mathcal{B}'_{IJ}\Gamma_{IJ} + \mathcal{C}'\gamma_{IJ})}{\sqrt{S_{n,I}(\frac{m_{\rm DM}}{2\pi})S_{n,J}(\frac{m_{\rm DM}}{2\pi})}} \right|. \tag{68}$$

$$\mathrm{SNR}^{\rm DP}_{IJ,j} \approx \left| \frac{2\sqrt{2}\epsilon_D^2 f_{\rm DP} T_{\rm eff}(\mathcal{B}_{IJ}\Gamma_{IJ} + \mathcal{C}(1+\frac{1}{3}\Omega^z_{\rm DP})\gamma_{IJ})}{\sqrt{S_{n,I}(\frac{m_{\rm DM}}{2\pi})S_{n,J}(\frac{m_{\rm DM}}{2\pi})}} \right|, \tag{69}$$

$$\mathrm{SNR}^{\rm DG}_{IJ,j} \approx \left| \frac{2\sqrt{2}\alpha^2 f_{\rm DG} T_{\rm eff}\mathcal{A}\gamma_{IJ}}{\sqrt{S_{n,I}(\frac{m_{\rm DM}}{2\pi})S_{n,J}(\frac{m_{\rm DM}}{2\pi})}} \right|, \tag{70}$$

For spin-0: $f_{\rm SD} \equiv \rho_{\rm SD}/\rho_{\rm DM}$ is the ratio of the energy density of the spin-0 DM to the total energy density of DM. α_A is the dimensionless coupling constant that depends on the coupling constants of the scalar DM particles to standard model ones, e.g. the electron and photon, and are given by Eq. 44-47 in [147]. γ_{IJ} is the overlap-reduction function that quantities the sensitivity loss by cross correlating detectors that are not co-located and co-aligned, and is given in Tab. I in [147] for different pairs of detectors. It specifically arises from the *spatial* displacement of mirrors by DM. Γ_{IJ} is the overlap-reduction function that arises from the finite-light time travel effects of the signal on the mirrors [139].

For spin-1: $f_{\rm DP} \equiv \rho_{\rm DP}/\rho_{\rm DM}$ is the ratio of the energy density of the spin-1 DM to the total energy density of DM. $\Omega^z_{\rm DP}$ is a term that depends on the polarization of DM, and $\Omega^z_{\rm DP} = 1/3$ is when the polarizations are randomized.

For spin-2: The SNR is independent of how the DM energy density is distributed in each polarization mode. $f_{\rm DG} \equiv \rho_{\rm DG}/\rho_{\rm DM}$ is the ratio of the energy density of the spin-2 DM to the total energy density of DM.

In all the expressions $T_{\rm eff} = T_{\rm obs}$ if $T_{\rm obs} < T_{\rm coh}$, and $T_{\rm eff} = \sqrt{T_{\rm obs}T_{\rm FFT}}$ if $T_{\rm obs} > T_{\rm coh}$. Furthermore, the definitions of the dimensionless coefficients $\mathcal{C}$, $\mathcal{B}_{IJ}$ and $\mathcal{A}$ are:

$$\mathcal{C} \equiv \frac{\rho_{\rm DM}e^2 v_0^2}{5\omega^2}\left(\frac{Q_D}{M}\right)^2, \tag{71}$$

$$\mathcal{B}_{IJ} \equiv \frac{8\rho_{\rm DM}e^2}{3\omega^4 L_I L_J}\left(\frac{Q_D}{M}\right)^2 \sin^2\left(\frac{\omega L_I}{2}\right)\sin^2\left(\frac{\omega L_J}{2}\right), \tag{72}$$

$$\mathcal{A} \equiv \frac{\rho_{\rm DM}}{5\omega^2 M_{\rm Pl}^2} \tag{73}$$

where $\omega = 2\pi f$ is the angular frequency of the ultralight dark matter, L_I and L_J are the arm-lengths of each interferometer,

2. *Excess power time-frequency method*

Cross-correlation is able to capture the phase information in each FFT; however, at the moment the software has not yet been implemented to change $T_{\rm FFT}$ to match $T_{\rm coh}$, which would result in optimal sensitivity to each DM mass. Thus, another method [103] was developed that can vary $T_{\rm FFT}$ as a function of frequency, and that is more robust against noise disturbances. It relies on creating time-frequency spectrograms in which frequencies in each FFT are only kept if their powers are (1) above a given threshold and (2) local maxima. After applying these cuts, a time-frequency "peakmap" is created, which is a collection of ones that indicates particular time/frequency points at which the aforementioned two conditions are met. A peakmap can be created every Hz, and $T_{\rm FFT}$ can be varied to match $T_{\rm coh}$ in each 1 Hz window. Because $T_{\rm FFT} \sim T_{\rm coh}$, the signal is expected to be sinusoidal. Thus, we can sum, in each frequency bin, the ones that are present, in essence creating a histogram. On this histogram, at each frequency, we compute a detection statistic called the "critical ratio":

$$CR = \frac{n-\mu}{\sigma} \tag{74}$$

where n is the number of peaks at a given frequency, and μ and σ are the mean and standard deviation of the

number of peaks in the histogram. The CR, like the SNR, follows a normal distribution. The minimum detectable strain amplitude of this method is:

$$\begin{aligned} h_{0,\min} &\approx \frac{\mathcal{G}}{N_{\rm FFT}^{1/4}\theta_{\rm thr}^{1/2}}\sqrt{\frac{S_n(f)}{T_{\rm FFT,max}}} \\ &\times \left(\frac{p_0(1-p_0)}{p_1^2}\right)^{1/4}\sqrt{CR_{\rm thr}-\sqrt{2}{\rm erfc}^{-1}(2\Gamma)}, \\ N_{\rm FFT} &= \frac{T_{\rm obs}}{T_{\rm FFT,max}}, \\ p_0 &= e^{-\theta_{\rm thr}}-e^{-2\theta_{\rm thr}}+\frac{1}{3}e^{-3\theta_{\rm thr}} = 0.0755 \text{ for } \theta_{\rm thr}=2.5, \\ p_1 &= e^{-\theta_{\rm thr}}-2e^{-2\theta_{\rm thr}}+e^{-3\theta_{\rm thr}} \ = 0.0692 \text{ for } \theta_{\rm thr}=2.5, \end{aligned} \tag{75}$$

where $\mathcal{G} = [1.3, 2.8, 2.08]$ for scalar, vector or tensor DM interactions, respectively. The $\mathcal{O}(1)$ differences arise from averages over the spin-1 or spin-2 polarizations. $\theta_{\rm thr}$ is a threshold on the equalized power in the time-frequency spectrogram, and Γ is the confidence level.

3. Logarithmic power spectral density (LPSD) method

To truly maximize the sensitivity towards DM signals, one must, with infinite precision, analyze chunks of data with $T_{\rm coh}$ as the DM mass changes. LPSD [117, 118, 148] is an attempt to do this, which creates spectra that are logarithmically spaced in frequency. It is extremely computationally intensive, since it requires an implementation separate from the discrete FFT. The benefit of using such an algorithm is its ability to estimate power spectral densities logarithmically, thereby capturing important features of the signals that could be missed when estimating the power spectral density across a linear frequency range. Given that the ultralight dark matter causes frequency variations of $\mathcal{O}(10^{-6})$, it is worthwhile to use LPSD to capture these tiny fluctuations in frequency.

Accounting for the strain on the test masses, the loss of sensitivity due to the number of round-trips of the laser light, as well, the induced strain can also be written in terms of transfer functions between scalar DM and the interferometers:

$$h(\omega) \approx \left(\frac{1}{\Lambda_\gamma}+\frac{1}{\Lambda_e}\right)\cdot\left(\frac{\hbar\sqrt{2\,\rho_{\rm DM}}}{m_{\rm DM}\,c}\right)A_{\rm cal}^{-1}(\omega) \tag{76}$$

where $A_{\rm cal}$ is a function given in [118] that encapsulates the transfer functions between the DM and the beam splitter and test masses, as well as the thicknesses and indices of refraction of the mirrors, the mirrors' transmissivities, and the GW/ detector transfer function. Then, $h(\omega)$ can be estimated from the data using Eq. 11 and 12 in [118], and Eq. 16 in [149], which can be mapped to constraints on the coupling constants using Eq. (76).

4. Stochastic summing method

This method leverages the fact that the signal power will be stochastically spread at frequencies above the characteristic one if $T_{\rm FFT} > T_{\rm coh}$, and essentially sums the power at those frequencies. Afterwards, a detection statistic, like the signal-to-noise ratio, is calculated by dividing by the noise power spectral density:

$$\rho(f_c) \equiv \sum_i^{N_{\rm FFT}} \sum_{f_0\le f_n\le f_0(1+\kappa^2 v_0^2/c^2)} \frac{4|\tilde{d}(f_n;t_i)|^2}{T_{\rm FFT}S(f_n;t_i)}, \tag{77}$$

where $\tilde{d}(f_n;t_i)$ is the FFT of $i^{\rm th}$ data chunk, $S(f_n;t_i)$ is the one-sided noise power spectral density at $t=t_i$, and $\kappa = 3.17$ to ensure that no more than 1% of signal power is lost by restricting the inner sum. The outer sum is over all chunks of length $T_{\rm FFT}$; the inner sum is over the frequency spread of the signal δf_v.

The sensitivity of this method has been estimated in [150] for both axions and dark photons, analytically and numerically in the case of $T_{\rm FFT} = T_{\rm obs}$. In the absence of a signal, assuming Gaussian noise, a detection threshold can be established as a function of the false alarm probability α (Eq. 47 in [150]), and this threshold can be fed back into an integral over the likelihood function (Eq. 46 in [150]), to compute, at a given confidence level, the minimum detectable signal amplitude $\bar{\lambda}_{\rm up}$:

$$\bar{\lambda}_{\rm up}(T_{\rm obs}) = \begin{cases} (\Delta_{X,\rm tot})^{-1/2}\sqrt{\frac{\ln(\alpha)}{\ln(\beta)}-1}, & \text{for } T_{\rm obs} < \tau/\kappa, \\ (\Delta_{X,\rm tot})^{-1/2}\sqrt{M_\alpha+M_{1-\beta}}\,(\kappa T_{\rm obs}/T_{\rm coh})^{1/4} & \text{for } T_{\rm obs} \gg T_{\rm coh}. \end{cases} \tag{78}$$

$\Delta_{X,\rm tot}$ encodes the deterministic part of the spectral shape of the signal, and depends on the relative motion of the DM velocity with respect to the interferometer arms. β is the detection probability. In principle, Eq. 11 and 17 of [150] give these relative motion terms; in practice, however, conservative ($\vec{v} = [0, 0, v_0]$) and optimistic ($\vec{v} = [v_0, 0, 0]$]) choices of the direction of the DM velocity with respect to the interferometers result in val-

ues of [0.38,0.81], respectively (see Eq. 52 in [150]). M_χ represents the relation between the peak width and the area of the Gaussian distribution defined by

$$\chi = \int_{M_\chi}^{\infty} dz \frac{1}{\sqrt{2\pi}} \exp(-z^2/2). \tag{79}$$

Depending on the type of DM signal assumed to be interacting with the interferometers, $\bar{\lambda}_{\rm up}$ can be equated to the following physical normalized (by the noise) DM signal amplitudes to obtain the upper limit on the corresponding coupling constant:

$$\begin{aligned}
\bar{\lambda}_{\rm axion} &= \frac{T_{\rm obs}}{\sqrt{T_{\rm obs} S_n}} g_{\alpha\gamma} \sqrt{\frac{\rho_{\rm DM}}{m^2}} \frac{m}{2k}, \\
\bar{\lambda}_{\rm time} &= \epsilon e \frac{2T_{\rm obs}}{\sqrt{T_{\rm obs} S_n}} \sqrt{\frac{2\rho_{\rm DM}}{3m^2}} \frac{(Q/M)_{\rm in}}{mL} \sin^2\left(\frac{mL}{2}\right), \\
\bar{\lambda}_{\rm space} &= \epsilon e \frac{2T_{\rm obs}}{\sqrt{T_{\rm obs} S_n}} \sqrt{\frac{2\rho_{\rm DM}}{3m^2}} \frac{(Q/M)_{\rm in} \bar{v}}{2\sqrt{2}}, \\
\bar{\lambda}_{\rm charge} &= \epsilon e \frac{2T_{\rm obs}}{\sqrt{T_{\rm obs} S_n}} \sqrt{\frac{2\rho_{\rm DM}}{3m^2}} \frac{|(Q/M)_e - (Q/M)_{\rm in}|}{2Lm}.
\end{aligned} \tag{80}$$

where L is the length of the interferometers and $(Q/M)_e, (Q/M)_{\rm in}$ are the charge-to-mass ratios of the end mirrors and input mirrors, respectively. The above approach works if $T_{\rm coh} \neq T_{\rm obs}$, however in practice, this does happen, since the data are typically broken in to smaller chunks with $T_{\rm FFT} \sim T_{\rm coh}$. The likelihood equation derived in [150] is actually unstable in this region, and so a numerical approach is used to estimate sensitivity and derive upper limits as in [151].

5. *Distinguishing amongst dark-matter models*

Only a couple of works [147, 152] have attempted to find ways of determining whether a particular type of DM interacted with GW detectors. In [152], the authors employ the Wiener filter [153] to compute the cross power across different detector pairs in the follow-up stages of the analysis, using different $T_{\rm FFT}$, to exploit the ways that types of DM will couple to different interferometer baselines. Not only was the Wiener filter shown to produce low residuals when the signal in the data matched the model, and high values when the data were filtered with the wrong signal but also it could, with high confidence, veto candidates returned in a real search of O3 data. Ref. [147] uses standard cross correlation to argue that the overlap reduction function can be used as way to distinguish amongst different spins of DM particles, since the cross power will be different. In both cases, cross power is important, since the individual power spectra are more or less indistinguishable for all types of ultralight dark matter, which arises because the phase evolutions for the considered types of ultralight dark matter here are the same.

B. Ground-based interferometers

Searches for DM particles interacting with the LIGO, Virgo, KAGRA and GEO600 interferometers have been performed using data from the most recent observing run, O3, resulting in constraints on dilatons and dark photons [117, 118, 151, 154]. We summarize the results that have arisen from each of the existing ground-based interferometers.

1. *LIGO, Virgo and GEO600*

In [154], two methods were used to search for ultralight dark matter: cross-correlation and excess power. Cross-correlation benefits from utilizing the phase information of the signal, something that is lost when using the time-frequency excess power method. On the other hand, the excess power method matches its coherence time $T_{\rm FFT}$ to the signal coherence time $T_{\rm coh}$ in every Hz band analyzed, allowing an improved sensitivity across the frequency range compared to cross-corelation, which fixed $T_{\rm FFT} = 1800$ s.

In Fig. 3, we show the upper limits on the coupling constant ϵ^2 for both methods, in comparison to existing experiments. We can see, across a broad frequency range, that results from GW interferometers surpass by orders of magnitude constraints from Eöt-Wash and the MICROSCOPE experiments. These upper limits were derived for cross-correlation and excess power by following the procedure outlined in Section III A 1 and Section III A 2, respectively. Both methods employed the Feldman-Cousins approach [155] to set upper limits, which is robust against non-Gaussian noise and has been shown to produce conservative upper limits with respect to those that would have been obtained through simulations [103].

Additionally, a recent search for scalar bosons interacting with LIGO was performed [118] using LPSD, resulting in tight constraints on the coupling constants given in Eq. (27). In Fig. 4, we can see, in blue, the constraints that have been derived, which supersede, at least a low masses, those that were derived in a GEO600 search for the same kind of DM [117]. The enhancement comes from the improved low-frequency sensitivity of LIGO relative to GEO600, as well as incorporating the interaction of scalar DM with the mirrors, as well as the beam splitter, into the search. These upper limits were derived for by following the procedure outlined in Section III A 3 and Section III A 2.

2. *KAGRA*

KAGRA is another interferometer in Japan that, while not yet as sensitive to GWs as LIGO and Virgo, can be used to search for DM. In particular, the different materials used in the mirrors in KAGRA can be exploited to be sensitive to vector DM that couples to baryon-lepton

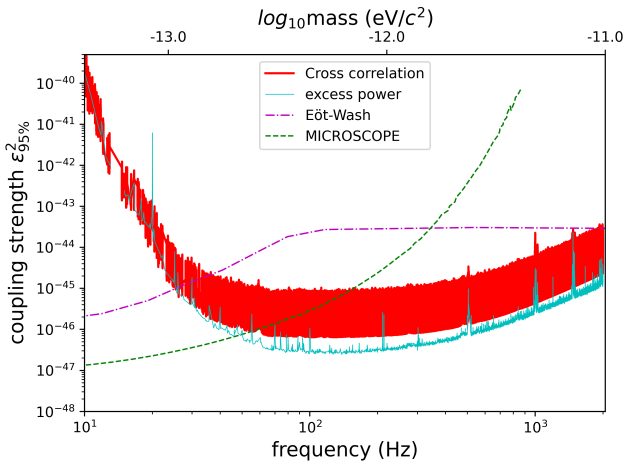

FIG. 3: Adapted from [154]. Upper limits obtained from analyzing LIGO O3 data on the coupling of dark photons to baryons $U(1)_{\rm B}$ in the LIGO mirrors. MICROSCOPE [62] and Eot-wash torsion balance upper limits are plotted as a comparison to the results here [60]. To produce limits on dark photon/baryon-lepton coupling, $U(1)_{\rm B-L}$ in the LIGO mirrors, these limits should be multiplied by four.

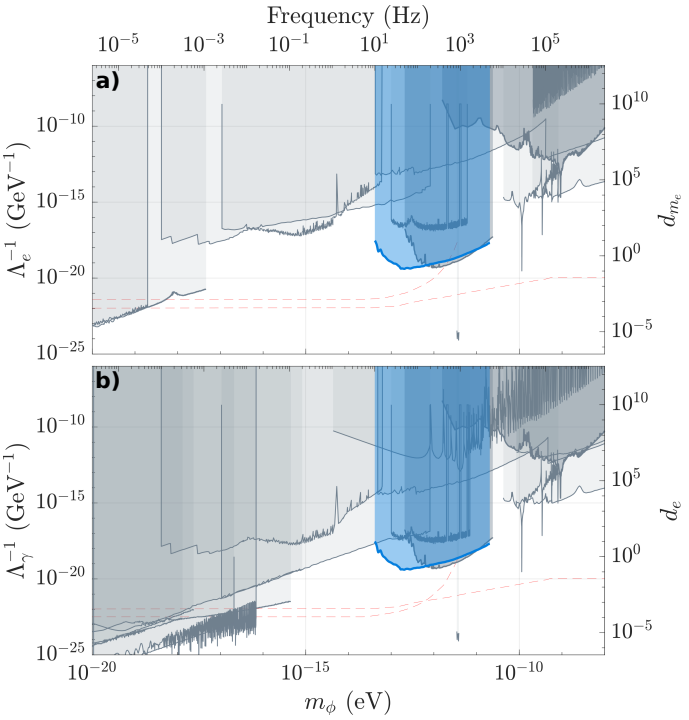

FIG. 4: Taken from [118]. 95% confidence-level upper limits on Λ_i^{-1}, the coupling of dilaton DM to electrons or photons, as a function of mass and frequency from LIGO O3 data, which would have cause time-dependent oscillations of the sizes and indices of refraction of the beamsplitter and the LIGO mirrors. **a**) and **b**) show these constraints compared to existing ones on Λ_e and Λ_γ, respectively. The results from the LIGO O3 search are shown by the thick blue line, constraints from direct experimental searches for DM [117, 156–168] are shown in thin grey, and constraints from searches for "fifth forces" [169, 170] are depicted by the dashed red lines.

number [171], since the signal-to-noise ratio is enhanced for objects with different charge-to-mass ratios, as indicated by Eq. (80). Furthermore, this kind of DM can actually be seen in non-GW channels, such as the auxiliary length channels PRCL and MICH. The raw outputs of PRCL and MICH are time-varying displacement sof the forms (we also write the GW channel for comparison, $\delta L_{\rm DARM}$) [151]:

$$\delta L_{\rm DARM} = \delta(L_{\rm x} - L_{\rm y}), \quad (81)$$
$$\delta L_{\rm MICH} = \delta(l_{\rm x} - l_{\rm y}), \quad (82)$$
$$\delta L_{\rm PRCL} = \delta[(l_{\rm x} + l_{\rm y})/2 + l_{\rm p}], \quad (83)$$

In KAGRA, $L_x = L_y = 3000$m is the arm length, $l_x = 26.7$m is the distance between the beam splitter and the input x mirror, $l_y = 23.3$m is the distance between the beam splitter and the input y mirror, and $l_p = 41.6$m is the the length of the power recycling cavity. All of these lengths are much shorter than the DM coherence length $L_{\rm coh}$. See Fig. 1 of [151] for a schematic of the interferometer.

These two channels contain both fused silica mirrors used for the beam splitter and power recycling mirrors, and cryogenic sapphire test masses. The charge-to-mass ratios for baryon-lepton number differ by $\sim 9 \times 10^{-3}$ for fused silica and sapphire, while for baryon number alone, these quantities differ by only $\sim 4 \times 10^{-5}$, showing a large enhancement of the baryon-lepton DM interaction signal.

No significant signals were found in this analysis of KAGRA O3 data [151], so upper limits, as shown in Fig. 5, were calculated following the procedure outlined in Section III A 4. The upper limits are shown for each channel analyzed, and many narrow-band noise artifacts are visible, which tends to limit the sensitivity of this search at low freqeuncies. The constraints are not as strong as those that come from LIGO; however, future searches with KAGRA are expected to yield powerful constraints on this type of DM due to the difference in charge-to-mass ratios of the mirrors [171].

C. Space-based interferometers

Spaced-based GW interferometers, such as LISA [172, 173], Taiji [174], Tianqin [175] and DECIGO [174], will hopefully fly within the next 10-15 years. The exquisite sensitivity of GWs in the μHz to mHz band also allows the prospect to probe ultralight dark matter with masses of $[10^{-19}, 10^{-14}]$ eV, a few orders of magnitude lower than those currently searched for in ground-based inter-

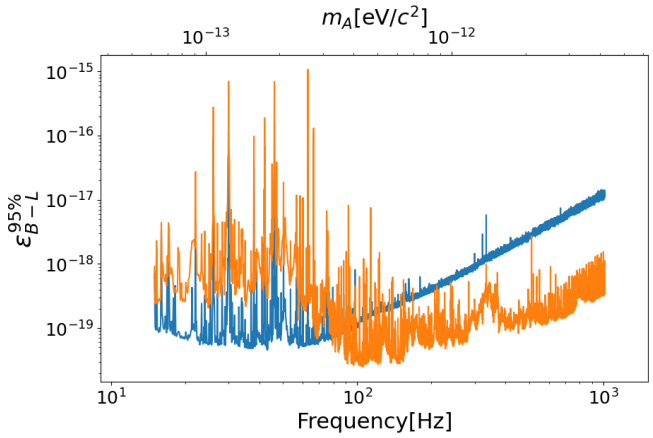

FIG. 5: Taken from [151]. 95% confidence-level upper limit on the strength of the coupling between dark photons and baryon-lepton number using KAGRA O3 data, derived from two particular interferometer channels: MICH (blue line) and PRCL (orange line). Because the KAGRA input mirrors, end mirrors, and power recycling mirrors are made of different material, the coupling strength of dark photons to baryon-lepton number is enhanced, and is more visible in these particular channels than in the ordinary strain one. In the low-mass (low-frequency) range, many narrow-band noise disturbances are seen, which arise due to unknown sources.

ferometers [176]. Until now, however, only a protoype for LISA, called LISA Pathfinder, has been flown as a "proof-of-concept" mission [177–179]. Nevertheless, pilot searches can be performed on LISA Pathfinder data as a way to prepare for when space-based detectors fly, which allows for the development of robust data analysis pipelines and for handling of the peculiarities of future data, e.g. glitches, downtimes, etc.

Such a search was preformed using LISA Pathfinder data [180] using the excess power method described in Section III A 2 for ultralight dark photons coupling to baryons, however, no physical constraints on the coupling strength were obtained, since the noise level was too high, the arm length was too short (only 40 cm compared to $\mathcal{O}(10^6)$ km), and only one arm existed. However, the search procedure designed will serve as a roadmap for future analyses of spaced-based detector data, since many problems, including limited sampling at low frequency, gaps, noise non-stationarities and glitches had to be handled in this analysis of data from a space-based detector.

After this search was performed, however, it was realized that the relative acceleration of the spacecraft and one of the test masses would produce a much stronger signal than that which was searched for previously, which was the relative acceleration of the two test masses [181]. A conservative upper limit on the baryon-lepton coupling was set without performing a search, assuming no signal would have been detected in LISA Pathfinder data, as shown in Fig. 6, by using a reference acceleration power spectral density of the spacecraft with respect to one of the test masses. We can see that the upper limits from the relative acceleration of space-craft/ test mass are much better than that from [180], labeled .(decoherence). The constraint on B-L coupling is stronger with respect to that of baryon coupling because the test mass and spacecraft are primarily made of gold, and gold/carbon, respectively.

Only B-L constraints are shown from [181] because those arising from coupling to baryons are not yet strong enough to probe a tighter constraint than provided by MICROSCOPE. However, many conservative assumptions were made in [181], including the composition of the spacecraft and the use of a reference acceleration power spectral density, both of which could, if studied in more detail, lead to more stringent constraints for both the baryon and B-L coupling scenarios.

D. Pulsar timing arrays

Because pulsars are extremely accurate clocks, they can also be used to search for GWs, which will distort the spacetime between earth and pulsars. Practically speaking, GWs will cause a change in the times of arrivals of pulses with respect to that in the absence of GWs. Of course, other effects between the pulsars and earth must be taken into account, e.g. interstellar medium dispersion and scattering, instabilities in the rotation of the pulsar itself, which makes these measurements particularly challenging. Nevertheless, pulsar timing arrays can be formed by cross correlating the times of arrivals from multiple pulsars in the galaxy, mitigating many of these effects.

Ultralight scalar DM will also cause deviations in the times of arrivals of pulses as given in [94], though the mass of such particles are 10 orders of magnitude lower than those probed with ground-based interferometers.

In Section II, we discussed various models of scalar DM that can be constrained with pulsar timing arrays. We again divide this section in the different types of DM that can be probed with pulsar timing arrays.

1. *Gravitationally-interacting ultralight dark matter*

As discussed before, DM could interact only via gravity, and alter the distances between the pulsars and earth, analgous to GWs. Using European pulsar timing array data, a search was performed in the residuals for this kind of DM interaction. In Fig. 7, we show recent constraints on ultralight scalar DM in two ways: (1) the minimum detectable strain amplitude as a function of DM mass, and (2) the fraction of DM that ultralight dark matter could compose. We can see that the masses below $\sim 10^{-23.2}$ eV can be well constrained by pulsar timing arrays, and that ultralight dark matter cannot make up

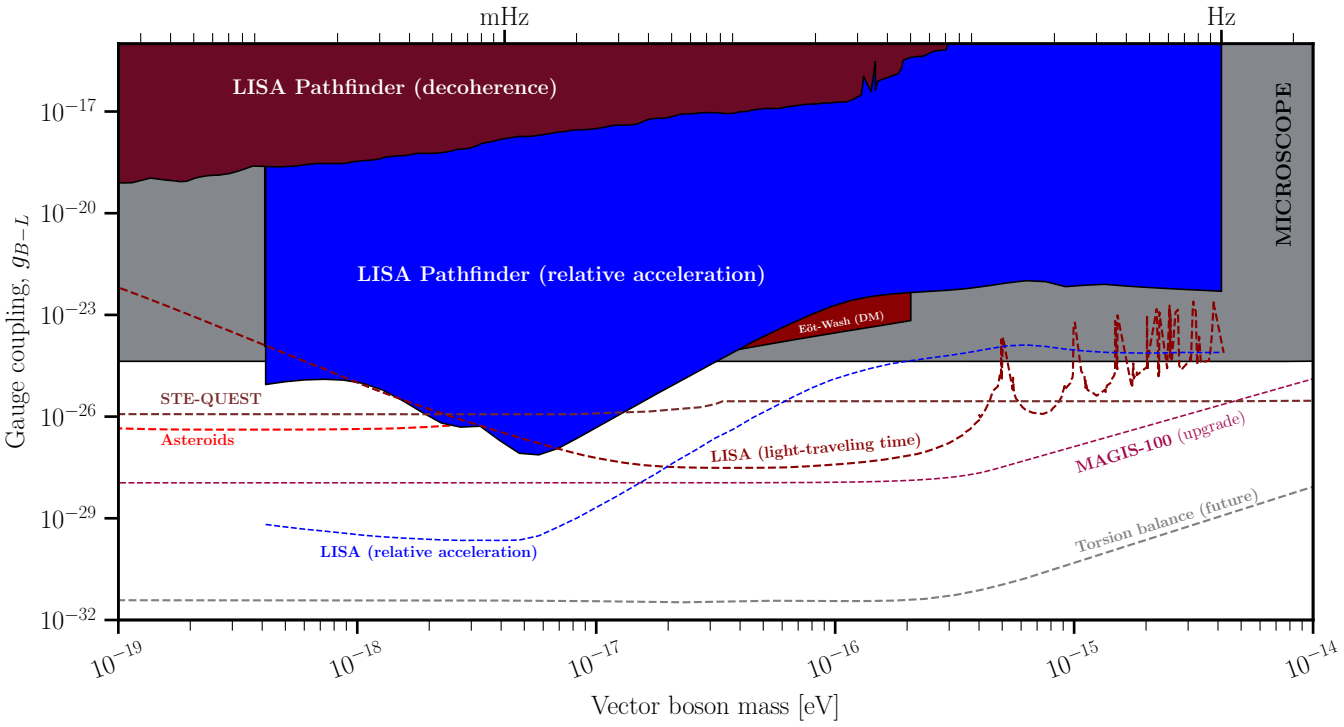

FIG. 6: Taken from [181]. Upper limits on the coupling of dark photons to baryon-lepton number considering the relative acceleration of the spacecraft and one of the test masses in LISA Pathfinder. The constraints derived from a search for the induced acceleration of the two test masses by dark photons in LISA Pathfinder data is shown as "decoherence" . Using the relative acceleration caused by dark photon interaction with baryon-lepton number allows for stringent constraints to be placed on the coupling, since the spacecraft and test masses are made of different materials. Constraints from other experiments and future projections for LISA are shown as well.

all of DM at these masses. Fig. 7 presents upper limits in three scenarios: (1) uncorrelated, (2) correlated and (3) pulsar-correlated.

1. "Uncorrelated" refers to the case when the ultralight dark-matter $L_{\rm coh}$ is less than the average pulsar separation and the earth-pulsar distance, and means that the pulsars experience different phases of the ultralight dark-matter signal. Thus, $\hat{\phi}_P^2$ and $\hat{\phi}_E^2$ are independent.

2. "Correlated" means that the earth-pulsar distance and the average distance between pulsars is smaller than $L_{\rm coh}$, and that the DM $L_{\rm coh}$ comprises the inner 20 kpc region of the galaxy for which galaxy rotation curves have been used to test the DM hypothesis. This means that each pulsar experiences the same phase of the ultralight dark-matter signal. In this case, the same coherence patch and local DM energy density are measured.

3. "Pulsar-correlated" means that $L_{\rm coh}$ is smaller than the radius of the galactic center sampled by experiments that derive galaxy rotation curves. However, estimates of the DM energy density are from different coherence patches and thus measurements averaged over different patches.

Each type of analysis optimally probes a different mass regime depending on the DM coherence length. Therefore, the "correlated" curve is valid for masses less than $\sim 2\times10^{-24}$ eV; the "pulsar-correlated" curve can be applied for $2\times10^{-24}\,\text{eV} \lesssim m_{\rm DM} \lesssim 5\times10^{-23}\,\text{eV}$ and the "uncorrelated" curve holds for $m_{\rm DM} \gtrsim 5\times10^{-23}$ eV. In both correlated cases, $\hat{\phi}_P^2 = \hat{\phi}_E^2$.

Additionally, NANOGrav data can be used to constrain this kind of ultralight dark matter. In Fig. 8, a similar constraint is shown on a quantity that relates to the fraction of the DM energy density that gravitationally-interacting DM could compose. S_ϕ is the spin of DM, which can be 0 or 1 in this model. NANOGrav writes the timing residuals for the $I^{\rm th}$ pulsar as:

$$h_I(t) = \sum_i A^i_{E,I}(\boldsymbol{x}_E)\sin(\omega t + \gamma^i_E) \tag{84}$$

$$+ A^i_{P,I}(\boldsymbol{x}_{P,I})\sin(\omega t + \gamma^i_{P,I})\,, \tag{85}$$

where i indicates the polarization (= 0 for spin-0 and = 1, 2, 3 for spin-1). This expression is divided into

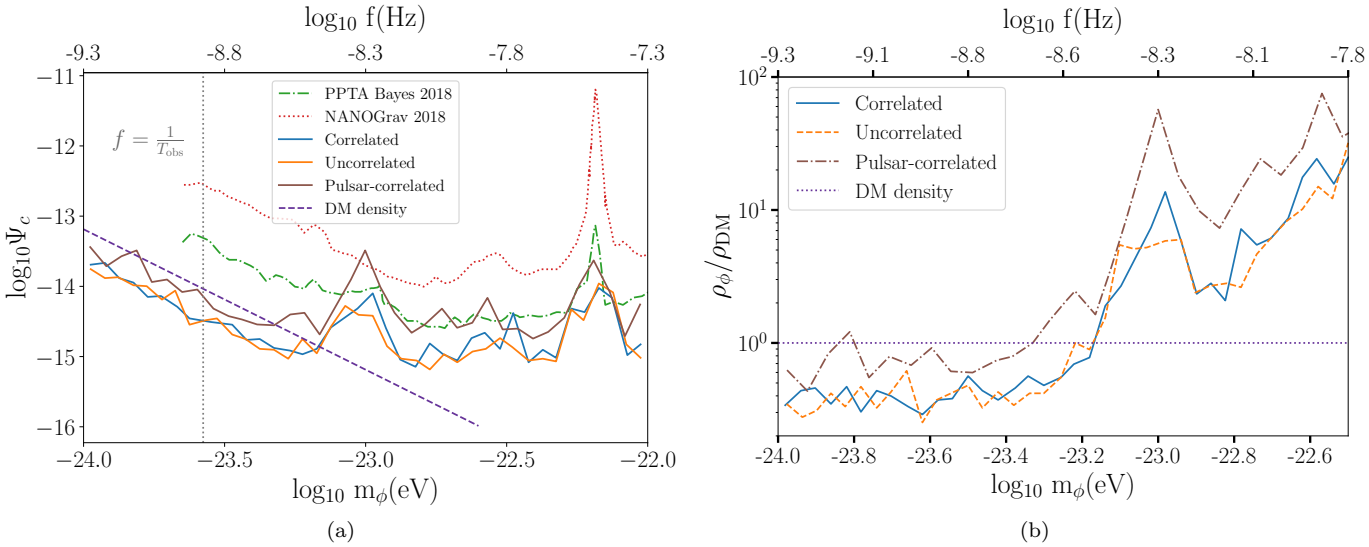

FIG. 7: Taken from [127]. 95% confidence-level upper limits from analyses of European pulsar timing array data on ultralight dark matter interacting only gravitationally and changing the times of arrivals of pulses in an analogous way as GWs do. The panels show (a) the dimensionless strain amplitude Ψ_c and (b) the fraction of the DM energy density that scalar DM could compose as a function of DM mass and frequency. $\rho_{\rm DM} = 0.4 {\rm GeV/cm}^3$. For comparison, upper limits on these quantities are shown from previous searches [126, 182]. In the right panel, we zoom in on the excluded ultralight dark matter masses. The horizontal dotted line represents the scenario in which ultralight dark matter is responsible for all of the local DM energy density . Scalar ultralight dark-matter particles with mass $-24.0 < \log_{10}\,(m_{\rm DM}/{\rm eV}) < -23.7$ can comprise at most $30 - 40$ % of $\rho_{\rm DM}$, while particles with masses $-23.7 < \log_{10}\,(m_{\rm DM}/{\rm eV}) < -23.3$ could comprise up to ~ 70 % of $\rho_{\rm DM}$.

"earth" and "pulsar" terms with amplitudes and arbitrary phases of $A^i_{E,I}(\boldsymbol{x}_E)$ and phase γ^i_E, and $A^i_{P,I}(\boldsymbol{x}_{P,I})$ and time-independent phase $\gamma^i_{P,I}$, respectively. These phases depend on the positions of the earth and the pulsar with respect to the ultralight dark-matter field (see Eq. 60 and 61 of [128]).

Like the EPTA, NANOGrav assumes a model of ultralight dark matter that induces metric perturbations and therefore changes in the times of arrivals of pulses [94]. The amplitude of the signal that is constrained is similar to Eq. (64):

$$A^i_{E,I}(\boldsymbol{x}_E) = A^i_{P,I}(\boldsymbol{x}_E) = A_{\rm grav} = (2S_\phi + 1)\,\frac{\pi G \rho_{\rm DM}}{2m^2_{\rm DM}}\hat{\phi}^2(\boldsymbol{x}) \tag{86}$$

where $S_\phi = 0$ or 1 for scalar and vector DM, respectively.

Fig. 8 shows the NANOGrav constraints on this amplitude, which can be compared to the right-hand panel of Fig. 7. NANOGrav cannot yet probe a physical constraint for the fraction of DM energy density that this model of DM could compose, likely because their dataset only spans 15 years, while the European pulsar timing array collaboration analyzed almost 25 years of data.

2. *Variation of fundamental constants constraints*

From the most recent NANOGrav dataset, constraints on ultralight dark matter that causes fundamental constants to oscillate [128] can be set as well for masses below 10^{-22} eV. In the case that ultralight dark matter causes changes in the moment of inertia of the pulsar, Fig. 9 depicts constraints on the couplings of the scalar DM particle to up- and down- quarks weighted by their masses ($\hat{m}$), electrons (d_e), muons (d_μ), photons (d_γ) and gluons (d_g). To derive these constraints, the simplest model of the equation-of-state of the neutron star is assumed, as outlined in Section II C 2, and, when constraining one particular coupling constant, the rest are assumed to be zero.

The strongest constraints from pulsar timing arrays are on the couplings to the electron and muons. Experiments that directly use atomic clocks to search for ultralight dark matter are insensitive to the electron coupling, since changing the electron mass does not affect the spacing between energy levels [122]. In terms of (the lack of) other constraints on muons, laboratory experiments do not have enough muons to harness on earth to study the coupling of DM to them, while, in contrast, neutron stars have an abundance of muons.

In Fig. 9, there is a gray-shaded region that indicates

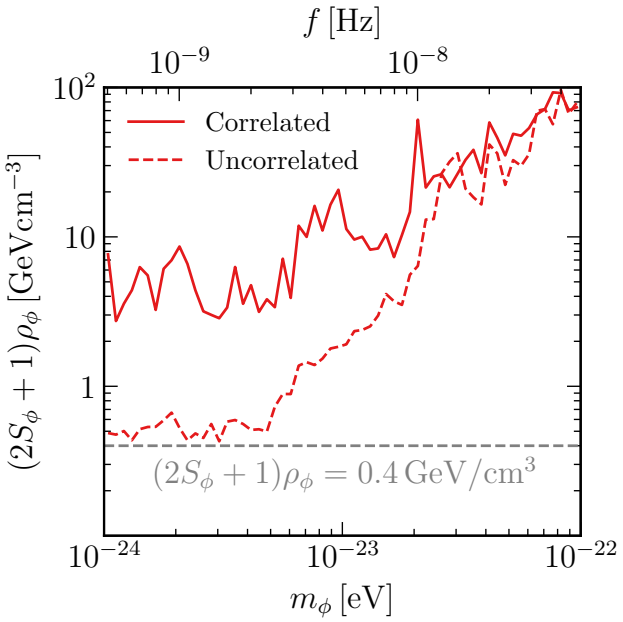

FIG. 8: Taken from [128]. Upper limits on the local ULDM density for the correlated (solid line) and uncorrelated (dashed line) signals at the 95% credible level using data from the NANOGrav pulsar timing array. The model of DM considered here is the same as that in Fig. 7. The gray dashed line indicates the predicted DM abundance.

the situation in which $A < A_{\rm grav}$, where A is given by the amplitude of Eq. (41) or Eq. (45). In other words, these constraints on ultralight dark matter coupling to standard-model particles are valid when the coupling of DM to gravity can be neglected, i.e. when [122]:

$$d_i \gtrsim \frac{4.5\times10^{-9}}{y_i}\left(\frac{10^{-23}\,\mathrm{eV}}{m_{\rm DM}}\right), \tag{87}$$

In the gray-shaded region, the interaction between gravity and DM is stronger, and thus constraints on ultralight dark matter coupling to standard-model particles alone would not be valid in that region. Furthermore, these constraints assume that scalar particles constitute all of DM, which may not be true. If they only comprise a fraction f of DM, then the constraints will be weakened by $\sqrt{f}$, because of the $\sqrt{\rho_{\rm DM}}$ term in the amplitude of these interaction signals.

The scalings of these constraints with the DM mass should be discussed. At high masses, the signal is essentially deterministic, and the signal-to-noise ratio scales as the square of the signal amplitude, which means that $d_i \propto m^2$. At low masses ($m < 1/T_{\rm obs}$), the signal is observed in different coherence patches, since the coherence length is shorter than the pulsar separation. The signal is no longer a sinusoid but can be expressed as a polynomial in mt. The first two terms of this polynomial (mt and $(mt)^2$) are degenerated with pulsar timing terms, and thus the first observable term is $(mt)^3$, meaning that the signal-to-noise ratio is proportional to m^3. Thus, $d_i \propto 1/m$, which explains the scaling at low masses. Still, though, red noise causes the constraints to flatten as the mass decreases, which, at first, hides this scaling.

3. *Constraints on vector dark matter*

As discussed in Section II D, DM could also be composed of spin-1 bosons that interact with standard model particles. In the case of pulsar timing arrays, the ultralight dark matter would cause oscillatory forces on the earth and on the pulsars themselves with strengths proportional to the charge-to-mass ratio of these objects.

Fig. 10 shows constraints on the coupling constants $g_B = \epsilon_B$ and $g_{B-L} = \epsilon_{B-L}$ as a function of the DM mass and oscillation frequency. Again, the gray-shaded region indicates the regime in which the coupling of DM to gravity becomes stronger than the coupling of DM to standard-model particles. We can see that the NANOGrav constraints greatly surpass those that come from MICROSCOPE at very low masses. Furthermore, these constraints assume that vector bosons constitute all of DM, which may not be true. If they only comprise a fraction f of DM, then the constraints will be weakened by $\sqrt{f}$, because of the $\sqrt{\rho_{\rm DM}}$ term in the amplitude of these interaction signals. Furthermore, the stochastic GW background w

4. *Constraints on conformal DM*

DM that conformally (universally) couples to gravity could alter the moment of inertia of rotating pulsars via a new gravity-mediated force between neutron stars and ultralight dark matter [187], which is called the Nordtvedt effect [188]. If such a coupling exists, the times of arrivals of pulsars would change in a deterministic way, and would also result in a violation of the equivalence principle. This model of conformal DM has been extensively constrained by looking for impacts on the timing solutions of measured binary pulsar [189, 190].

Ref. [191] uses European pulsar timing array data to constrain linear (Fierz-Jordan-Brans-Dicke (FJBD) theory) [192–195] and quadratic (Damour-Esposito-Farese (DEF) theory) [196, 197] conformal DM couplings to gravity by deriving how the pulsar times of arrivals would change in the presence of the ultralight dark matter fields. In the case of FJBD conformal coupling, the residuals would appear as:

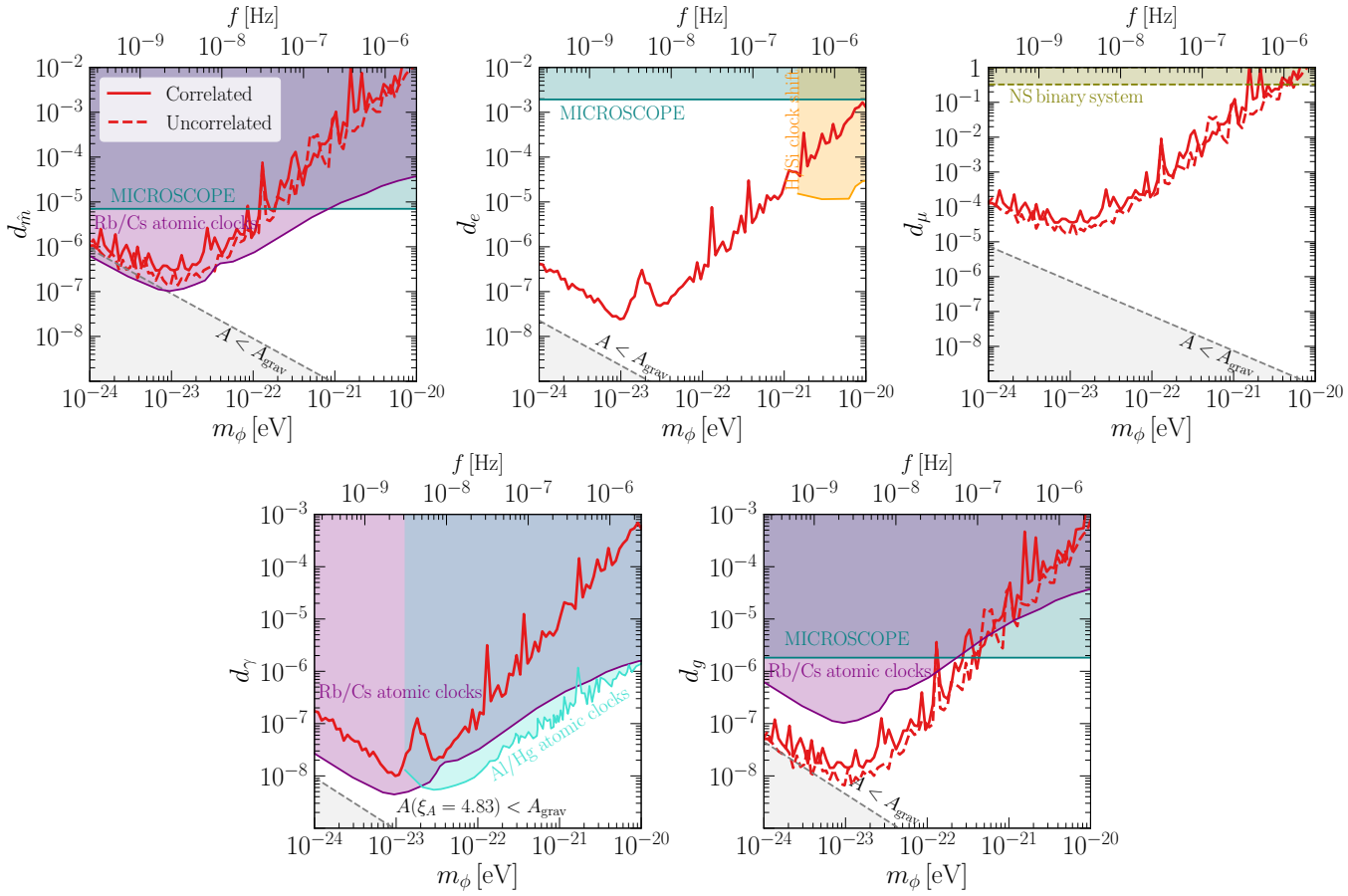

FIG. 9: Taken from [128]. Upper limits from an analysis of NANOGrav data on the coupling of ultralight dark matter to various standard-model particles: quarks, electrons, muons, photons and gluons, shown in red for the correlated case, and red dashed for the uncorrelated case. In this model, DM would alter the moment of inertia of neutron stars and thus affect the times of arrivals of pulses in pulsar timing arrays. The constraints on one coupling constant assume that all other coupling constants are set to 0. The black dashed line, and the gray shaded region, indicate where the amplitude of the signal would be less than the amplitude of the signal arising from DM coupling only to gravity. Current constraints "Rb/Cs atomic clocks" (purple) are from [183], "Al/Hg atomic clocks" (turquoise) are from [165], "MICROSCOPE" (teal) are from [62], "H/Si clock shift" (orange) are from [165], and "NS binary system" are from [184] and [185].

$$\Delta t(t) = -\int \mathrm{d}t \frac{\delta\Omega_{\rm obs}}{\bar{\Omega}} = 2\alpha s_I \frac{\sqrt{\rho_{\rm DM}}}{M_{\rm Pl} m^2} \hat{\phi}(\boldsymbol{x}) \sin(m_{\rm DM} t + \theta(\boldsymbol{x})) \Big|_{t_{\rm start} - \frac{d}{c}}^{t_{\rm end} - \frac{d}{c}}, \tag{88}$$

where s_I is the angular moment sensitivity parameter computed in [187] and is of $\mathcal{O}(1)$ in FJBD theory, α is the strength of the coupling, and $\hat{\phi}$ is a stochastic parameter whose value depends on whether the correlated, uncorrelated or pulsar correlated scenarios are considered. $\theta(\mathbf{x})$ is a random phase.

In Fig. 11, we show the upper limits on the linear coupling parameter α using European pulsar timing array data. However, Ref. [191] notes that there is some evidence for additional signal power at two masses: $m \sim 10^{-22.7}$ eV and $m \sim 10^{-21.4}$ eV, but note that other physical processes could responsible for these excesses.

5. *Constraints on axions through polarization measurements*

Changes in polarization of light by axions could also be probed in pulsar timing array experiments [106, 107]. Just as in ground-based interferometers, axions could induce cosmic birefrigence, an oscillation of the polarization plane of a linearly polarized source. Since pulsars constantly emit light that is beamed at earth, its polarization can be measured over time, and any changes in it could be attributed to axion-like DM/photon interactions. In Fig. 12, we show upper limits on this coupling

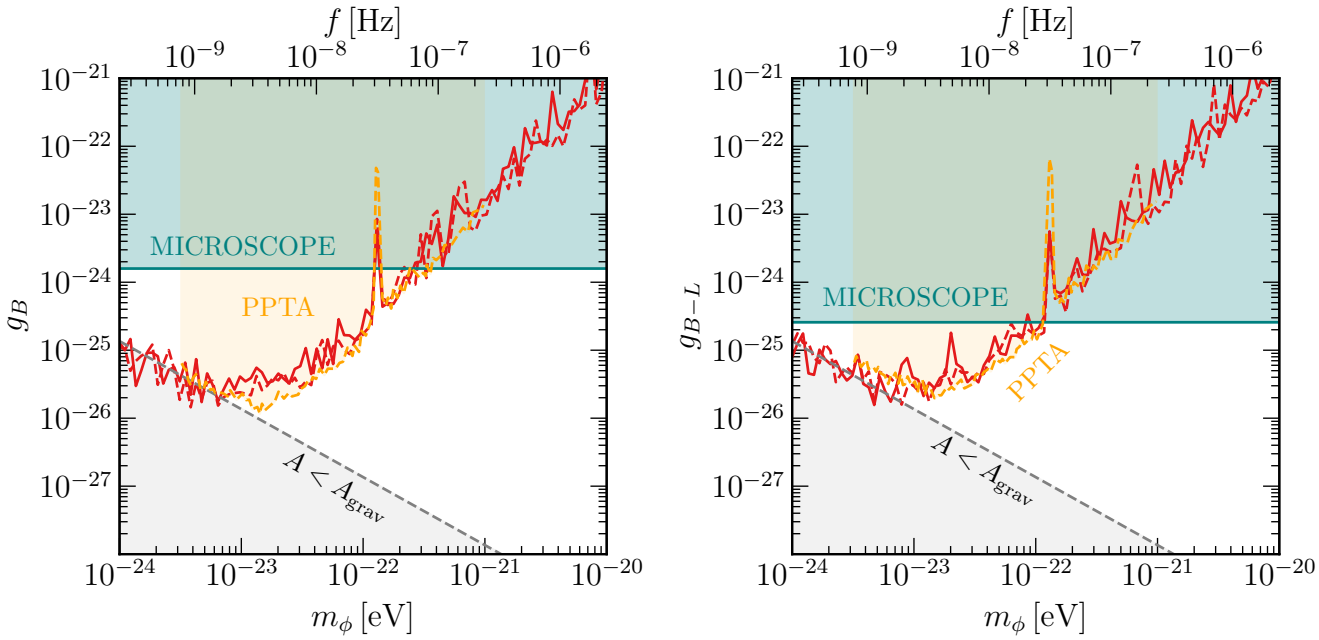

FIG. 10: Taken from [128]. Upper limits from analyses of NANOGrav pulsar timing array data on the coupling of DM to baryon and baryon-lepton number for the correlated (solid lines) an uncorrelated (dashed line) cases. In this case, dark photon DM would couple to standard model particles in the earth and the pulsars themselves. The black dashed line, and the gray shaded region, indicates where the amplitude of the signal would be less than the amplitude of the signal arising from DM coupling only to gravity. The constraints from tests of the equivalence principle ("MICROSCOPE") are shown in teal [62], and the constraints previously set by the PPTA Collaboration are reported in yellow [186].

from the Parkes Pulsar Polarization Array (PPPA), the first search of its kind. The constraints here outperform existing experiments at low axion masses.

E. Prospects for detecting the coupling of ultralight dark matter to the interferometers

Though no searches so far have yielded conclusive evidence of any DM/standard model coupling with the interferometers, impressive constraints, relative to existing DM experiments, have been set on these interaction models. The current searches and their constraints have been framed only in terms of upper limits on dilatons, dark photons and DM that couples to gravity; however, they are actually sensitive to *any* kind of DM interaction that would cause a differential strain in the interferometers. In fact, to derive these constraints, we first compute the minimum detectable signal amplitude for a generic quasi-monochromatic signal as a function of frequency, and then map these values to constraints on the DM/standard model coupling constants. It is thus simply a matter of a few relations that these results are interpreted in terms of two relatively well-motivated DM models.

Of course, ultralight dark matter could take on any mass a priori, and ground-based GW detectors only allow us to probe a small region of this parameter space, from $\sim 10^{-14} - 10^{-12}$ eV. Space-based GW detectors will permit being sensitive to masses a few orders of magnitude smaller, while high-frequency gravitational-wave (HFGW) detectors could see DM particles a few orders of magnitude larger [198]. However, it should be noted that when placing constraints on ultralight dark matter, the stochasisity of the signal could affect the limits: if we happen to "get unlucky" and observe the signal when the phase offset reduces the signal amplitude to zero, as can be seen at the zero points in Fig. 2, we would have no constraint. Such considerations were made in [150, 199] for ground-based interferometers and pulsar timing arrays.

The prospects for future ground-based GW interferometers, such as ET and Cosmic Explorer, to observe ultralight dark matter interactions are bright. Within a decade or so of observation, such detectors, currently a couple of orders of magnitude behind fifth-force constraints, could actually be competitive in this portion of the parameter space, thus permitting an extremely strong probe of new physics [24, 139].

Though GW interferometers can probe extremely small DM/standard model couplings, we do not have an estimate of a minimum strength of these interactions. We thus have no guarantee, in any search that we do, that

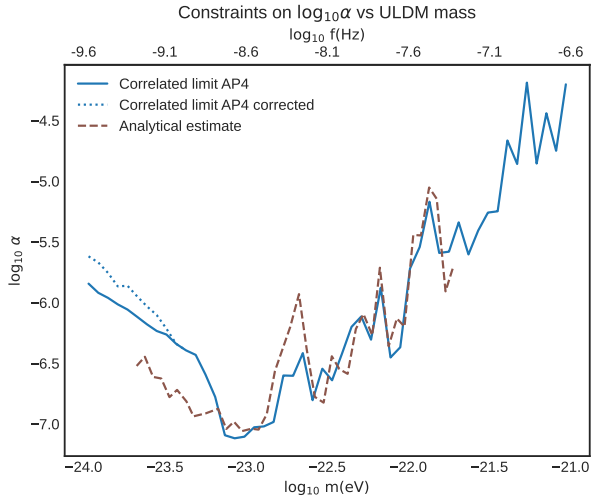

FIG. 11: Taken from [127]. Constraints on the coupling $\log_{10}\alpha$ of conformal DM to gravity at the 95% confidence-level (solid line) for the correlated case compared to the analytical estimate obtained by using the upper limits from the European pulsar timing array search in [127] to estimate α (brown dashed lines). $\rho_{\rm DM} = 0.4\,{\rm GeV/cm^3}$. Here, this model of DM would change the moment of inertia of neutron stars in the used in pulsar timing arrays, resulting in changes of the times of arrival of the pulses. If the true density of DM that conformal DM composes is less than $\rho_{\rm DM}$, the limits will suffer, which is shown by the dotted line, for values of ρ given in [127]. AP4 is a particular equation-of-state of neutron stars [73].

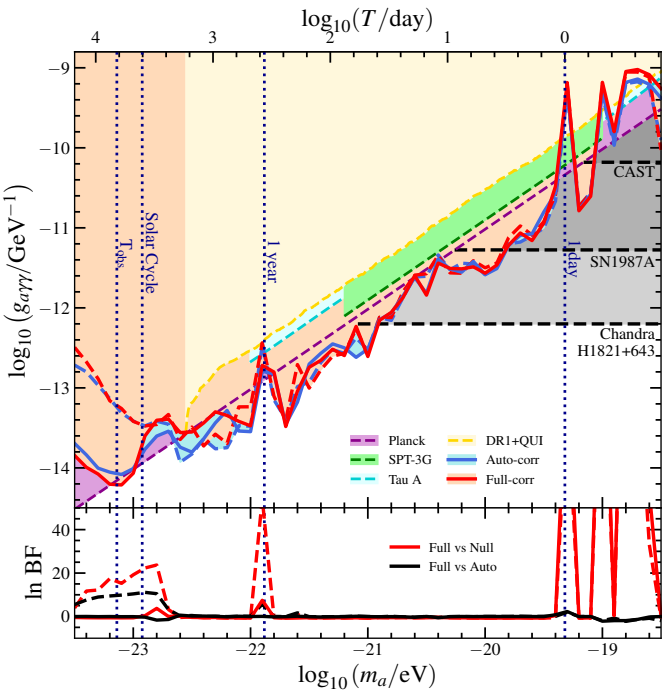

FIG. 12: Taken from [106]. Upper limits from analyses of European pulsar timing array data on the coupling of axion-like DM to photons.$\rho_{\rm DM} = 0.4\,{\rm GeV/cm^3}$. The blue and red curves correspond to the limits derived using the auto-correlation-only and full-correlation signal models, respectively. Excluded portions of the axion mass /coupling parameter space lie above these curves, and constraints from different experiments are also shown. Key timescales are shown with vertical dotted lines, included $T_{\rm obs} = 18$ years. The lower panel shows the Bayes factors for each of the scenarios.

we are getting closer to probing the true coupling value between ordinary matter and the dark sector. Such a caveat is balanced by the relatively model agnostic nature of our searches, which make minimal assumptions about the signal model, and essentially just look for correlated noise. While we probably cannot believe just one model for DM/standard model interactions, we can be sure that our techniques are sensitive to a wide range of theories, even ones that have yet to be thought of.

IV. MACROSCOPIC DARK MATTER TRANSITING THROUGH THE INTERFEROMETERS

A. Background

As mentioned in Section I, the mass of DM can span many orders of magnitude, including being "macroscopic", that is, from being $M_{\rm DM} \sim [1, 10^9]$ kg [102]. If DM exists in this mass range, it could transit through GW interferometers, and thus be searched for in LIGO, Virgo and KAGRA data. The event rate, however, depends on the mass of DM, and there are orders of magnitude fewer heavy DM particles in any given region of space than the number of ultralight dark-matter particles [102]:

$$\rho_{\rm DM} = M_{\rm DM} n_{\rm DM} \quad \Longrightarrow \quad \frac{L_{\rm DM}}{10^4\ {\rm km}} \simeq 1.2 \times \left(\frac{M_{\rm DM}}{1\ {\rm kg}}\right)^{1/3}, \tag{89}$$

where $n_{\rm DM}$ is the number density of DM, and $L_{\rm DM}$ is a characteristic length scale for the transiting DM. For 1-kg DM, the flux of DM through a given region of space is given by $\Phi \sim n_{\rm DM} v_0 \sim 3\times10^{-10}\ {\rm km^{-2}\ s^{-1}}$, meaning that approximately one transient event could be observed per year if the impact parameter of such an event is 10 km, which is similar in size to the three or four kilometer-long arms of LIGO, Virgo and KAGRA.

B. Yukawa-like interactions

If DM only couples to gravity, it seems unlikely that GW interferometers could detect this interaction

[102, 200]; however, if there is a Yukawa-like coupling between the standard model and DM, allowing for self-interactions as well, DM transiting through the interferometers could very well be detectable. The following potential V_{i-j} is assumed to govern the (self-) interactions between the standard model and DM

$$V_{i-j} = -M_i M_j \frac{G}{r}\Big(1 + (-1)^s\ \delta_i \delta_j \exp[-r/\lambda]\Big) \quad \text{where} \quad i,j = \text{SM,DM}. \tag{90}$$

where $\delta_{i,j}$ parametrizes the standard model and DM couplings, r is a length scale, λ is the screening length, s is the spin, and $M_{i,j}$ are the two masses. By assuming that the size of DM is much larger than the size of GW detectors and the range of the DM force, but smaller than the average distance between the detectors, the scattering cross section from this process can be derived:

$$\sigma_{\text{DM-DM}} = 16\,\pi \times \frac{G^2\, M_{\text{DM}}^2\, \delta_{\text{DM}}^4}{v_0^4} \times \log\left[\frac{\lambda}{r_{\text{DM}}}\right], \tag{91}$$

where r_{DM} is the size of the DM objects. While $|\delta_{\text{SM}}| < 5 \times 10^{-4}$ has been strongly constrained by equivalence principle experiments [201], the DM coupling constant could be much larger, as the only constraints come from how DM self-interaction would have influenced structure formation [202] and collisions between galaxies [203].

The lack of observed deceleration of DM in the bullet cluster collision constrained the cross-section of DM to be less than ~ 1 cm^2/g [204], which provides limits on the coupling constant of self-interacting DM to be:

$$|\delta_{\text{DM}}| \lesssim 5 \times 10^9 \times \left(\frac{1\ \text{kg}}{M_{\text{DM}}}\right)^{1/4}, \tag{92}$$

in which $\log\left[\frac{\lambda}{r_{\text{DM}}}\right] = 5$. Based on the current upper limits on δ_{SM} and δ_{DM}, the coupling of standard-model particles to DM ones could be quite large, and would thus permit an observation of a transit event in GW interferometers. Furthermore, $\delta_{\text{DM}} \gg 1$ would actually alleviate some problems with the cold DM scenario, including overly dense areas of dwarf galaxies found in simulations, and a prediction that the Milky Way produces more stars than are observed [205].

C. Projected constraints on Yukawa-like interactions

By using the potential given in Eq. (90), the differential acceleration visible on interferometers can be computed, and from that, the matched-filter signal-to-noise ratio:

$$\rho^2 = 4 \int \frac{|a(f)|^2}{S_n(f)} df \tag{93}$$

where $a(f)$ is the Fourier transform of the integral of the differential acceleration $a(t) = a_y^{\text{EM}} - a_y^{\text{IM}} - (a_x^{\text{EM}} - a_x^{\text{IM}})$ between the input mirror (IM) and the end mirror (EM) [206], and $S_n(f)$ is the acceleration power spectral density of the noise. By using sensitivity curves of LIGO, Virgo and KAGRA and a threshold on $\rho > 8$, the number of detections per year of transiting DM with different masses and different screening lengths can be computed, and is shown in Fig. 13 using a power spectral density for advanced LIGO at design sensitivity.

Further work was done regarding the detection of macroscopic DM in much more detail [200], in which the different kinds of effects of DM on the test masses were derived. Ref. [200] derives the strain on the detector in terms of three observables: (1) the Doppler effect (previously considered in [102]), (2) the Shapiro delay (light is curved near objects with mass and thus will take a longer time to travel down the interferometer arms, and (3) the Einstein Delay (time runs slower near more massive objects than less massive ones). Unfortunately, all effects are extremely weak because they are solely gravitational, and thus DM would have to couple to the standard model in some way to be detectable. As in [102], Ref. [200] computes the expected constraints on the effective coupling of DM to the standard model with an effective parameter $\tilde{\alpha} \sim \delta_i \delta_j$, which are shown in Fig. 14 for a variety of GW detectors and for two choices of screening lengths: $\lambda = 1$ m and $\lambda = 10^6$ m. Existing constraints from the bullet cluster [202], MICROSCOPE [62] and neutron-star kinetic heating with and without interactions between DM and baryons that could enhance energy transfer [207]. While the constraints that could be obtained from GW interferometers do not appear to beat existing ones, it should be noted that if only a part of DM can be explained by a new fifth force, the Bullet cluster constraints on self-interacting DM disappear, while GW bounds fall off linearly with this fraction of DM charged under this fifth force [200].

Given that such deterministic signals may not be detectable in LIGO, Virgo and KAGRA, it was worth considering whether a stochastic background arising from many transiting DM events could be seen [102, 200]. However, again, it is necessary to include the Yukawa interaction to have a chance of detecting a stochastic background.

Finally, another study [208] considered specifically how heavy transiting DM would appear in KAGRA, as well as the directional dependence of the signal-to-noise ratio, which turns out to be strong due to the geometry of the detector. In KAGRA, it is shown that the suspension system can be particularly sensitive to DM-standard model interactions, between [1,130] Hz.

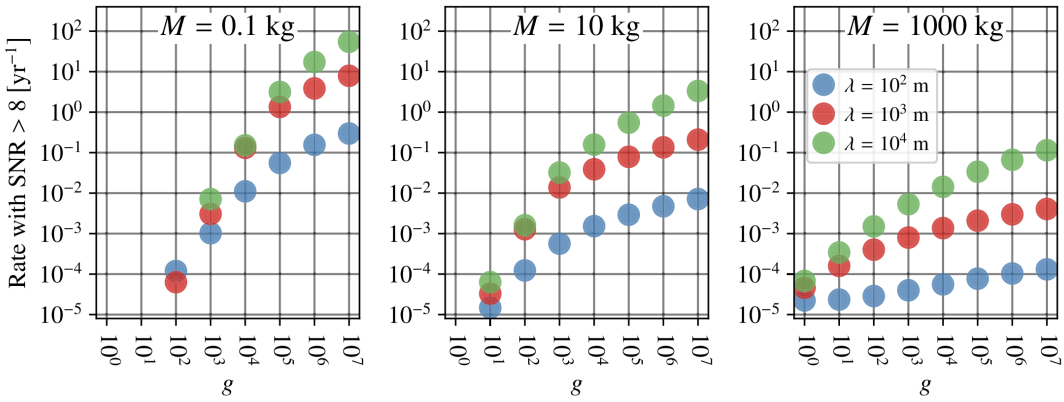

FIG. 13: Taken from [102]. Expected number of macroscopic DM transit events per year with $\rho > 8$ as measurable with advanced LIGO operating at design sensitivity, as a function of the DM mass, the screening length λ and the coupling $g = \delta_{\rm SM}\delta_{\rm DM}$ between DM and the standard model.

V. GWS FROM ULTRALIGHT BOSONIC CLOUDS AROUND ROTATING BHS

If a new ultralight boson[5] exist, it will have a particular mass, frequency and Compton wavelength. Quantum fluctuations could then allow bosons to pop into existence near a rotating BH, whose characteristic length scale is given by half of its Schwarzschild radius. Some bosons will fall in; others will scatter off, and the extent to which either of these scenarios happens depends on the properties of the black hole and the boson. If the following superradiance condition, relating the BH angular frequency Ω to the boson angular frequency ω via the magnetic quantum number m, is met [91]:

$$\omega < m\Omega, \tag{94}$$

the boson will extract energy from the BH, and thus the "bosonic wave" will be amplified. This amplification will be maximized if the Compton wavelength of this new particle comparable to the characteristic length of a BH. The massive bosons then become bound to the BH, allowing for successive scatterings, thus permitting a huge number of bosons to appear around the BH as a cloud in a given energy state (no limit on the occupation number of these particles exists a priori).. This process is called "superradiance".

More quantitatively, solving the Klein-Gordon equation for a Kerr BH hole in the presence of a massive scalar field results in a Schrondinger-like equation that exhibits a $1/r$ potential, resulting from the gravitational interaction between the bosons and the BH. Such an equation can be solved to show that the energy states of the boson cloud are quantized analogously to those of the hydrogen atom, allowing us to describe the boson cloud as a "gravitational atom in the sky" [209].

Qualitatively, superradiance will occur regardless of the spin of the boson; however, the timescales to build the cloud, as well as to deplete it, will differ. In all cases, however, as we will see, the GW emission timescale will be shorter than the time to build up the cloud, making these systems excellent sources of GWs.

For the black hole to be spun down such that the condition in Eq. (94) is no longer satisfied, scalar and vector clouds require [210]:

$$\tau^{(\rm s)}_{\rm inst} \approx 27\,{\rm days}\left(\frac{M_{\rm BH}}{10\,M_\odot}\right)\left(\frac{0.1}{\alpha}\right)^9\frac{1}{\chi_i}\,, \tag{95}$$

and

$$\tau^{(\rm v)}_{\rm inst} \approx 2\,{\rm minutes}\left(\frac{M_{\rm BH}}{10\,M_\odot}\right)\left(\frac{0.1}{\alpha}\right)^7\frac{1}{\chi_i}\,, \tag{96}$$

where χ_i is the BH spin at birth, and the GW fine-structure constant is

$$\alpha \equiv \frac{r_g}{\lambda\!\!\!^{-}_\mu} = \frac{GM_{\rm BH}}{c}\frac{m_b}{\hbar}, \tag{97}$$

where m_b is the mass of the boson. This new boson could have a spin of 0, 1 or 2, where spin-0 could correspond to the pseudo-scalar QCD axion (or axion-like) particle [91, 211], spin-1 could indicate dark photons arising through kinetic mixing with the ordinary photon [138], or spin-2 tensor bosons that could arise from modified theories of gravity [211].

After the cloud builds up, GWs can be emitted in three different ways: (1) through boson-boson annihilation, (2) through boson energy-level transitions, and (3) after a "bosenova".

It has been shown, under a wide range of assumptions of BH populations, spins, redshift distributions, etc., that

[5] In the context of boson clouds around rotating black holes, this new particle could, but need not, be DM

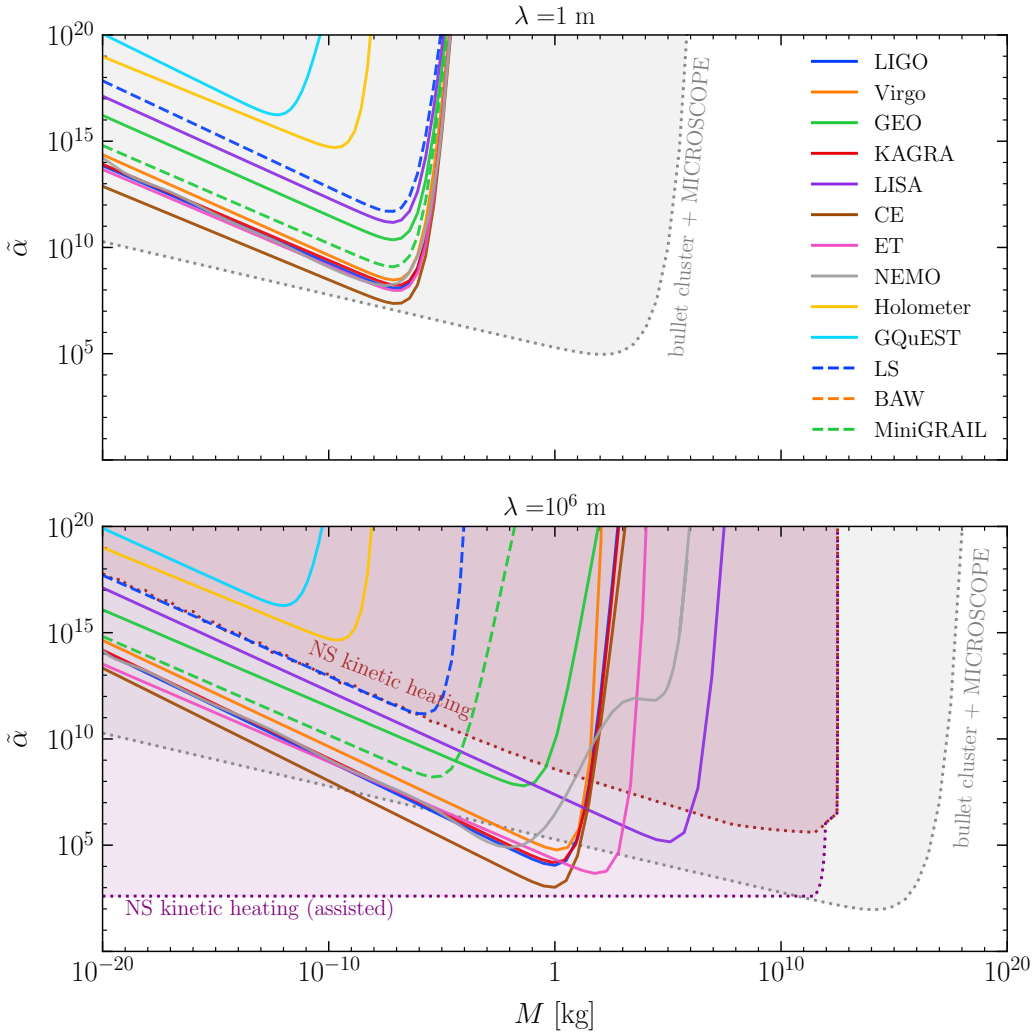

FIG. 14: Taken from [200]. 90%-projected sensitivity on the standard model/DM interaction parameter $\tilde{\alpha} \sim \delta_{\rm SM}\delta_{\rm DM}$ that can be probed from macroscopic DM transiting through several GW experiments, compared to existing constraints from others. One year of observation is assumed, and two choices for the screening length are made. Dotted lines denote existing constraints. Existing constraints are shown in dotted lines. In particular, Bullet cluster and MICROSCOPE constraints are shown in gray [62, 202], MICROSCOPE ones. The purple and red lines denote constraints from neutron star kinetic heating [207] with and without additional short-range interactions between baryons and DM that would enhance energy transfer.

such systems would be detectable by CW searches in advanced LIGO, Virgo and KAGRA data and/or in future detectors, such as ET and Cosmic Explorer [212, 213]. Furthermore, both galactic BHs [214] and remnants of mergers of BHs outside the galaxy could also be detected, the latter of which, in the scalar case, only being visible in ET and Cosmic Explorer [210, 212, 215]. Annihilating vector boson cloud systems, however, emit stronger, though shorter, GW signals [91, 216–219], and potentially may contain electromagnetic counterparts if the vector boson kinetically mixes with the ordinary photon [138].

The boson mass is fixed by the GW frequency, and could in principle take on any ultralight mass. That is why GW experiments across the frequency spectrum have been or are being designed to search for these boson cloud systems. While most of the literature focuses on ground-based GW interferometers, we note that HFGW detectors will also be able to probe BH superradiance of heavier bosons than those detectable by LIGO, Virgo and KAGRA [198], e.g. [220], and space-based GW interferometers will probe lighter masses [212, 221], and space-based detector analyses can be used to aid in discovering boson clouds in the band of ground-based GW interferometers [222].

As will be discussed, boson cloud self-interactions could have a significant impact on (1) whether the superradiance condition is saturated [223–225], (2) how

quickly a binary black hole system will approach merger [226, 227], and (3) the rate of change of the GW frequency of an isolated boson cloud [228]. Self-interactions would also allow higher energy levels to grow faster. The strength of these interactions will affect the detection prospects in ET and Cosmic Explorer [229], as well as recent search results which have not yet accounted for moderate or strong interactions.

Note that while spin-0 and spin-1 boson clouds are relatively well understood theoretically, spin-2 clouds are much more complicated. The superradiant instability of spin-2 fields occurs much faster than the others [230], and since the backreaction of the instability has not been computed due to difficulties arising from a nonlinear coupling between the spin-2 particle and gravity, it is not yet known whether the observational signatures are similar to the vector or scalar cases, and whether there is a dependency on the specific nonlinear theory chosen.

A. Annihilation signal

When Eq. (94) is no longer satisfied, the cloud stops growing. Since ultralight bosons are their own antiparticles, they will start to annihilate, producing GW radiation at a frequency fixed by the boson mass and slightly redshifted by the BH mass (in the non-relativistic limit $\alpha \ll 1$), which predominately applies to the equations shown in this work). In the scalar boson case [231]:

$$f_{\rm gw} \simeq 483\,{\rm Hz}\left(\frac{m_{\rm b}}{10^{-12}\ {\rm eV}}\right)\times\left[1-7\times10^{-4}\left(\frac{M_{\rm BH}}{10M_\odot}\frac{m_{\rm b}}{10^{-12}\ {\rm eV}}\right)^2\right] \tag{98}$$

Qualitatively, the GWs emitted are monochromatic because the mass of the boson is fixed, and all the bosons are in the same energy state. As alluded to before, the timescales for GW emission are much longer than the time it takes to build the cloud [210]:

$$\tau^{\rm (s)}_{\rm GW} \approx 2\times 6.5\times10^4\,{\rm yr}\left(\frac{M_{\rm BH}}{10\,M_\odot}\right)\left(\frac{0.1}{\alpha}\right)^{15}\frac{1}{\chi_i}. \tag{99}$$

$$\tau^{\rm (v)}_{\rm GW} \approx 2\times 1\,{\rm day}\left(\frac{M_{\rm BH}}{10\,M_\odot}\right)\left(\frac{0.1}{\alpha}\right)^{11}\frac{1}{\chi_i}. \tag{100}$$

where we have explicitly noted a factor of 2 that is missing from the original reference [210], as pointed out in [217]. There will also be a classical depletion of the cloud over time, as the number of bosons starts to decrease, resulting in the following drifts in frequency over time [210]:

$$\dot f^{\rm (s)}_{\rm gw} \approx 3\times10^{-14}\,{\rm Hz/s}\left(\frac{10M_\odot}{M_{\rm BH}}\right)^2\left(\frac{\alpha}{0.1}\right)^{19}\chi_i^2\,, \tag{101}$$

$$\dot f^{\rm (v)}_{\rm gw} \approx 1\times10^{-6}\,{\rm Hz/s}\left(\frac{10M_\odot}{M_{\rm BH}}\right)^2\left(\frac{\alpha}{0.1}\right)^{15}\chi_i^2\,. \tag{102}$$

We note that relativistic computations of the frequency drift have also been performed [217, 232]. In the non-relativistic limit $\alpha \ll 1$, the signals will have the corresponding amplitudes of [210]:

$$h^{\rm (s)}_0 \approx 8\times10^{-28}\left(\frac{M_{\rm BH}}{10M_\odot}\right)\left(\frac{\alpha}{0.1}\right)^7\left(\frac{\rm Mpc}{r}\right)\left(\frac{\chi-\chi_f}{0.1}\right) \tag{103}$$

$$h^{\rm (v)}_0 \approx 4\times10^{-24}\left(\frac{M_{\rm BH}}{10M_\odot}\right)\left(\frac{\alpha}{0.1}\right)^5\left(\frac{\rm Mpc}{r}\right)\left(\frac{\chi-\chi_f}{0.1}\right) \tag{104}$$

where the final spin χ_f is

$$\chi_f = \frac{4\alpha_f m}{4\alpha_f^2+m^2} \tag{105}$$

These equations indicate interesting properties for scalar and vector boson cloud annihilation signals. For bosons whose Compton wavelengths are optimally matched to the size of the BH, scalar bosons will annihilate over timescales that greatly exceed the observation time of ground- or space-based GW interferometers, and their frequencies will hardly drift over time. Thus, this signal can be thought of as a quasi-sinusoidal and persistent. On the other hand (and with the same caveat of optimal matching), the GW signal from annihilating vector boson clouds lasts significantly shorter than the scalar one, and thus can be thought of more as a "transient" CW, lasting for durations for $\mathcal{O}$(hours-days), i.e. much longer than mergers of black holes routinely detected now by LIGO, Virgo and KAGRA, but much shorter than scalar boson cloud annihilation signals. Furthermore, vector signals emit much more GW power per unit time than scalar ones, but for scalar signals, analysis methods are able to integrate over the entire data collection period of LIGO, Virgo and KAGRA to improve the signal-to-noise ratio. If, in the vector case, the size of the BH does not match the Compton wavelength of the boson, the signals could resemble CWs.

B. Transition signal

In the scalar boson case, just as electrons jump between energy levels in atoms, so too can bosons transition between different energy states, so long as these states are populated. Significant transition signals will only be possible if the $l = 4$ energy state can be populated, and would start occurring between the $5g$ and $6g$ levels. The transition signal can last for durations much longer than the typical observing time of GW interferometers, and would have a frequency of [212]:

$$f_{\rm gw} \sim 15\ {\rm Hz}\left(\frac{m_b}{10^{-11}\ {\rm eV}/c^2}\right) \tag{106}$$

and a frequency drift over time that relates to the duration of the signal T and the axion decay constant f_a [212]:

$$\frac{df}{dt} \simeq 10^{-11} \frac{\mathrm{Hz}}{\mathrm{s}} \left(\frac{f_{\mathrm{gw}}}{90\,\mathrm{Hz}}\right)\left(\frac{M_{\mathrm{BH}}}{10 M_\odot}\right)\left(\frac{10^{17}\mathrm{GeV}}{f_a}\right)^2 \left(\frac{5\mathrm{yr}}{T_{\mathrm{obs}}}\right)^2 \tag{107}$$

Unfortunately, the expected event rate of transitions in ground-based detectors is not expected to exceed one even in ~ 3.5 years of observing time in advanced LIGO (Fig. 5 in [212]). But, if self-interactions occur, transitions could happen and be detectable [229].

In the vector boson case, transitions could also occur, and the overtone modes could actually grow faster than the fundamental modes at small angular numbers and for fine-structure constants and BH spin values [233]. The higher overtones could saturate much quicker than lower ones, implying that transitions to lower states could occur, thus allowing BHs to become unstable to increasing energies at lower modes. Different energy states of the boson cloud could thus be populated at the same time, enriching the kind of physics searchable via transitions.

C. Bosenova signal

If the self-interactions between bosons become stronger than the gravitational binding energy of the cloud, the cloud starts to deform and can no longer be described analogously to the Hydrogen atom [219, 229, 234, 235]. Instead, it can collapse and explode in what is known as a "bosenova". This phenomenon would occur if the potential energy of the cloud is approximately equal to the self-interaction energy. Bosenovas have been observed on earth in condensed matter laboratories, in which repulsive forces were switched to attractive ones in a material that formed a Bose-Einstein condensate via a tuneable external magnetic field [236]. There are a lot of uncertainties around whether the bosenova would occur, and it seems that including self-interactions in the cloud limits bosenovas to a corner of the allowed parameter BH-boson mass parameter space [228].

In particular, in the axion case, originally proposed in [237], bosenovas would likely *not* occur. While early papers assumed that the boson cloud reached large enough amplitudes to produce GW emission [223–225], subsequent studies in the non-relativistic [228] and relativistic [238] regimes confirmed that dissipative nonlinear effects would prevent large-enough cloud amplitudes from occurring to cause a bosenova. In the vector case, bosenovas could actually occur if strings are formed the Higgs-Abelian mode [220, 239, 240].

Though GWs from boson clouds described above may seem independent, they could in principle be happening at the same time. In particular, if ultralight scalar or vector bosons have some self-interactions, the GW signal will change. If these clouds are composed of string axions (as opposed to the QCD axion), a non-linear self-interaction may cause a bosenova if, during superradiance, the value of the scalar field approaches the axion decay constant f_a, which, for string axions, could be below the grand unification theory (GUT) scale [215, 223–225]. This bosenova would halt the superradiance process, as about 5% of the boson cloud mass would fall back into the BH, but superradiance would immediately start again until the next bosenova is triggered. Such periodic bosenovas could sustain superradiance for much longer durations than those in the conventional scenario, permitting annihilating clouds even around extremely old BHs. Furthermore, we note that boson annilation could alter the GW of an inspiraling binary, potentially visible in space-based GW detectors [241], in a similar way that dynamical friction does.

In more general models of axions than in the axiverse, self-interactions could suppress annihilation signals as they get stronger, and transitions could occur for moderate interaction strengths. In particular, GW power sourced by annihilation would be reduced due to the smaller cloud size that can be sustained because of self-interactions, while scalar radiation, a new energy loss mechanism, consumes a portion of the energy that would source GW emission. But, multiple levels could be populated with self-interactions, allowing transitions to occur more than in the non-self-interaction scenarios [228].

D. Clouds in binary black hole systems

We know that BHs form binaries, and if ultralight dark matter exists in the form of ultralight bosons, it should imprint some signature in the GWs arising from inspiraling binary black holes [209]. The GW signal will be modified due to tidal disruptions induced by the companion, and the multiple moments of the cloud [209, 242, 243]. These kinds of signals could be visible in future space-based detectors, since the deviations primarily occur in the early inspiral stages of the system, i.e. at frequencies much lower than currently accessible by ground-based GW interferometers. In both cases, observations of the inspiral of binary systems could indicate the presence of boson clouds around one or both of the objects. Additionally, once the binary reaches a certain stage of its evolution, the impact of both the spin-induced quadrupole moment and tidal forces will lessen, since the clouds will become disrupted by their companions. If we can observe variations in both the spin-induced quadrupole moment, parameterized as κ, and the tidal deformability, parameterized as Λ, over the course of the lifetime of the binary, it would indicate the presence of a (disrupted) boson cloud [209]. More recently, it has been show that the boson cloud could be "ionized" as the orbital separation approaches the size of the cloud. Self-interactions could also play a role in the evolution of a binary, in which two types of clouds can actually coexist around the rotating BH through mode coupling [226, 227, 244]. We will now describe different ways in which boson clouds could affect

GWs from binary black hole systems.

1. Spin-induced quadrupole moment

The spin-induced quadrupole moment is often parameterized in terms of a dimensionless quantity $\kappa = \frac{Q}{J^2/M_{\rm BH}}$, which has been normalized by the object's angular moment J and mass BH. This parameter enters into the waveform at the second post-Newtonian order. Thus, the spin-induced quadrupole moment, regardless of its source, has a significant impact on the GW signal from compact objects inspiraling towards one another.

Ref. [245] showed that κ can be used as a distinguishing parameter for different kinds of objects, and also a test of the no-hair theorem: as an example, $\kappa = 1$ for BHs [246], while $\kappa \sim [1.4, 8]$ for neutron stars depending on the equation-of-state [247, 248]. In the case of boson cloud systems, κ will take on vastly different values, of $\mathcal{O}(1000)$, depending on the boson cloud and BH masses, and the extent to which the Kerr metric is altered in the presence of a cloud with enough mass compared to the BH.

2. Tidal disruptions

Because the boson cloud is much less compact than the BH, we expect that tidal disruptions from the companion could occur when the two objects in the binary black hole are close enough to each other [222]. To characterize the effects of tides in a binary system, the tidal deformability parameter Λ is used, which depends on the mass and radius of the compact objects. For BHs, this quantity is 0, while for neutron stars, it can take on values of $\mathcal{O}(100-1000)$ [249]. For boson clouds, $\Lambda \sim 10^7$, which is a remarkable departure from that expected from conventional astrophysical binaries [242]. In [250], the authors considered the impact that superradiance would have on hierarchical BH mergers, and showed that the reduction of spin in BHs implies smaller recoil velocities of binary black hole mergers. Smaller recoil velocities imply that remnants could remain inside clusters, leading to higher chances of hierarchical formation and merger of binary black holes. Such disruptive effects of bosons on not just individual BHs but also on the BH population, imply that boson clouds, if they exist, would significantly impact the formation and evolution histories of BHs.

3. Binary-induced transitions

Over the course of the inspiral, the presence of the boson cloud will induce transitions between different energy levels of the boson clouds that would be visible in space-based GW detectors if (1) the orbital frequency matches the hyperfine splitting between two energy levels (hyperfine resonance), and (2) the growing mode mixes with decaying modes (Bohr resonance). Both kinds of transitions would also be smoking-gun signatures of the presence of boson clouds around rotating BHs in a binary [209]. More recently, by considering the slow evolution of the orbital frequency through resonances of the boson cloud system, that is, when the orbital frequency matches the energy spacing between adjacent levels, it can be shown that Landau-Zener transitions occur and significantly affect the inspiral GW signal [243].

4. Ionization

Another transition arises when the binary system separation becomes comparable to the size of the cloud: an "ionization" of the boson cloud occurs as the cloud becomes unbounded from its host BH [251–253]. The energy from the binary sources this effect, and is significantly larger than that emitted via GWs; thus, the inspiral of the binary becomes driven by the boson cloud, instead of simply perturbed by it. Ionization will also tend to circularize the binary if it formed through dynamical capture, while leaving any orbital inclinations unaffected [254]. It has been recently found, however, that as the resonances in the boson cloud evolve during the orbit, the boson cloud is unperturbed and ordinarily visible in LISA if the cloud and binary are counter rotating; otherwise, the cloud is destroyed because of the resonances, but a distinct mark is left on the binary. That is, the binary is forced to co-rotate with the boson cloud, and its eccentricity is driven to a particular value, which allows the possibilty of doing statistics with detected binary black hole systems in LISA to probe the boson cloud hypothesis [255].

VI. GW CONSTRAINTS ON BOSON CLOUDS

The extensive theoretical background on boson clouds around rotating BHs, coupled with the potential for them to be DM, have motivated GW probes of boson cloud/BH systems. Different GW interferometers probe vastly different mass regimes of ultralight dark matter boson clouds. While ground-based detectors are sensitive to annihilation signals from bosons of masses between $\sim 10^{-14} - 10^{-12}$ eV [212], space-based detectors can probe a few orders of magnitude lower than that, $\sim 10^{-20} - 10^{-16}$ eV [209], and HFGW detectors could see systems with masses around $\sim 10^{-9}$ eV [198]. At the moment, only ground-based GW interferometers exist, and so we focus on methods and search results from the most recent LIGO, Virgo and KAGRA observing runs.

A. Constraints from the spins of detected binary black holes

We note that constraints on boson clouds can be inferred from the spin measurements of binary black hole systems [212, 216, 221, 256–258]. Recently, a Bayesian method has been developed by combining the information from each system [259], assuming a distribution for the initial BH spins and requiring that the BHs have had enough time to undergo superradiance before merging. Such a study has been applied to the second GW transient catalog (GWTC-2) [260], and has resulted in essentially a joint posterior on the scalar boson mass and the spin distribution of BHs at their formation [261]. The latter is required because BHs born with high spins that have been spun down by superradiance is partially degenerate with BHs simply born with low spins in a universe without superradiance. The study presented in [261] tentatively rules out scalar bosons in the mass range $[1.3, 2.7] \times 10^{-13}$ eV.

B. Search methods

While the aforementioned constraints from measured BH spins can disfavor particular masses or even confirm the presence of an ultralight boson, they rely on assumptions about the spin distribution at formation, on whether the boson clouds have time to form (which could be impacted by eccentricity at formation [262, 263]), and are a function of the (strongest) BH mergers that we see with GWs. To that end, different methods to actually search for long-lived GWs from isolated BHs (or those present in a known x-ray binary system) have been developed and used in real searches in LIGO, Virgo and KAGRA data. Detecting GW emission from an isolated BH would provide smoking-gun evidence of the existence of an ultralight bosonic field around BHs.

1. Excess power

One method to search for boson clouds around rotating BHs lightly models the boson cloud signal as monochromatic within the entire observation time that could come from anywhere in the sky, hence inducing a Doppler modulation. This method creates time-frequency maps and corrects each of them for different sky positions, leaving behind a monochromatic signal [264]. It employs different coherence times $T_{\rm FFT}$ for the analysis in order to be robust against possible theoretical uncertainties in the GW signal model. Shorter $T_{\rm FFT}$, while less sensitive than longer ones, provide larger frequency bins that allow the signal frequency to wander more, and thus are more sensitive to deviations from the monochromatic signal model.

In Fig. 15, we show the core stage of this method, which involves creating the time-frequency peakmap from raw time-domain strain data, correcting for the Doppler modulation from a particular sky location, and then integrating over time to collect all peaks at a given frequency to highlight the presence of a signal. Note that while we show the color to indicate the ratio of signal to noise power, the method does *not* actually use it: it only requires that a given point in the time-frequency plane is above a given threshold. When moving from Fig. 15(b) to Fig. 15(c), all time-frequency points above this threshold are given a weight of "1", and the ones are summed over time in order to create this histogram.

2. Viterbi

Another method that is more robust against stochastic frequency variations relies on Hidden Markov Models (HMMs) to find arbitrary tracks in the time-frequency plane. The main idea is to model a time-frequency GW signal probabilistically as a Markov chain of transitions between "hidden" (unobservable) frequency states and use a detection statistic to relate "observed" frequency states with the hidden ones [265]. In the framework for this method, the probability to jump to a new state at a given time only depends upon the previous hidden state. In total, there would be $N_Q^{N_T+1}$ possible paths through the hidden states, where N_Q is the total number of hidden states and N_T is the total number of times at which we have observed frequency states.The Viterbi algorithm provides a recursive, computationally efficient way of maximizing the probability that the hidden set of states is responsible for the observed sequence of states.

In Fig. 16, taken from [210], we show the optimal path found by the Viterbi method for injected boson cloud signals in white noise that has an associated random walk of the frequency, which is meant to simulate unknown theoretical features of the signal. We can see that in both cases, with less and more variability of the signal, the Viterbi algorithm can find the appropriate track of the signal.

Recently, the Viterbi algorithm has also been adapted to search for GWs from annihilating vector boson clouds, which have timescales significantly shorter than in the scalar case [218, 219], and for which numerical waveforms must be used to gauge sensitivity [217, 233].

3. Cross-correlation and other methods

We have already discussed in Section III A 1 cross correlating detector data to search for ultralight dark matter that could interact directly with GW interferometers; however, it is important to note that such a method could also be used to search for boson clouds around rotating BHs, both deterministically and for a stochastic GW background composed of the superposition. Furthermore, virtually *any* method in the CW community could be tuned to look for such boson cloud systems because such methods already analyze almost monochromatic sig-

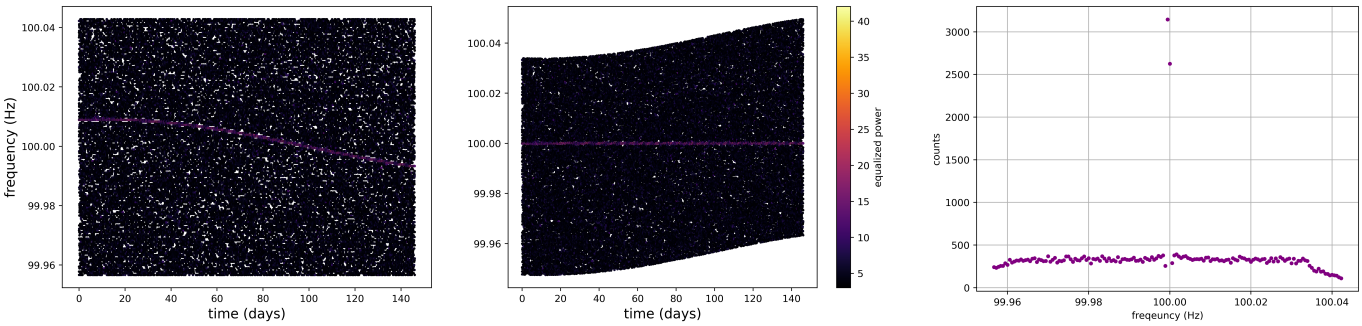

(a) (b) (c)

FIG. 15: This plot shows how the method described in Section VI B 1 works for a simulated GW signal from an annihilating scalar boson cloud system. (a) The Doppler-modulated time-frequency peakmap of the GW signal coming from a particular position in the sky (b) The time-frequency peakmap after the Doppler correction, which has made the signal monochromatic. (c) The projected time-frequency map is shown here, which corresponds to an integral over time in each frequency bin. Note that each time-frequency point is labeled simply as "one" if it is above a threshold, and is zero otherwise. This histogram thus is a count of the number of times at which the equalized power exceeded a given threshold.

nals focusing on spin-downs but could also extend their parameter spaces to include spin-ups.

C. Recent search results for scalar boson clouds

We can choose different BHs to point at depending on whether we are looking for scalar or vector clouds, or annihilation or transition signals. Current GW interferometer and algorithm sensitivities indicate that annihilation signals from scalar boson clouds could be observed for galactic and relatively young black holes [231]. Or, particular, known black hole systems, such as Cyg-X1, could be targeted for such clouds as well [266]. Finally, the stochastic GW background, composed of the superposition of signals from all of the annihilating boson cloud systems in the universe, can be probed as well through cross-correlation analyses. We go through each of these scenarios in the following subsections.

1. *All-sky search constraints*

The excess power method described in Section VI B 1 has been used to analyze LIGO O3 data to search for the presence of annihilating scalar boson clouds around isolated BHs within our galaxy [231]. This search was very computationally expensive, since each sky position had to be analyzed individually. A separate search towards the galactic center was also performed, targeting both spinning down neutron stars and spinning up boson cloud systems [267] No evidence for scalar boson cloud systems were found in either case, and thus upper limits were placed on the presence of boson clouds with different ages, spins, and distances away from earth in two different ways [214, 231, 268]:

1. Exclude the existence of BH/boson cloud pairs certain distances away from us with particular spins and ages.

2. Assume mass and spin distributions for BHs in the universe, draw different BHs from these distributions, and determine the maximum distance reach that could be attained for different boson cloud masses.

The first way is agnostic towards whether such BHs exist in the galaxy, while the second one contains some (uncertain) astrophysics regarding the properties of astrophysical BHs, but allows for some physical intuition into the reach of such searches.

Constraints from the first way are shown in Fig. 17 for two different distances (1 kpc and 15 kpc), for BHs with spin of 0.9 and for a few ages of the BH/boson cloud system. The search on LIGO O3 data can thus exclude the existence of BH/boson cloud systems that have these particular combinations of parameters at certain distances away from us.

Constraints from the second way are shown in Fig. 18, in which a Kroupa BH mass distribution $f(m) \propto M_{\rm BH}^{-2.3}$ [269] between $[5,\ 50]M_\odot$ and $[5,\ 100]M_\odot$ is assumed, as well as a uniform initial BH spin distribution between [0.2,0.9]. For fixed BH age, the maximum distance reach as a function of boson mass indicates that at least 5% of GWs from BH/boson cloud systems would have been detected by the search, i.e. their strain amplitudes are larger than the minimum detectable amplitudes at a given confidence level (the upper limits) of the search. As expected, on average when $50M_\odot$ is the maximum BH mass considered, the distance that can be reached

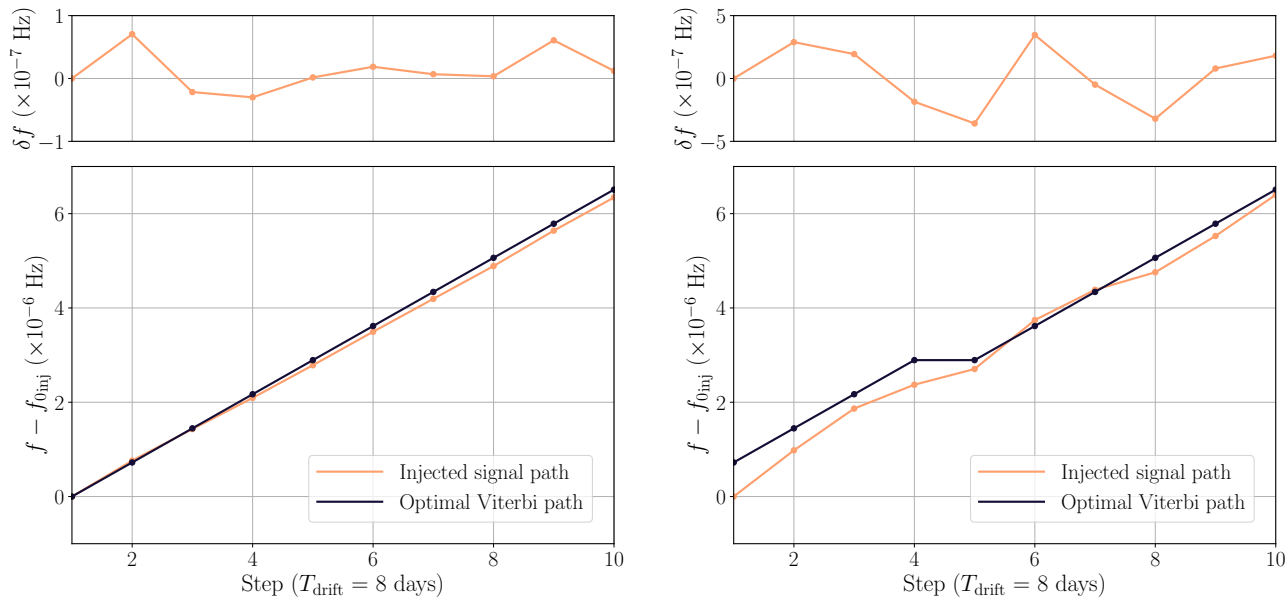

(a)Less variability

(b)More variability

FIG. 16: Taken from [210]. This figure illustrates how the Viterbi HMM algorithm described in Section VI B 2 works to identify tracks in the time-frequency plane. In particular, these plots shows two examples of injected and recovered boson cloud signals with random walk frequency variations $|\delta f| \leq 0.1\Delta f$ (weak variation) and (b) $|\delta f| \leq 0.5\Delta f$ (strong variation). The top panels show the injected random walk frequency evolutions, which cannot be seen by eye in the time-frequency tracks. The Viterbi optimal path results in a good match to the injected signal path. $f_0(t)$ (light curves) and optimal Viterbi paths (dark curves) for the injected signals with (a) weaker random walk $|\delta f| \leq 0.1\Delta f$ and (b) stronger random walk $|\delta f| \leq 0.5\Delta f$. Each step in time on the x-axis is 8 days. Injection parameters are in Table II of [210] and the signal strain is $h_0 = 5 \times 10^{-26}$.

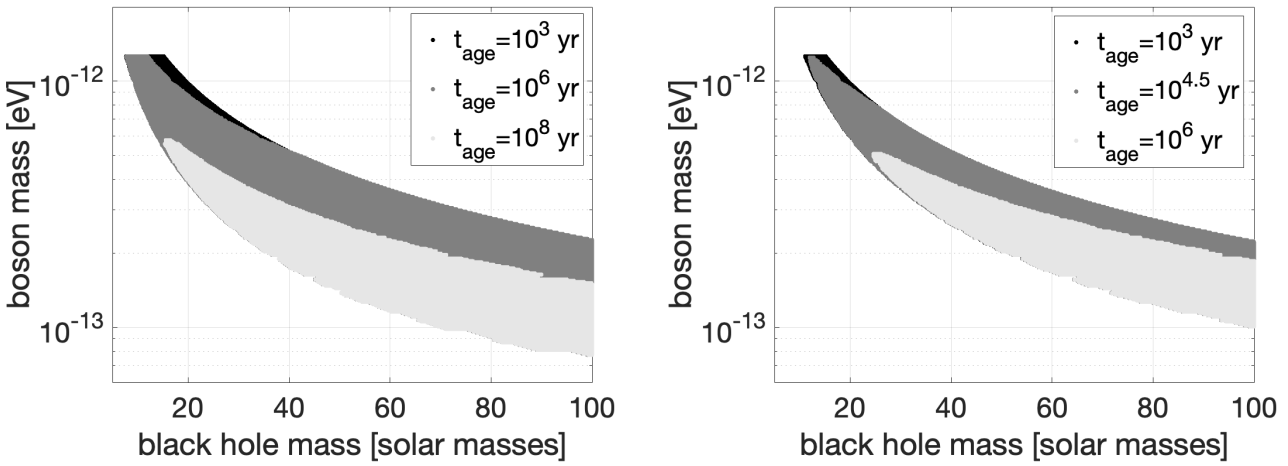

FIG. 17: Taken from [231]. Using upper limits from the O3 LIGO search for GWs from annihilating boson cloud systems, exclusion region of particular boson mass /BH mass pairs are derived assuming different ages and distances (left: 1kpc; right: 15 kpc) for BHs with initial spins of $\chi_i = 0.9$. This is the most model-agnostic way to probe boson clouds around rotating BHs using upper limits obtained from an all-sky search for CWs from isolated BHs.

is also smaller, since the GW amplitudes scales strongly with the BH mass.

We note that the search constraints present in, for example, [87, 270, 271], could also be cast in terms of all-sky or directed search constraints on scalar or vector boson clouds, but with particular caveats that would have be worked out depending on the actual search parameter space.

2. Cygnus X-1 constraints

Cygnus x-1 is an x-ray binary that is close by, has a large spin, ~ 0.9, and has relatively well-measured orbital parameters, which make it a reasonable BH to target. Since the sky position is known, searches based on the Viterbi algorithm discussed in Section VI B 2 can use much longer coherence times than those used in [231], thus permitting exquisite sensitivity towards almost monochromatic signal, while also being robust to theoretical uncertainties in boson cloud source.

In Section VI C 2, we show constraints on the strain amplitude arising from annihilating scalar boson cloud particles as a function of the boson mass. The search results $h_0^{95\%}$ are given as the black line, while the two curves represent the numerically obtained strain from this system, accounting for the spin, age, mass and distance of Cyg x-1 ($t_{\rm age} = 5 \times 10^6\,{\rm yr}$ and $1 \times 10^5\,{\rm yr}$). The region in which the search results are below the theoretical curves denote boson masses that are disfavored as having formed around Cyg x-1.

All constraints presented so far do not assume any boson self-interactions. If self interactions do occur, the available parameter space to probe would change. But, if the self-coupling is weak enough, standard searches can probe this scenario without modification. An example for the string axiverse scenario is shown in Fig. 20. The white region indicates the portion of the parameter space in which bosenovas do not occur, and thus cannot be constrained with the current search, while, again, portions of the colored parameter space above the black line indicate that those boson masses are disfavored. However, these constraints contain a number of caveats, namely: (1) the periodic bosenovas do not alter the time-frequency evolution of the GW signal, though they actually might induce oscillations every few minutes [224], and (2) the signal must last for longer than the age of the BH. Future studies are needed to determine to what extent CW searches can actually probe this particular model for string axion boson clouds around BHs, as well as to incorporate self-interactions more systematically into how CW searches are performed.

3. Constraints on luminous dark photons clouds

As alluded to in Section V, if the dark photon DM kinetically mixes with the ordinary photon and forms clouds around rotating BHs, it could produce both electromagnetic and GW signals, which, if detected, could enable a major multi-messenger discovery [138]. This additional coupling implies that soon after exponential growth of the boson cloud begins, electromagnetic fields act on charged particles in the vicinity of the BH, producing electron/positron pairs essentially out of vacuum, i.e. through the photon-assisted Schwinger mechanism [272–274]. At this point, a pair-production cascade ensues [275, 276], sourced by the electromagnetic fields, creating a plasma around the BH in a state of turbulent quasi-equilibrium. This plasma emits copious amounts of electromagnetic radiation, sourced by energy injections through dissipative processes in the cloud (e.g. at magnetic reconnection sites, Landau damping, turbulence), potentially even periodically. The luminosity of these sources depends on the strength of the kinetic mixing parameter, but could be at the level of supernovae or known pulsars, and it could be periodic [138]. If the dark photon has a mass around $\sim 10^{-12}$ eV, it will induce the formation of clouds around stellar-mass BHs, and give off radio emission that would look remarkably similar to, and potentially indistinguishable from, known pulsars in the ATNF catalog [277].

The lack of observation of CWs from pulsars, and the potential of dark-photon clouds to act as "pulsar mimickers", motivates a search for such clouds around targets in the ATNF catalog that could be mislabeled as pulsars. In Ref. [278], the authors consider this possibilty by analyzing a subset of, spinning up "pulsars" from the ATNF catalog that might actually be but stellar-mass BHs with a dark-photon luminous cloud around them. Using a variety of methods – one that assumes perfect phase coherence between the observed electromagnetic radiation and GW emission, one that allows small deviations in frequency around a narrow band of the observed frequency of each compact object, and one that is most robust against theoretical uncertainties in the signal but least sensitive to GW emission –, upper limits on the dark photon/ordinary photon kinetic mixing parameter are set as a function of boson mass for the 34 sources considered in this analysis, as shown in Fig. 21. To obtain this plot, particular BH populations and electromagnetic emissions are assumed to determine the number of events on the color bar, so the bounds are not necessarily robust against changes in these choices. For the BH population, the relevant distributions are over position in the galaxy (black holes follow the stellar distribution) and mass (Salpeter), spin (uniform) and age (uniform) of the BH systems.

Though particular population models are assumed, the constraints only require ten "events" to have been observable, which is conservative with respect to the potentially $\mathcal{O}(10^3)$ that would be expected at such coupling/mass combinations, as shown in the right-hand panel of Fig. 3 of [278]. Here, "events" just means the number of rotating BHs that could have given off a detectable signal, that is, with a GW amplitude larger than the upper limit

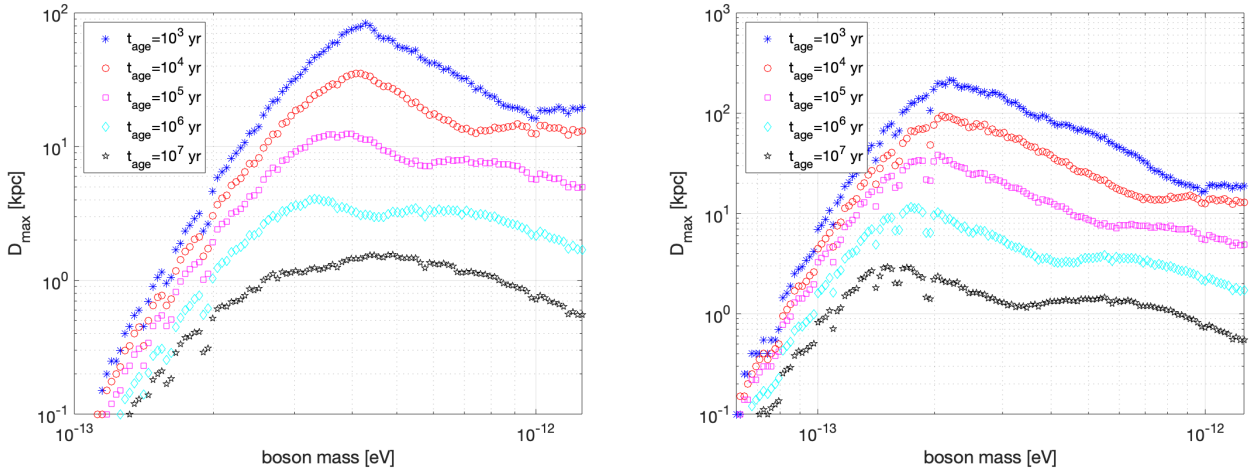

FIG. 18: Taken from [231]. Using upper limits from the O3 LIGO search for GWs from annihilating boson cloud systems, the maximum distance that the search in [231] could reach at which at least 5% of a simulated BH population would have been detectable, that is, with a strain greater than the value of the upper limit, is shown here. To create this plot, Ref. [231] assumed a uniform spin distribution between [0.2,0.9], different ages, and a Kroupa mass distribution with maximum mass $50M_\odot$ (left) and $100M_\odot$ (right).

strain amplitude, in an assumed population of 10^8 BHs in the galaxy. In the end, a dark photon mass range between, roughly $[10^{-13}, 10^{-12}]$ eV could not have a kinetic mixing more than roughly $[10^{-9}, 10^{-7}]$.

4. Stochastic gravitational-wave background constraints

The superposition of GWs arising from annihilating scalar boson clouds could form a stochastic GW background detectable by current-generation GW interferometers. In [283], the authors designed a model of the stochastic GW background arising from isolated BHs formed in two ways: (1) from remnants of core collapse supernovae, and (2) from remnants of mergers of BHs or neutron stars. The authors also performed search on LIGO O1 data using cross-correlation to look for evidence of a stochastic GW background [283]. No signal was found, and no range of boson masses could be robustly excluded unfortunately, except under optimistic assumptions about BH formation rates and spin distributions, which would disfavor the regime $2 \times 10^{-13} \leq m_b \leq 3.8 \times 10^{-13}$ eV at 95% confidence. The major reason for the inability to robustly exclude boson masses is that there exist degeneracies between the boson mass and BH astrophysical quantities, such as spins. The search was repeated in the second observing run as well, finding no evidence for any stochastic GW background of vector boson clouds around rotating BHs [284], in particular disfavoring vector boson cloud masses between $[0.8, 6] \times 10^{-13}$ eV at 95% confidence. Additionally, Ref. [285] has also disfavored bosons with masses between $[1.5, 17] \times 10^{-13}$ eV depending upon what is assumed for the uniform spin distribution, with wider constraints present when higher-spinning BHs dominate the priors. Furthermore, the stochastic GW background from tensor bosons around rotating BHs has been computed and searched for in [286], and has disfavored boson masses between $[10^{-13.4}, 10{-}11.7]$ eV depending on the range of uniform spin distributions assumed [286].

D. Prospects for GW probes of boson clouds

At the moment, despite the vast theoretical playground of ultralight dark matter boson clouds, only a few searches have actually been performed for GWs due to boson-boson annihilations. This is primarily due to the fact that the rich physics present in boson cloud binary black hole systems, and from transitions in isolated ones, can only be probed in space-based GW detectors, which are expected to be operational in the 2030s. Moreover, scalar boson clouds are by far easier to work with theoretically than vector or tensors, which has restricted the search parameter space primarily to what can be probed by CW searches. However, as the theoretical calculations of vector boson cloud waveforms improve [217, 233], new methods are being developed to search for annihilating vector boson clouds as well [218, 219]. Additionally, there are also significant astrophysical uncertainties, namely: what are the distributions of BH spins, masses, distances and ages in the galaxy and beyond. Such known unknowns limit potential constraints to be quite model agnostic (not so astrophysically informative) or too tied to uncertain BH population models. These conundrums are not yet resolved, and probably will not be until we start detecting significantly more BHs than we currently do.

The chosen targets of GW searches should also be eval-

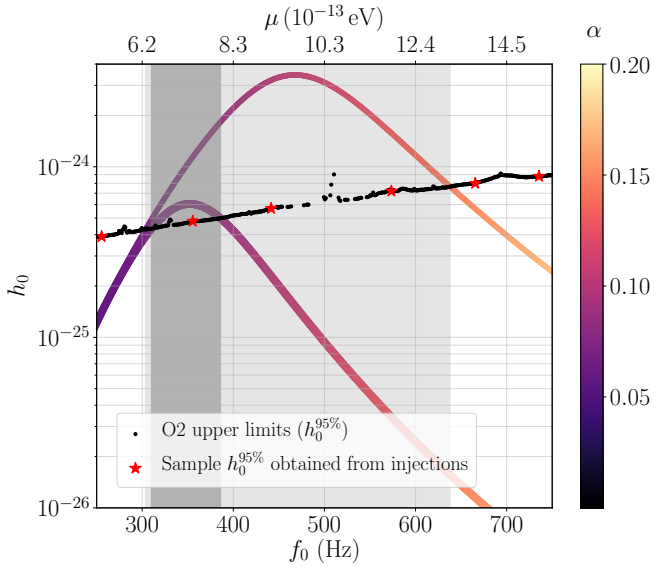

FIG. 19: Taken from [266], a search using O2 LIGO data for annihilating boson cloud systems around Cyg X-1. (a) Upper limits at 95% confidence on the strain amplitude of annihilating scalar boson clouds coming from the BH in Cyg X-1. The black curve indicates the upper limits from the search on O2 data, with the red stars denoting upper limits derived in frequency bands with injections. The two different curves correspond to different choices for the (unknown) age of the system (lower curve: 10^6 years; upper curve: 5×10^6 years. The GW fine structure constant is colored, and the gray region denotes boson masses disfavored under the two different age assumptions. $M = 14.8 M_\odot$, $\chi_i = 0.99$, and $d = 1.86\,\mathrm{kpc}$ for the two curves.

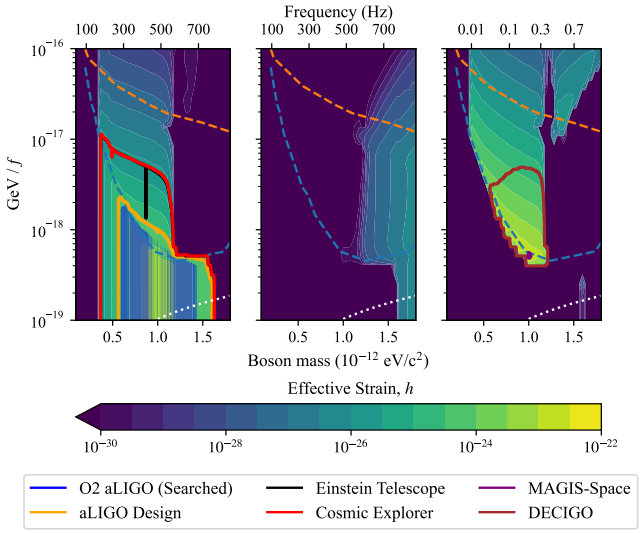

FIG. 20: Taken from [229]. Constraints on the string axiverse scenario (in blue from O2), in particular the axion decay constant. The regions are divided into three regimes: (1) strong-interactions (above the orange dashed-line), (2) intermediate interactions (between the dashed-blue and dashed orange lines) and no self-interactions (below the dashed-blue line). The three plots correspond to annihilations in different energy levels (left and middle) and to transitions between these energy levels (right). Sensitivities of future detectors are also shown on this plot for comparison.

uated. While having accurate measurements of the mass, spin and age of remnants of binary black hole mergers would allow us to ignore astrophysical population models [113], these systems are currently too far to be detected if the clouds are composed of scalar bosons [210], though could be seen up to Gpc now if they are composed of vector bosons [218]. On the flipside, GWs from vector boson clouds suffer from even more theoretical uncertainties than scalars [233], and so the robustness of search results by targeting remnants would have to be evaluated.

All-sky searches for such boson cloud systems could also be enhanced. At the moment, especially in light of boson self-interactions that could alter the GW signal significantly. Potentially, new methods to track quickly-evolving waveforms, such as those in [218, 219], could be useful in a variety of contexts. Furthermore, the all-sky search specifically for scalar boson cloud systems did not consider any grid in spin-up, which limited it to be sensitive to boson clouds whose frequency drift did not exceed one frequency bin during the entire observation time. Such modifications to searches, coupled with additional theoretical understanding of the GW signal itself, could increase chances of detecting a signal.

It is also difficult to say with certainty that a particular boson mass is "ruled out", since the constraints are either population agonistic or depend on some assumptions about BH formation, spin or mass distributions. Ref. [287] attempts to unify the way in which constraints are set in a Bayesian way by handling the subtleties associated with population assumptions. The authors encourage that posteriors on mass and spin be made publicly available in order to incorporate into their future analyses. Furthermore, Ref. [288] shows that bosons could be transferred from a growing level to a depleting one if both BHs in a binary system have clouds around them, which may affect the GW waveform and hence would need to be considered in future GW searches.

VII. GW PROBES OF SOLITON DM

If DM has a mass of $\sim 10^{-24} - 10^{-22}$ eV [289], its Compton wavelength will be comparable to the size of the galactic halo, which actually limits the minimum mass of DM [290]. In this mass regime DM could form so-called "solitons", self-gravitating structures prevented from collapsing from degeneracy pressure, at the centers of galaxies [291]. To probe this kind of DM, these masses imply

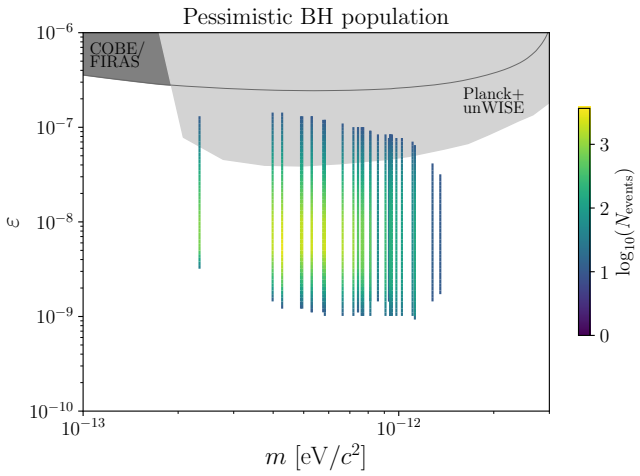

FIG. 21: Taken from [278]. For each of the targets of the search in [278], the upper limit at 95% confidence on the kinetic mixing parameter ϵ is plotted as a function of the boson mass for which at least 10 systems would have been detected with signal amplitudes above the strain upper limits. The color corresponds to the number of events that should have been detected, assuming a "pessimistic" population model for BHs. The bounds reproduced from other experiments can be found in [279], specifically from the conversion of CMB photons into dark photons, which would cause distortions in the black body spectrum measured by COBE/FIRAS [280, 281] (dark gray), and from measurements by Planck and unWISE galaxies of cross correlations between temperature anisotropies in the CMB [282] (light gray).

that the oscillation frequencies will be of $\mathcal{O}$(nHz), making pulsar timing arrays the ideal probe [292]. In essence, DM would affect the waveform arising from the superposition of inspiraling supermassive BHs, causing the BHs to experience dynamical friction, thus weaking the signal strain in the nHz regime. But this is not the only way to detect this mass regime of ultralight dark matter: as we will show, LISA and next-generation ground-based GW interferometers could also be used. To probe this kind of DM with conventional GW sources, low-frequency information needs to be contained in relatively higher-frequency carrier GW. The GW frequency becomes modified during its propagation between its source and the earth as it passes through the DM soliton, i.e. it is "heterodyned", or gravitationally redshifted, analogously to the Sachs-Wolfe effect that induces fluctuations in the cosmic microwave background [293].

A. Impact on phase evolution of binary systems

Space-based GW detectors will observe the quasi-infinite inspiral of galactic white dwarf binaries and extreme-mass ratio inspirals of ordinary compact objects with much heavier BHs [294, 295]. The long-durations of such signals permit the possibility of detecting a low-frequency modulation when passing through the ultralight dark matter soliton [296–298]. Ref [297] has found that the impact of dynamical friction on the phase evolution of GW signals from white dwarf binaries exceeds that of the low-frequency DM-induced modulation for masses above 10^{-21} eV, essentially providing two orders of magnitude of mass that could be probed in the future. Unfortunately, even at these masses, the density of DM would have to be at least 10^4 times higher than in the solar system in order to observe any changes to the phase evolution GW. This is broadly consistent with previous work by [296], which assumed an enhancement of the DM density by eight orders of magnitude relative to that on earth, and showed that DM with a mass of $\sim 10^{-23}$ eV could be detected with LISA. Furthermore, Ref. [298] assumes a representative population of white dwarf binaries, a fraction of which are detectable in LISA, and concludes that DM masses above $\sim 10^{-23}$ eV will remain unconstrained by LISA. However, the mass regime $\sim [2\times10^{-22}, 3\times10^{-21}]$ eV could be constrained if DM has stronger, quadratic couplings to ordinary matter.

B. Imprint of DM on CW signal from neutron star

In addition to modulating the millihertz frequency of GWs from binaries in space-based GW detectors, soliton ultralight dark matter could induce changes in the CWs arising from deformed neutron stars, thus allowing the possibility of detecting this effect in future ground-based detectors [298]. These GWs are sourced from the rotational power of the neutron stars, thus spinning down the neutron stars as GWs are emitted [299]. In ET and Cosmic Explorer, we expect to detect $\mathcal{O}(100)$ or more neutron stars spinning down due to the emission of CWs [300], all of which could be modulated by ultralight dark matter solitons.

Using CWs from deformed neutron stars, the soliton mass regime $\sim [2\times10^{-22}, 3\times10^{-21}]$ eV becomes accessible in ET for both linear and quadratic couplings, and improves with the number of neutron stars that are detected. The constraints will even outperform existing pulsar timing array ones, since the signal-to-noise ratio scales linearly with the carrier GW frequency. This is shown in Fig. 22 for LISA, ET and Cosmic Explorer, and demonstrates the powerful probe that CWs from neutron stars will be of this particular DM model.

C. Pulsar-timing constraints on soliton ultralight dark matter

The evidence for a GW background from NANOGrav results can be used to put constraints on soliton DM [292]. Essentially, ultralight dark matter would induce

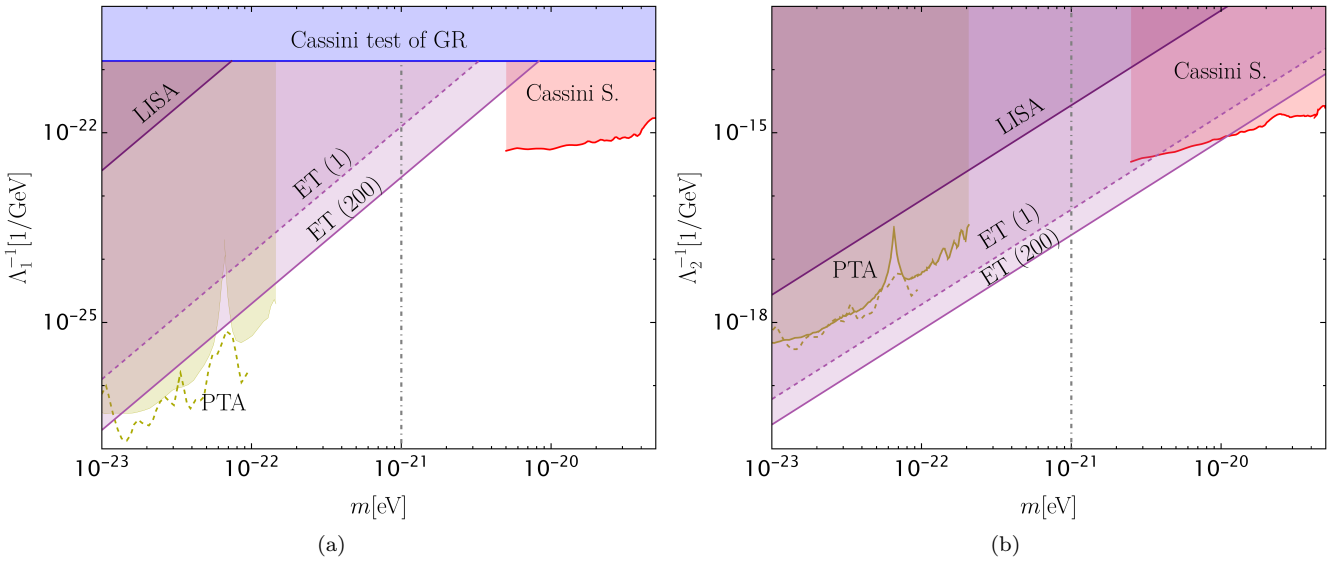

FIG. 22: Taken from [298]. Projected constraints on the linear (left) and quartic coupling parameters (right) for both LISA and ET from low-frequency soliton DM modulating ("heterodyning") high-frequency carrier GW signals via changes to the moment of inertia of neutron stars, which alters CWs from deformed neutron stars (ET), or to changes in the inspiral frequency of inspiraling binary black holes (LISA). The curves for ET assume one or 200 detections of CWs from isolated neutron stars. The LISA curve is determined by the impact of soliton DM on GW frequencies from binary systems.$\bar{\rho}_0 = 10^3 M_\odot \mathrm{pc}^{-3}$. The olive regions are excluded by the pulsar timing array analysis in [191], while blue and red are constrained away via Cassini tests of general relativity (violet) and on a stochastic GW background (red).

dynamical friction in the inspiral of supermassive BHs, speeding up the orbit, which suppresses the GW strain at nanohertz frequencies. The supermassive BHs are too massive to be prevented from merging, as would be the case for lighter BHs [289, 301]. Using the most accurate limit at 3.92 nHz on the GW strain from supermassive BHs in the right-hand panel of Fig. 1 of [128], Ref. [292] derives constraints on the soltion DM mass-to-BH mass ratio parameter space, as shown in Fig. 23. These bounds are derived by using Eq. 17 of [292], which depends on how much energy is lost via GW emission normally and in the presence of the ultralight dark matter soliton, and on the differential density populations of supermassive BHs. The latter can be written analytically in terms of the the galaxy-stellar mass functions, galaxy merger rates and galaxy pair fractions [302]. It is then a matter of integrating Eq. 17 in [292] over these different distributions (which may depend on decently uncertain astrophysics) for different choices of ultralight dark matter mass to derive the constraint on mass ratio of soliton DM to supermassive BH mass, and determine if the integrated strain exceeds the error bar on the GW strain obtained by NANOGrav.

VIII. GW PROBES OF WIMP DARK MATTER

A. Transmuted black holes in binaries

Non-annihilating WIMPs that interact with nucleons could lose energy through single or multiple scatterings off of celestial objects [303, 304], eventually becoming gravitationally bound to them over time. After repeated interactions between the WIMPs and ordinary nucleons, the WIMPs become thermalized, forming a compact core with a higher density than that of the celestial object. If the density of the particles is sufficient, gravitational collapse (in the case of bosons) or Chandrasekhar collapse (in the case of fermions) of the WIMP core will occur, thus resulting in a newborn BH. After formation, the celestial object could accrete surrounding DM on a given timescale, and if enough matter becomes bound to the object quickly enough compared to the Hawking evaporation timescale, the entire object could collapse into what is known as a transmuted black hole (TBH) [93, 305–308]. If the sum of the time to accrete new particles and the time to collapse is smaller than the age of the universe, TBHs should form.

TBHs forming from inspiraling neutron stars were first considered in [305]. Since DM would induce neutron stars to transmute into BHs, from the observational perspective, there is no difference between electromagnetically silent neutron stars and low-mass BHs. Therefore, the

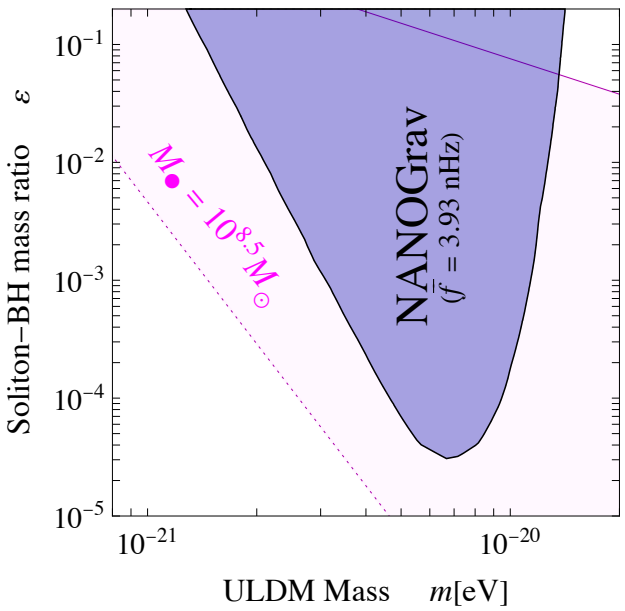

FIG. 23: Taken from [292]. Upper limits from NANOGrav data on the DM mass and solition-BH mass ratio parameter space, obtained by noting that inspiraling supermassive BH background for which NANOGrav found evidence would be modulated by the dynamical friction induced by soliton DM. Magenta lines show the scaling relations derived through DM-only numerical simulations (solid), and ones in which supermassive BHs dominate scaling relations suggested by DM-only numerical simulations and SMBH dominance (dashed).

non-detection of low-mass binary black holes by LIGO, Virgo and KAGRA can be used to constrain weak interaction cross-sections, since the progenitor neutron stars provide an extremely strong gravitational field to accrete and retain DM particles [307, 308]. In Fig. 24(a), we show the excluded bosonic DM mass/cross-section parameter space based on null search results from the LIGO, Virgo and KAGRA collaborations for sub-solar mass compact objects [309]. Additionally, a projection for this constraint is shown for 50x more exposure time, which may be possible for the future GW network[6].While analyses of LIGO, Virgo and KAGRA data cannot yet constrain new parameter space for this model of DM, future searches should be able to surpass the pulsar constraint, which comes from the fact that the nearby Gyr-old pulsar PSR 0437−4715 has not actually collapsed into a BH in its lifetime.

In contrast, stars, being less compact than neutron stars, could sustain DM cores with stronger interaction cross-sections, because of the weaker gravitational field around the star [93]. In Fig. 24(b), we show the potential excluded parameter space for null detection of TBHs arising from slowly inspiraling non-compact binaries that could be visible in space-based GW detectors. These binaries would be inspiraling for durations of order of the age of the universe, and thus exhibit CW signals in the millihertz regime. The results are parameterized in terms of α, which denotes the fraction of stellar-mass binaries that form close enough to exist within the millihertz band. Essentially, α parametrizes our ignorance about how closely the population of sun-like stars form to each other.

Comparing Fig. 24(a) and Fig. 24(b), we note the vastly different interaction cross-section ranges from these two complementary GW probes of WIMP DM. For both low-mass BHs and sun-like stars, fermionic DM has also been constrained in similar ways as bosonic DM has, see [93, 307] for more details.

B. GWs to probe the GeV excess

Annihilating WIMP DM and a collection of unresolved millisecond pulsars are two leading explanations for the unexpected excess of GeV gamma rays observed by the Fermi-LAT experiment coming from the Galactic Center [52, 310]. At first, the GeV excess appeared spherically symmetric and well-fit by annihilating DM models [311–315]. But still, an astrophysical explanation of millisecond pulsars cannot yet be ruled out [316–320].

GWs can be used to weigh in on this debate. If the millisecond pulsars are deformed, they will emit CWs as they rotate, and this radiation could be detectable by the LIGO, Virgo and KAGRA if the degree of deformation, called the ellipticity (defined in terms of the principle moments of inertia as $\epsilon = \frac{I_{xx}-I_{yy}}{I_{zz}}$), is large enough [321].

First, a stochastic GW background of GWs from millisecond pulsars in the Galactic Center was considered, and projected constraints on the average ellipticity of this population were obtained as a function of the total number of millisecond pulsars in the Galactic Center [95]. The authors showed that $\mathcal{O}(10^4)$ millisecond pulsars with ellipticities of $\sim 10^{-7}$ could be detectable by current detectors and be consistent with the diffuse electromagnetic radiation coming from the Galactic Center, as shown in Fig. 25(a). However, they did not go so far as to link GW observations with Fermi-LAT ones.

On the other hand, Ref. [96] considered different models for how the deformations on the millisecond pulsars were sustained, either through the internal magnetic field [322–324] or simply as a fraction of the total electromagnetic radiation from the star. It is then assumed that the unresolved population of millisecond pulsars follows the same spin and ellipticity distribution of the known pulsars [277], and, from that, the probability of observing a CW in the search be computed, given upper limits on ellipticities from searches for isolated neutron stars

[6] https://observing.docs.ligo.org/plan/

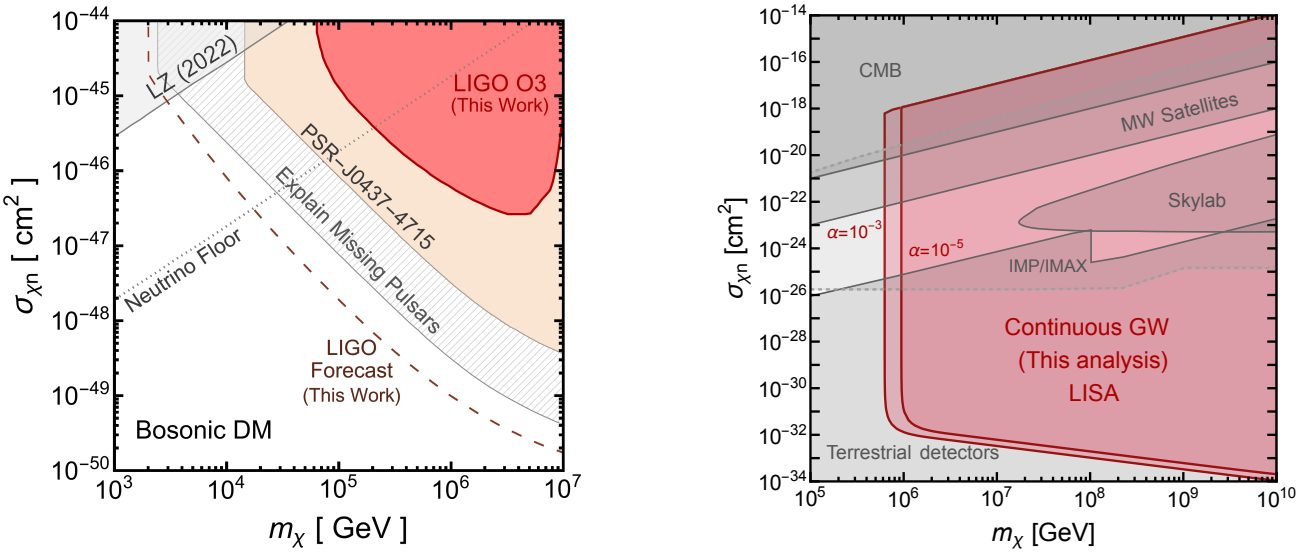

(a) (b)

FIG. 24: Taken from [307] and [93]. (a) Constraints and (b) projected constraints in the DM mass (m_χ) and interaction cross-section ($\sigma_{\chi n}$) plane for Bosonic DM particles that could induce the collapse of celestial objects to BHs. (a): The red shaded region shows the current limit from O3 data [309], while the brown dashed line represents the forecast with a 50× sensitivity increase. (See Fig.1 of Ref. [307]). (b): The red shaded region indicates the exclusion based on the proposed sensitivity of LISA, with α being the fraction of sun-like star binaries that form close enough to be in the LISA band. For $\alpha < 10^{-5}$, this method excludes no parameter space. Further details on other existing constraints and other scenarios (Fermionic DM, Bose Einstein Condensate formation) are in the original references [93, 307].

or those in binary systems [86, 96]. Once this quantity is computed, we can determine the number of millisecond pulsars in the Galactic Center by fitting parameters of luminosity functions to match the observed Galactic Center GeV excess [325–327]. By multiplying the predicted number of millisecond pulsars with the probability of detecting them, we can rule out luminosity function parameters that would have led to at least one millisecond pulsar being detected via GWs.

Fig. 25(b) shows the parameter space of a simplistic luminosity function, and the constraints that can be obtained through null results from CW searches, assuming particular ellipticity and frequency distributions for the millisecond pulsars. We can see that GW searches probe a complementary portion of the parameter space to what Fermi-LAT does: if there are more millisecond pulsars that are dimmer electromagnetically, this means more rotational power may go into GWs, and more of them are necessary to explain the GeV excess. Thus, GW searches would have more millisecond pulsars to find, and not seeing at least one of them rules out particular luminosity function parameters. Likewise, Fermi performs better when less millisecond pulsars are more luminous.

Most recently, Ref. [97] simulated a population of $\sim$ 40000 millisecond pulsars in the Galactic Center that could explain the Galactic Center GeV excess, and found that the GW signal could lie between [200,1400] Hz, and would have strain amplitudes of $\mathcal{O}(10^{-30} - 10^{-28})$ based on the population parameters chosen (e.g. moment of inertia around $\sim 10^{38}$ kg$\cdot$ m^2, ellipticities mostly smaller than 10^{-9}, and Boxy vs. spherical spatial distributions of the millisecond pulsars). It is argued that such signals are too weak to be detected by current and future GW observatories; however, this conclusion depends heavily on the assumed ellipticity distribution and the number of millisecond pulsars chosen to be in the population. If millisecond pulsars appear in larger numbers than assumed here, they would each be dimmer, since the luminosity of the GeV excess is fixed. In fact, the constraints from [96] are strongest for larger populations than assumed in [97]. Additionally, the ellipticity distribution employed in [97] only reaches a maximum of $\sim 2 \times 10^{-9}$, which is consistent with the minimum ellipticity of neutron stars as predicted by [328], but may be too conservative. Upper limits on ellipticities at the Galactic Center from CW searches have not yet constrained ellipticities to be less than $\sim 10^{-6}$ [86, 87, 267], which is consistent with the maximum ellipticity employed in [96] up to 10^{-6}.

If GWs can rule out more and more of the luminosity function parameter space to explain the GeV excess, then this will give significant weight to the annihilating WIMP DM hypothesis.

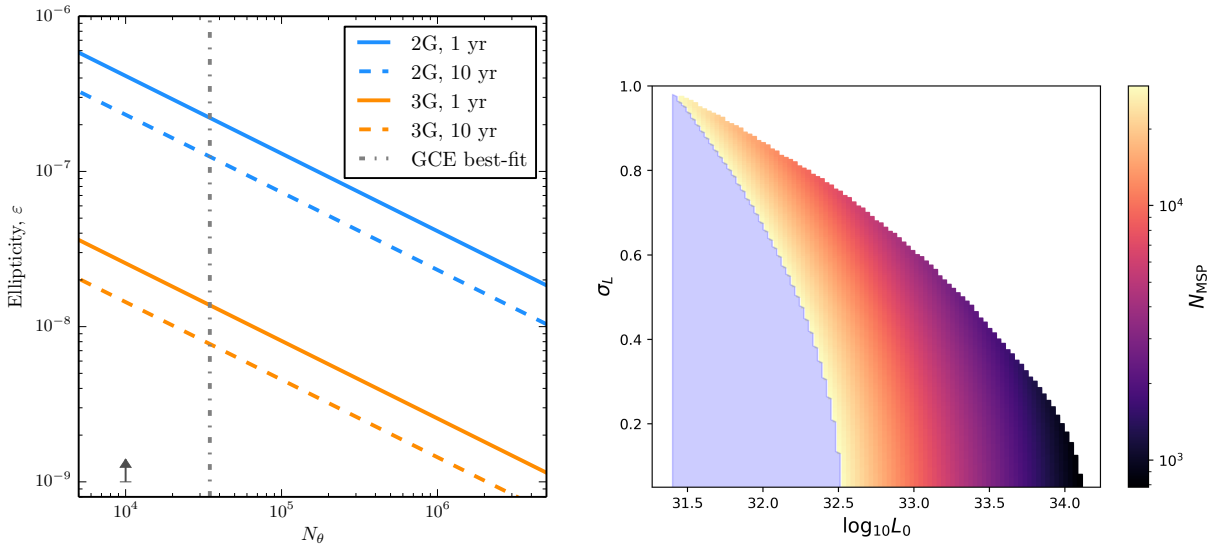

(a) (b)

FIG. 25: Taken from [95] and [96]. Projected constraints from current generation (2G) and next-generation (3G) ground-based GW interferometers on the average ellipticity of a population of millisecond pulsars arising from a null result from a search for the stochastic GW background of signals from deformed, rotating neutron stars coming from anywhere in the sky, for different observation times [95]. The vertical line denotes the total number of millisecond pulsars in the bulge required by fits of the Galactic Center excess based on [329]. (b) Constraints from an all-sky search on O3 LIGO/Virgo data for isolated neutron stars in [86] on a portion of the luminosity function space, in light blue, that would have given rise to a high enough number of millisecond pulsars such that at least one would have been detected by the search [96] L_0 and σ_L are the parameters of a log-normal luminosity function distribution. To obtain this plot, the Galactic Center is assumed to be 8 kpc away, the moment of inertia of the unknown millisecond pulsars is assumed to be $I_{zz} = 10^{38}\text{kg}\cdot\text{m}^2$, a frequency distribution following pulsars in the ATNF catalog is used, and an ellipticity distriution derived from the ATNF catalog assuming that 1% of rotational energy goes into GWs is used.

IX. GW PROBES OF DM SPIKES

A. Background

It was first recognized in [330] that BHs in the DM halo accreting DM adiabatically (slowly) could allow a high-density region of DM to form, called a "spike", which could enhance the DM annihilation rate inside the spike. Subsequent studies showed that if such spikes formed around supermassive BHs at the center of galaxies, they would would likely have been disrupted during host galaxy mergers [331], if the BH formed off-center [332], or if DM particles scattered off of nearby stars [333, 334]. Though, recently, upper bounds on the DM densities for supermassive BHs have been forecasted with LISA [335]. However, intermediate-mass BHs (IMBHs) could sustain such spikes [336], since their spikes may not have been torn apart through mergers over cosmic time. Furthermore, recently it has been shown that astrophysical BHs and PBHs could also host DM spikes [337–342].

The density of the DM spike is characterized by the following equation [343]:

$$\rho(r) = \rho_{\rm sp}\left(\frac{r_{\rm sp}}{r}\right)^{\alpha} \quad (r_{\rm min} \leq r \leq r_{\rm sp}), \tag{108}$$

where $\rho_{\rm sp}$ is a normalization constant for the DM density of the spike, $r_{\rm min}$ is the minimum separation between the two objects, often taken to the radius at the innermost stable circular orbit, and $r_{\rm sp}$ is the spike radius. Here, $\rho_{\rm sp} = 379\ M_\odot/\text{pc}^3$ and $r_{\rm sp} = 0.33\text{pc}$ if the mass of the IMBH is $M_{\rm BH} = 10^3 M_\odot$ and the DM spike has a mass of $M_{\rm halo} = 10^6 M_\odot$. The power-law index α denotes how the concentration of DM particles falls off as one moves away from the host BH. Astrophysically speaking, measurements of α would allow us to glean important information regarding whether the host BH evolved from the DM halo and/or experienced mergers in the past [343].

B. Dephasing due to dynamical friction of IMRI systems

Ref. [343] first showed that the phase evolution of an intermediate-mass ratio inspiral (a binary composed

to a $\mathcal{O}(1000)M_\odot$ and an $\mathcal{O}(1)M_\odot$ object) would be significantly modified at milli-hertz frequencies due to the presence of a DM spike around the intermediate-mass BH. This occurs because the less massive object sweeps through the DM spike as it orbits around the more massive one, losing energy via dynamical friction (in addition to via GWs) and speeding up the orbit. Such effects will primarily be relevant in space-based GW detectors [344, 345], since IMBHs inspiral and merge at much lower frequencies than stellar-mass BHs [346].

In the future, if matched filtering analyses are performed that do not account for the DM spike, dephasing with respect to the vacuum templates may occur. In Fig. 26, we show how the signal-to-noise ratio degrades as a function of the observation time, the initial frequency $f_{\rm ini}$, and the power-law index α of the DM spike). As described in [343], dynamical friction affects the early stages of the inspiral, and as the system progresses toward, the DM spike becomes disrupted, reducing its impact on the GW signal. That is why in Fig. 26, lower initial frequencies start to lose signal-to-noise ratio at smaller values of α. Furthermore, it is clear that above $\alpha \simeq 2$, templates that include dynamical friction will be required to successfully recover IMRI signals in space-based GW interferometers. This conclusion was significantly expanded in [347], in which the authors demonstrated how accurately the power-law index α could be measured from a detection of an IMRI signal in LISA. This accuracy is quantified in terms of the power-law index itself and the masses of the two objects that are inspiraling. If the IMRI system consists of smaller primary and secondary masses, and a larger power-law index, the power-law index can be measured more accurately. This is because higher values of α induce a larger phase difference, and smaller masses in the IMBH system ensures that it spends more cycles in the LISA band before merging.

PBHs could also host DM spikes, and must do so, since, at most masses, the fraction of DM that they could compose is less than one [26, 348]. Thus, Ref. [349] showed that ET and Cosmic Explorer could probe the existence DM spikes around binary PBH systems, where the primary has a mass of $[1, 10]M_\odot$ and the system has a mass ratio of 10^{-3}. However, just as in astrophysical binary black hole systems, these exotic mergers would be missed if the DM spike is not taken into account in matched-filtering searches in ET and Cosmic Explorer. Multi-band observation of inspirals/mergers constraining DM spikes are also possible with future deci-hertz and ground-based GW interferometers, which would enhance the constraints on the power-law index and spike-density factors by orders of magnitude relative to individual constraints from each of these detectors [350, 351].

Recently, it has also been shown that these dephasing effects are unique enough to allow distinguishing between three BH environments: accretion disks, DM spikes, and ultralight boson clouds [352], as well as distinguishing between environmental effects and modified theories of gravity [353]. However, Ref. [354] argues that practically speaking, dephasing could result from a variety of (also unmodelled) sources, and would be difficult (computationally and algorithmically speaking) to track with long-duration templates in matched filtering. Though, Ref. [355] has indicated this could be possible within a parameterized post-Einsteinian framework. They thus propose more model-agnostic ways (i.e. periodic forces) that may influence the evolution of the binary and leave characteristic signatures on the GW signal. Such problems with matched filter, could, however, be handled by the use of alternative, non-matched filtering CW methods meant to handle intermediate-duration signals, e.g. [210, 356–365], and those discussed already in this review.

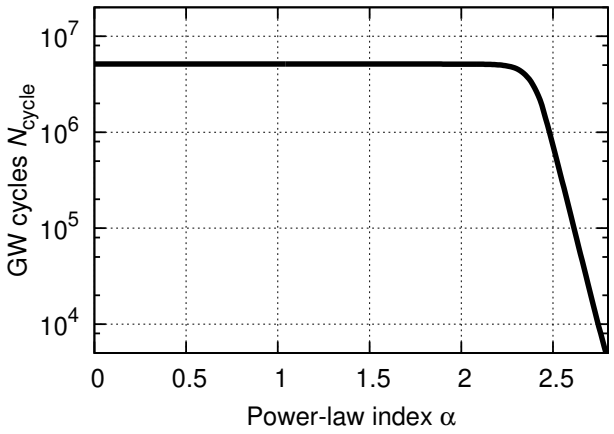

FIG. 26: Taken from [347]. The number of cycles $N_{\rm cycle}$ spent in the GW band $f \in [f_{\rm min}, f_{\rm max}]$ for a primary BH with mass $M_{\rm BH} = 1000M_\odot$ and a companion of $1M_\odot$. At large α, the DM solition causes large dephasing between the injected waveform and the one that would be used to recover the signal. Thus, the number of cycles that are captured in-band drops significantly.

Perhaps more surprising, it has been proposed that equal-mass systems could sustain DM spikes even in the last ten orbits of binary black hole merger [366]. Initially, it had been shown through N-body simulations that heavy, particle-like DM environments would be disrupted well before equal-mass binary black hole systems merge [334, 367]. But, for wave-like, ultralight dark matter, though there have been many works that have modeled the motion of binary black holes through DM environments,[368–376] or with boson clouds [209, 217, 233, 243, 252–254, 377–391], the point during the inspiral at which the environment becomes disrupted is not clear, motivating further studies into this [392]. Ref. [366] found that amount of dephasing that exists within the last ten orbits of a binary black hole merger depends strongly the scalar DM mass and the masses of the BHs:

$$\mu \approx 5 \times 10^{-17} \left(M/10^6 M_\odot\right)^{-1} \text{ eV}, \qquad (109)$$

which gives the optimal DM mass to cause the most de-

phasing during the last ten orbits of the binary, and determines the DM density as

$$\rho_0 \approx 10^{20} \left(\frac{M}{10^6 M_\odot}\right)^{-2} \frac{M_\odot}{\mathrm{pc}^3} \,. \tag{110}$$

which gives the DM density necessary to induce dephasing. Though the DM density presented here is larger than the average, it results from a measured dephasing over a short period of time. If the effect of the DM spike on the binary black hole system turns on at larger separations, as may be expected from previous works [349, 352], then smaller densities could cause significant dephasing over the lifetime of the binary.

C. Upper limits on BH environments

Because vacuum phase-evolution waveforms confirmed the detection of many binary black hole mergers by LIGO, Virgo and KAGRA, any deviations due to environmental effects, such as a DM spike, must be small enough to be inconsequential to the detected GW signals. Knowing this, Ref. [393] modeled dynamical friction and other possible environmental effects as additional (negative) PN corrections to the waveform, and placed upper limits on the density of environment around BHs by requiring the induced dephasing to be small with respect to the phase evolution of the binary black hole systems in vacuum. While the results were used to eliminate dynamical fragmentation [394] as a possible binary formation channel, they are generic enough to apply to *any* BH environment. Unfortunately, the upper limits on environments affected by dynamical friction, which would be relevant for the DM spike scenario, are, at best, about seven orders of magnitude larger than the maximum density of the spike (10^{-6} g/cm^3 [330, 395]. The upper limits are shown to drastically improve in DECIGO because the dynamical friction (and other environments) affect the early inspiral of the binary black hole system much more than at the time of merger. These findings are consistent with those found in N-Body simulations about how the dynamics of the DM spike affect the inspiral, and the detectability of these effects by LISA [396].

X. GW PROBES OF ATOMIC DM

A. Background

It is possible that the dark sector is actually much more complicated than a single new particle with a single coupling to gravity or the standard model. In fact, a atomic DM models exist [397, 398] composed of dark protons and dark electrons that interact via a massless dark photon with a particular coupling. With such a model, DM can form bounds states analogous to the Hydrogen atom, and dissipate energy via Bremsstrahlung, recombination, and collisional excitation processes [399]. If DM collects in small-enough regions of space, it will collapse and form "dark BHs [400].

Such dark BHs could form in binary systems, as astrophysical BHs do; thus, LIGO, Virgo and KAGRA observations of binary black hole mergers can constrain the existence of these objects, just as they do for PBHs [92, 309, 401].

B. Constraints from observations of binary black holes

Ref. [400] first considered the prospects of detecting dark BH mergers with advanced LIGO and ET, finding that these interferometers could set stringent constraints on the fraction of DM that dark BHs could compose. If the BH merger of GW190425 [402] is interpreted as the merger of two dark BHs, the Chandrasekhar mass [403] can be constrained to be below $1.4M_\odot$ at $> 99.9\%$, bounding the lower-most value mass of the dark proton as 0.95 GeV and the spacing of energy levels in a dark atom to be near 10^{-3} eV [92].

These constraints on the mass of the dark proton and the Chandrasekhar limit of the mass of dark BHs are derived using [92, 400, 403]:

$$M_{\rm DC} \simeq 1.4 M_\odot \left(\frac{m_p}{m_\chi}\right)^2 . \tag{111}$$

The range of the dark proton mass m_χ can be obtained by setting $M_{\rm DC} = M_{\rm min}$ for the values of $M_{\rm min}$ for which the fraction of DM that dark BHs could compose is less than 1:

$$\sqrt{\frac{1.4M_\odot}{M_{\rm min}^{\rm max}}} m_p < m_\chi < \sqrt{\frac{1.4M_\odot}{M_{\rm max}^{\rm max}}} m_p \tag{112}$$

$M_{\rm min}$ is the minimum mass in a distribution of dark BHs masses that is assumed, as described below.

Further constraints on the fraction of DM composed of dark BHs are presented in three cases, assuming that (1) none of the detected BHs by LIGO, Virgo and KAGRA are dark, (2) half are dark, and (3) GW190425 and/or GW190814 [404] are dark. Here, we limit ourselves to case (1) and case (3). These constraints rely on an assumed mass distribution of dark BHs based on Population III star formation works [405], which is chosen to be $P(m) \propto m^{-b}$ along with a mass range of $[M_{\rm min}, rM_{\rm min}]$. The parameters $b = [-1, 2], r = [2, 100]$ determine the mass distribution of dark BHs. With these assumptions, we show in Fig. 27 the constraint on the fraction of DM that dark BHs could compose as a function of the average mass of the BHs considered, in relation to other limits, in case (1) and in case (3). Assuming all BHs are not dark, the constraint beats existing ones by several orders of magnitude; assuming that GW190425 and GW190814

are dark BHs, a region in this parameter space is carved out of possible average mass/ DM fractions. More observations of dark BHs would be needed to further narrow this region. However, it must be emphasized that while GW190425 and GW190814 being dark BHs are not yet excluded by other experiments, this work does not provide a way of distinguishing astrophysical BHs from dark BHs.

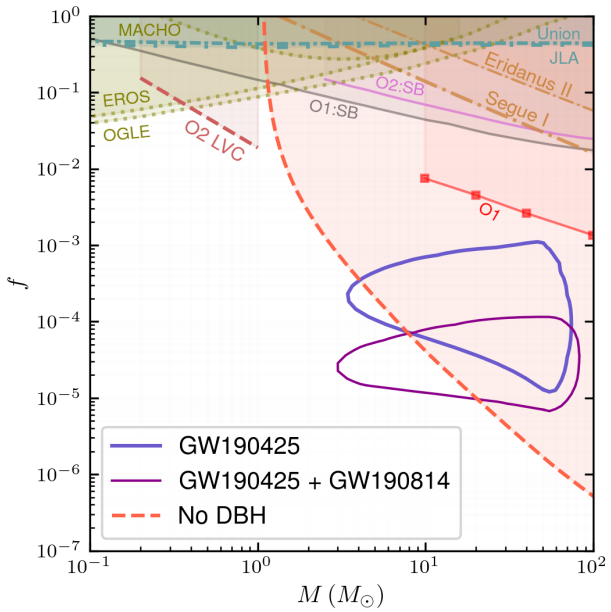

FIG. 27: Taken from [92]. Constraints on the fraction of DM that dark BHs could compose relative to other experimental upper limits using all binary black holes detected in the first three observing runs of LIGO, Virgo and KAGRA. These plots assume an atomic model of DM that forms dark BHs. Even in the absence of any dark BHs, the constraints obtained in [92] significantly outperform existing microlensing experiments [18, 406, 407] and those from dynamics of dwarf galaxies [408, 409]. Additional constraints arise from PBH searches [410–414]. SB stands for stochastic background and refers to analyses of the first and second observing runs of LIGO, Virgo and KAGRA data for stochastic GW backgrounds from generic systems.

C. Constraints from sub-solar mass binary black hole searches

The lack of smoking-gun evidence for dark BHs in current LIGO, Virgo and KAGRA observations motivates the need to consider sub-solar mass BHs, whose origins, if detected, cannot be explained by astrophysical means. Searches for GWs from sub-solar mass compact objects in binary systems have grown in popularity in recent years, covering mass ranges of roughly $[10^{-11}, 1]M_\odot$ [86, 309, 401, 415–419], and, traditionally, have put constraints on the fraction of DM that PBHs could compose. However, as discussed in [92], these searches do not assume a particular formation mechanism for these compact objects, and the binaries can thus be interpreted as arising from not only PBHs, but also dark BHs.

In the most recent analysis of LIGO, Virgo and KAGRA data from the second half of the third observing run, constraints on dark BHs with masses below $1M_\odot$ were placed, as shown in Fig. 28, using different matched filtering methods, again assuming a power-law dependence for the mass distribution of dark BHs and as a function of the minimum mass of this distribution. Nuisance parameters in the mass distribution are marginalized over. These limits do not go below $\sim 10^{-2}M_\odot$ because the maximum mass probed is between $[2, 1000]M_\odot$, and so the distribution tends to disfavor smaller masses. Moreover, the limits do not go above a solar mass because the search is only for sub-solar mass objects.

From this work [309], the mass of the dark proton has been constrained to be [0.66,8.8] GeV, which is actually broader than the constraint in [92] of [0.91,4.76] GeV since there are no assumed detections of dark BHs. Additionally, the energy spacing between dark atomic energy levels can also be constrained, assuming values for the mass of the dark fermions, the dark fine structure constant, and the Jeans mass, and using Eq. 1 of [92] and Eq. 4 of [400].

XI. CONCLUSIONS

There is no shortage of observable signatures that DM could leave on GW sources when the particle, mass and couplings of DM the standard model are varied. We do not assume to have covered every single DM model in this work, but we hope to have provided an overview for the interested reader that wishes to pursue more details about different ways that GWs can be used to probe the existence of particle DM.

In this work, we have explored (1) how ultralight dark matter could couple to GW interferometers, (2) how macroscopic DM could transit through the interferometers, (3) how boson cloud systems formed through a superradiance process around rotating BHs could emit GWs by annihilation, (4) how soliton DM could induce changes in GWs arising from binary systems and isolated neutron stars, (5) how WIMP DM could collect around celestial objects and induce them to collapse into BHs detectable via GW emission, (6) how environmental effects of DM spikes around BHs could affect GW signals in future detectors, and (7) how GW observations and non-observations can be used to probe atomic models of DM. Some of these types for DM have been extensively constrained through analysis of terrestrial GW detector data; others will require the advent of space-based and next-generation ground-based GW interferometers to obtain insight into these types of DM.

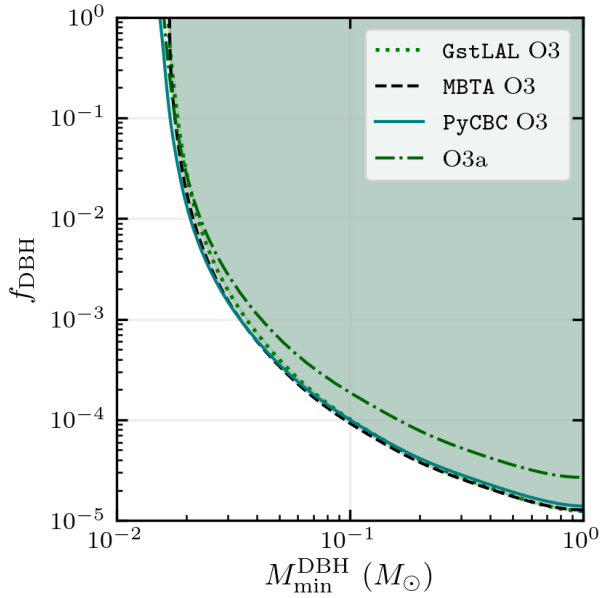

FIG. 28: Taken from [309]. Constraints on the fraction of DM that dark BHs could compose in the atomic DM scenario. A mass distribution for dark BHs is assumed with the shown minimum mass on the x-axis, and the constraints are shown for three different matched filtering algorithms: `GstLAL` (*dotted*), `MBTA` (*dashed*) and `PyCBC` (*solid*). Constraints from a previous search for sub-solar mass compact objects in the first half of the third observing run of LIGO, Virgo and KAGRA are also shown [401].

Despite the "WIMP miracle" announced decades ago, WIMPs have not yet been detected, and are only one of numerous possible ways that DM could exist in the Universe. The lack of detection of WIMPs over the years has opened up both the experimental and theoretical playgrounds for new probes of DM, one of which is through its impact on GW signals, or as a signal in interferometer data itself. Moreover, it has been assumed in this work, and almost all those cited, that DM is *the* way to solve the puzzling cosmological observations on a variety of scales. However, modified theories of gravity are real contenders to solve this problem as well, though their community is a lot smaller and not quite as popular as the DM one. These two communities – DM and modified gravity – act entirely independently, choosing to break, respectively, one of the two assumptions of "classical" physics: (1) the matter in the universe is mostly baryonic and luminous, and (2) general relativity and, in the limit of slow-moving objects, Newtonian theory, are correct [420]. It may be that these assumptions need to be broken simultaneously, or that these two distinct fields have more in common than it appears, as argued in [420].

We only briefly mentioned PBHs in this review, which have been reviewed extensively elsewhere [26, 33]. PBHs could also comprise a fraction of or the totality of DM, and recent observations of binary black holes by the LIGO, Virgo and KAGRA with low spins whose merging rates are consistent with PBHs have reignited interested in this hypothesis [31, 421, 422]. While analyses of PBHs typically receive criticism for using monochromatic mass functions to place constraints, all of the results presented here implicitly assume that DM is *only* composed of particles that are being constrained[7]. It could be that multiple forms of DM co-exist, e.g. in the atomic DM models, or that there is a whole dark sector.

Nevertheless, GWs provide a new window to probe the existence of DM in a variety of ways. Most of the actual analyses performed on GW data do not assume particular models for DM, and only constrain them later when one interprets null (or actual) results in terms of a DM model. GW searches are therefore powerful, relatively model-agnostic probes of DM that permit the detection of a variety of DM signatures.

ACKNOWLEDGMENTS

We thank William East, Alexandre Gottel, Dana Jones, Jun'ya Kume, Sachiko Kuroyanagi, Ling Sun, and Yue Zhao for reviewing this manuscript.

This material is based upon work supported by NSF's LIGO Laboratory which is a major facility fully funded by the National Science Foundation

This research has made use of data, software and/or web tools obtained from the Gravitational Wave Open Science Center (https://www.gw-openscience.org/), a service of LIGO Laboratory, the LIGO Scientific Collaboration and the Virgo Collaboration. LIGO Laboratory and Advanced LIGO are funded by the United States National Science Foundation (NSF) as well as the Science and Technology Facilities Council (STFC) of the United Kingdom, the Max-Planck-Society (MPS), and the State of Niedersachsen/Germany for support of the construction of Advanced LIGO and construction and operation of the GEO600 detector. Additional support for Advanced LIGO was provided by the Australian Research Council. Virgo is funded, through the European Gravitational Observatory (EGO), by the French Centre National de Recherche Scientifique (CNRS), the Italian Istituto Nazionale della Fisica Nucleare (INFN) and the Dutch Nikhef, with contributions by institutions from Belgium, Germany, Greece, Hungary, Ireland, Japan, Monaco, Poland, Portugal, Spain.

We would like to thank all of the essential workers who put their health at risk during the COVID-19 pandemic, without whom we would not have been able to complete this work.

[1] G. Bertone and D. Hooper, Rev. Mod. Phys. **90**, 045002 (2018), arXiv:1605.04909 [astro-ph.CO].
[2] K. C. Freeman, Astrophys. J. **160**, 811 (1970).
[3] D. Rogstad and G. Shostak, Astrophysical Journal, vol. 176, p. 315 **176**, 315 (1972).
[4] R. N. Whitehurst and M. S. Roberts, Astrophysical Journal, vol. 175, p. 347 **175**, 347 (1972).
[5] M. Roberts and A. Rots, Astronomy and Astrophysics, Vol. 26, p. 483-485 (1973) **26**, 483 (1973).
[6] P. J. E. Peebles, Astrophys. J. Lett. **263**, L1 (1982).
[7] S. Burles and D. Tytler, Astrophys. J. **507**, 732 (1998), arXiv:astro-ph/9712109.
[8] H. Pagels and J. R. Primack, Phys. Rev. Lett. **48**, 223 (1982).
[9] M. Davis, J. Huchra, D. W. Latham, and J. Tonry, Astrophysical Journal, Part 1, vol. 253, Feb. 15, 1982, p. 423-445. **253**, 423 (1982).
[10] G. R. Blumenthal, S. M. Faber, J. R. Primack, and M. J. Rees, Nature **311**, 517 (1984).
[11] M. Davis, G. Efstathiou, C. S. Frenk, and S. D. M. White, Astrophys. J. **292**, 371 (1985).
[12] J. F. Navarro, C. S. Frenk, and S. D. M. White, Astrophys. J. **462**, 563 (1996), arXiv:astro-ph/9508025.
[13] B. Paczynski, Astrophys. J. **304**, 1 (1986).
[14] C. Alcock *et al.* (Supernova Cosmology Project), Nature **365**, 621 (1993), arXiv:astro-ph/9309052.
[15] E. Aubourg *et al.*, Nature **365**, 623 (1993).
[16] C. Alcock *et al.* (MACHO), Astrophys. J. **542**, 281 (2000), arXiv:astro-ph/0001272.
[17] T. Lasserre (EROS), Astron. Astrophys. **355**, L39 (2000), arXiv:astro-ph/0002253.
[18] P. Tisserand *et al.* (EROS-2), Astron. Astrophys. **469**, 387 (2007), arXiv:astro-ph/0607207.
[19] R. D. Peccei and H. R. Quinn, Phys. Rev. Lett. **38**, 1440 (1977).
[20] R. D. Peccei and H. R. Quinn, Phys. Rev. D **16**, 1791 (1977).
[21] S. Weinberg, Phys. Rev. Lett. **40**, 223 (1978).
[22] P. Galison and A. Manohar, Phys. Lett. B **136**, 279 (1984).
[23] B. Holdom, Phys. Lett. B **166**, 196 (1986).
[24] A. Pierce, K. Riles, and Y. Zhao, Phys. Rev. Lett. **121**, 061102 (2018), arXiv:1801.10161 [hep-ph].
[25] A. Filippi and M. De Napoli, Rev. Phys. **5**, 100042 (2020), arXiv:2006.04640 [hep-ph].
[26] A. M. Green and B. J. Kavanagh, J. Phys. G **48**, 043001 (2021), arXiv:2007.10722 [astro-ph.CO].
[27] S. Hawking, Mon. Not. Roy. Astron. Soc. **152**, 75 (1971).
[28] B. Carr, K. Kohri, Y. Sendouda, and J. Yokoyama, Phys. Rev. D **81**, 104019 (2010), arXiv:0912.5297 [astro-ph.CO].
[29] S. Clesse and J. García-Bellido, Phys. Rev. **D92**, 023524 (2015), arXiv:1501.07565 [astro-ph.CO].
[30] B. Carr, F. Kuhnel, and M. Sandstad, Phys. Rev. D **94**, 083504 (2016), arXiv:1607.06077 [astro-ph.CO].
[31] S. Clesse and J. García-Bellido, Phys. Dark Universe **15**, 142 (2017).
[32] S. Clesse and J. Garcia-Bellido, Phys. Dark Univ. **38**, 101111 (2022), arXiv:2007.06481 [astro-ph.CO].
[33] A. L. Miller, (2024), arXiv:2404.11601 [gr-qc].
[34] A. Belenchia *et al.*, Phys. Rept. **951**, 1 (2022), arXiv:2108.01435 [quant-ph].
[35] G. Jungman, M. Kamionkowski, and K. Griest, Phys. Rept. **267**, 195 (1996), arXiv:hep-ph/9506380.
[36] J. Goodman, M. Ibe, A. Rajaraman, W. Shepherd, T. M. P. Tait, and H.-B. Yu, Phys. Rev. D **82**, 116010 (2010), arXiv:1008.1783 [hep-ph].
[37] D. S. Akerib *et al.* (CDMS), Phys. Rev. D **68**, 082002 (2003), arXiv:hep-ex/0306001.
[38] D. S. Akerib *et al.* (CDMS), Phys. Rev. Lett. **96**, 011302 (2006), arXiv:astro-ph/0509259.
[39] Z. Ahmed *et al.* (CDMS), Phys. Rev. Lett. **102**, 011301 (2009), arXiv:0802.3530 [astro-ph].
[40] R. Agnese *et al.* (SuperCDMS), Phys. Rev. D **99**, 062001 (2019), arXiv:1808.09098 [astro-ph.CO].
[41] J. Angle *et al.* (XENON), Phys. Rev. Lett. **100**, 021303 (2008), arXiv:0706.0039 [astro-ph].
[42] J. Angle *et al.* (XENON10), Phys. Rev. Lett. **107**, 051301 (2011), [Erratum: Phys.Rev.Lett. 110, 249901 (2013)], arXiv:1104.3088 [astro-ph.CO].
[43] E. Aprile *et al.* (XENON100), Astropart. Phys. **35**, 573 (2012), arXiv:1107.2155 [astro-ph.IM].
[44] E. Aprile *et al.* (XENON), Phys. Rev. D **94**, 092001 (2016), [Erratum: Phys.Rev.D 95, 059901 (2017)], arXiv:1605.06262 [astro-ph.CO].
[45] E. Aprile *et al.* (XENON), Eur. Phys. J. C **84**, 784 (2024), arXiv:2402.10446 [physics.ins-det].
[46] D. S. Akerib *et al.* (LUX), Nucl. Instrum. Meth. A **704**, 111 (2013), arXiv:1211.3788 [physics.ins-det].
[47] D. S. Akerib *et al.* (LUX), Phys. Rev. Lett. **116**, 161302 (2016), arXiv:1602.03489 [hep-ex].
[48] J. Aleksic *et al.* (MAGIC), Astron. Astrophys. **541**, A99 (2012), arXiv:1111.5544 [astro-ph.HE].
[49] J. Aleksić *et al.*, Astropart. Phys. **72**, 61 (2016), arXiv:1409.6073 [astro-ph.IM].
[50] J. Holder *et al.*, AIP Conf. Proc. **1085**, 657 (2009), arXiv:0810.0474 [astro-ph].
[51] F. Aharonian *et al.* (H.E.S.S.), Astron. Astrophys. **457**, 899 (2006), arXiv:astro-ph/0607333.
[52] D. Hooper and L. Goodenough, Phys. Lett. B **697**, 412 (2011), arXiv:1010.2752 [hep-ph].
[53] M. Aguilar *et al.* (AMS 01), Phys. Lett. B **646**, 145 (2007), arXiv:astro-ph/0703154.
[54] M. Aguilar *et al.* (AMS), Phys. Rev. Lett. **110**, 141102 (2013).
[55] L. Bergstrom, T. Bringmann, I. Cholis, D. Hooper, and C. Weniger, Phys. Rev. Lett. **111**, 171101 (2013), arXiv:1306.3983 [astro-ph.HE].
[56] A. A. Abdo *et al.* (Fermi-LAT), Phys. Rev. Lett. **102**, 181101 (2009), arXiv:0905.0025 [astro-ph.HE].
[57] M. Ackermann *et al.* (Fermi-LAT), Phys. Rev. Lett. **108**, 011103 (2012), arXiv:1109.0521 [astro-ph.HE].
[58] F. Petriello and K. M. Zurek, JHEP **09**, 047 (2008), arXiv:0806.3989 [hep-ph].
[59] Y. Su, B. R. Heckel, E. G. Adelberger, J. H. Gundlach, M. Harris, G. L. Smith, and H. E. Swanson, Phys. Rev.

[7] The exception to this statement is superradiance probes of BHs– these bosons need not be DM.

D **50**, 3614 (1994).
[60] S. Schlamminger, K. Y. Choi, T. A. Wagner, J. H. Gundlach, and E. G. Adelberger, Phys. Rev. Lett. **100**, 041101 (2008), arXiv:0712.0607 [gr-qc].
[61] P. Touboul, G. Metris, V. Lebat, and A. Robert, Class. Quant. Grav. **29**, 184010 (2012).
[62] J. Bergé, P. Brax, G. Métris, M. Pernot-Borràs, P. Touboul, and J.-P. Uzan, Phys. Rev. Lett. **120**, 141101 (2018), arXiv:1712.00483 [gr-qc].
[63] N. Du *et al.* (ADMX), Phys. Rev. Lett. **120**, 151301 (2018), arXiv:1804.05750 [hep-ex].
[64] J. Aasi, B. P. Abbott, R. Abbott, T. Abbott, M. R. Abernathy, K. Ackley, C. Adams, T. Adams, P. Addesso, and et al., CQGra **32**, 074001 (2015), arXiv:1411.4547 [gr-qc].
[65] F. Acernese, M. Agathos, K. Agatsuma, D. Aisa, N. Allemandou, A. Allocca, J. Amarni, P. Astone, G. Balestri, G. Ballardin, and et al., CQGra **32**, 024001 (2015), arXiv:1408.3978 [gr-qc].
[66] Y. Aso, Y. Michimura, K. Somiya, M. Ando, O. Miyakawa, T. Sekiguchi, D. Tatsumi, and H. Yamamoto (KAGRA), Phys. Rev. D **88**, 043007 (2013), arXiv:1306.6747 [gr-qc].
[67] M. Sieniawska and M. Bejger, Universe **5**, 217 (2019), arXiv:1909.12600 [astro-ph.HE].
[68] R. Tenorio, D. Keitel, and A. M. Sintes, Universe **7**, 474 (2021), arXiv:2111.12575 [gr-qc].
[69] K. Riles, Living Rev. Rel. **26**, 3 (2023), arXiv:2206.06447 [astro-ph.HE].
[70] O. J. Piccinni, Galaxies **10**, 72 (2022), arXiv:2202.01088 [gr-qc].
[71] A. L. Miller (LIGO Scientific Collaboration, Virgo, KAGRA), in *57th Rencontres de Moriond on Gravitation* (2023) arXiv:2305.15185 [gr-qc].
[72] K. Wette, Astropart. Phys. **153**, 102880 (2023), arXiv:2305.07106 [gr-qc].
[73] A. Akmal, V. R. Pandharipande, and D. G. Ravenhall, Phys. Rev. C **58**, 1804 (1998), arXiv:nucl-th/9804027.
[74] C. Cutler, Physical Review D **66**, 084025 (2002), gr-qc/0206051.
[75] A. Lyne, G. Hobbs, M. Kramer, I. Stairs, and B. Stappers, Science **329**, 408 (2010), arXiv:1006.5184 [astro-ph.GA].
[76] B. Krishnan, A. M. Sintes, M. A. Papa, B. F. Schutz, S. Frasca, and C. Palomba, Physical Review D **70**, 082001 (2004), arXiv:gr-qc/0407001 [gr-qc].
[77] S. Dhurandhar, B. Krishnan, H. Mukhopadhyay, and J. T. Whelan, Phys. Rev. D **77**, 082001 (2008), arXiv:0712.1578 [gr-qc].
[78] P. Astone, A. Colla, S. D'Antonio, S. Frasca, and C. Palomba, Physical Review D **90**, 042002 (2014).
[79] S. Suvorova, L. Sun, A. Melatos, W. Moran, and R. J. Evans, Physical Review D **D93**, 123009 (2016), arXiv:1606.02412 [astro-ph.IM].
[80] J. Bayley, G. Woan, and C. Messenger, Phys. Rev. D **100**, 023006 (2019), arXiv:1903.12614 [astro-ph.IM].
[81] R. Abbott *et al.* (LIGO Scientific, Virgo, KAGRA), Astrophys. J. **913**, L27 (2021), arXiv:2012.12926 [astro-ph.HE].
[82] R. Abbott *et al.* (LIGO Scientific Collaboration, VIRGO, KAGRA), Astrophys. J. **935**, 1 (2022), arXiv:2111.13106 [astro-ph.HE].
[83] A. Ashok, B. Beheshtipour, M. A. Papa, P. C. C. Freire, B. Steltner, B. Machenschalk, O. Behnke, B. Allen, and R. Prix, Astrophys. J. **923**, 85 (2021), arXiv:2107.09727 [astro-ph.HE].
[84] A. Ashok, P. B. Covas, R. Prix, and M. A. Papa, Phys. Rev. D **109**, 104002 (2024), arXiv:2401.17025 [gr-qc].
[85] A. G. Abac *et al.* (LIGO Scientific, VIRGO, KAGRA), (2025), arXiv:2501.01495 [astro-ph.HE].
[86] R. Abbott *et al.* (LIGO Scientific Collaboration, Virgo, KAGRA), Phys. Rev. D **106**, 102008 (2022), arXiv:2201.00697 [gr-qc].
[87] B. Steltner, M. A. Papa, H. B. Eggenstein, R. Prix, M. Bensch, B. Allen, and B. Machenschalk, Astrophys. J. **952**, 55 (2023), arXiv:2303.04109 [gr-qc].
[88] H.-K. Guo, K. Riles, F.-W. Yang, and Y. Zhao, Commun. Phys. **2**, 155 (2019), arXiv:1905.04316 [hep-ph].
[89] H. Grote and Y. Stadnik, Physical Review Research **1**, 033187 (2019).
[90] M. A. Ismail, C. S. Nugroho, and H. T.-K. Wong, Phys. Rev. D **107**, 082002 (2023), arXiv:2211.13384 [hep-ph].
[91] R. Brito, V. Cardoso, and P. Pani, Lect. Notes Phys. **906**, pp.1 (2015), arXiv:1501.06570 [gr-qc].
[92] D. Singh, M. Ryan, R. Magee, T. Akhter, S. Shandera, D. Jeong, and C. Hanna, Phys. Rev. D **104**, 044015 (2021), arXiv:2009.05209 [astro-ph.CO].
[93] S. Bhattacharya, A. L. Miller, and A. Ray, Phys. Rev. D **110**, 043006 (2024), arXiv:2403.13886 [hep-ph].
[94] A. Khmelnitsky and V. Rubakov, JCAP **02**, 019 (2014), arXiv:1309.5888 [astro-ph.CO].
[95] F. Calore, T. Regimbau, and P. D. Serpico, Phys. Rev. Lett. **122**, 081103 (2019), arXiv:1812.05094 [astro-ph.HE].
[96] A. L. Miller and Y. Zhao, Phys. Rev. Lett. **131**, 081401 (2023), arXiv:2301.10239 [astro-ph.HE].
[97] K. Bartel and S. Profumo, Phys. Rev. D **110**, 123036 (2024), arXiv:2409.12271 [astro-ph.HE].
[98] K. Kadota, J. H. Kim, P. Ko, and X.-Y. Yang, Phys. Rev. D **109**, 015022 (2024), arXiv:2306.10828 [hep-ph].
[99] J. H. Kim and X.-Y. Yang, (2024), arXiv:2407.14604 [astro-ph.CO].
[100] M. C. Smith, G. R. Ruchti, A. Helmi, R. F. Wyse, J. P. Fulbright, K. C. Freeman, J. F. Navarro, G. M. Seabroke, M. Steinmetz, M. Williams, *et al.*, Monthly Notices of the Royal Astronomical Society **379**, 755 (2007).
[101] P. F. de Salas and A. Widmark, Rept. Prog. Phys. **84**, 104901 (2021), arXiv:2012.11477 [astro-ph.GA].
[102] E. D. Hall, R. X. Adhikari, V. V. Frolov, H. Müller, M. Pospelov, and R. X. Adhikari, Phys. Rev. D **98**, 083019 (2018), arXiv:1605.01103 [gr-qc].
[103] A. L. Miller *et al.*, Phys. Rev. D **103**, 103002 (2021), arXiv:2010.01925 [astro-ph.IM].
[104] K. Nagano, T. Fujita, Y. Michimura, and I. Obata, Physical Review Letters **123**, 111301 (2019).
[105] K. Nagano *et al.*, Physical Review D **104**, 062008 (2021).
[106] X. Xue *et al.*, (2024), arXiv:2412.02229 [astro-ph.HE].
[107] N. K. Porayko *et al.* (EPTA), (2024), arXiv:2412.02232 [astro-ph.CO].
[108] J. Preskill, M. B. Wise, and F. Wilczek, Phys. Lett. B **120**, 127 (1983).
[109] L. Abbott and P. Sikivie, Phys. Lett. B **120**, 133 (1983).
[110] M. Dine and W. Fischler, Phys. Lett. B **120**, 137 (1983).
[111] Y. Cho and Y. Keum, Mod. Phys. Lett. A **13**, 109 (1998), arXiv:hep-ph/9810379.
[112] Y. Cho and J. Kim, Phys. Rev. D **79**, 023504 (2009),

arXiv:0711.2858 [gr-qc].
[113] A. Arvanitaki, J. Huang, and K. Van Tilburg, Phys. Rev. D **91**, 015015 (2015), arXiv:1405.2925 [hep-ph].
[114] Y. Stadnik and V. Flambaum, Physical Review Letters **114**, 161301 (2015).
[115] Y. Stadnik and V. Flambaum, Physical Review Letters **115**, 201301 (2015).
[116] Y. Stadnik and V. Flambaum, Physical Review A **93**, 063630 (2016).
[117] S. M. Vermeulen *et al.*, Nature **600**, 424 (2021).
[118] A. S. Göttel, A. Ejlli, K. Karan, S. M. Vermeulen, L. Aiello, V. Raymond, and H. Grote, Phys. Rev. Lett. **133**, 101001 (2024), arXiv:2401.18076 [astro-ph.CO].
[119] A. Derevianko, Phys. Rev. A **97**, 042506 (2018), arXiv:1605.09717 [physics.atom-ph].
[120] A. A. Geraci, C. Bradley, D. Gao, J. Weinstein, and A. Derevianko, Phys. Rev. Lett. **123**, 031304 (2019), arXiv:1808.00540 [astro-ph.IM].
[121] E. Hall and N. Aggarwal, (2022), arXiv:2210.17487 [hep-ex].
[122] D. E. Kaplan, A. Mitridate, and T. Trickle, Phys. Rev. D **106**, 035032 (2022), arXiv:2205.06817 [hep-ph].
[123] T. Damour and J. F. Donoghue, Phys. Rev. D **82**, 084033 (2010), arXiv:1007.2792 [gr-qc].
[124] S. L. Shapiro and S. A. Teukolsky, *Black holes, white dwarfs, and neutron stars: The physics of compact objects* (1983).
[125] N. F. Bell, G. Busoni, and S. Robles, JCAP **06**, 054 (2019), arXiv:1904.09803 [hep-ph].
[126] N. K. Porayko *et al.*, Phys. Rev. D **98**, 102002 (2018), arXiv:1810.03227 [astro-ph.CO].
[127] C. Smarra *et al.* (European Pulsar Timing Array), Phys. Rev. Lett. **131**, 171001 (2023), arXiv:2306.16228 [astro-ph.HE].
[128] A. Afzal *et al.* (NANOGrav), Astrophys. J. Lett. **951**, L11 (2023), [Erratum: Astrophys.J.Lett. 971, L27 (2024), Erratum: Astrophys.J. 971, L27 (2024)], arXiv:2306.16219 [astro-ph.HE].
[129] V. V. Flambaum, D. B. Leinweber, A. W. Thomas, and R. D. Young, Phys. Rev. D **69**, 115006 (2004), arXiv:hep-ph/0402098.
[130] A. E. Nelson and J. Scholtz, Physical Review D **84**, 103501 (2011).
[131] P. Arias, D. Cadamuro, M. Goodsell, J. Jaeckel, J. Redondo, and A. Ringwald, Journal of Cosmology and Astroparticle Physics **2012**, 013 (2012).
[132] P. W. Graham, J. Mardon, and S. Rajendran, Physical Review D **93**, 103520 (2016).
[133] P. Agrawal, N. Kitajima, M. Reece, T. Sekiguchi, and F. Takahashi, Physics Letters B **801**, 135136 (2020).
[134] R. T. Co, A. Pierce, Z. Zhang, and Y. Zhao, Phys. Rev. D **99**, 075002 (2019), arXiv:1810.07196 [hep-ph].
[135] M. Bastero-Gil, J. Santiago, L. Ubaldi, and R. Vega-Morales, JCAP **04**, 015 (2019), arXiv:1810.07208 [hep-ph].
[136] J. A. Dror, K. Harigaya, and V. Narayan, Phys. Rev. D **99**, 035036 (2019), arXiv:1810.07195 [hep-ph].
[137] A. J. Long and L.-T. Wang, Physical Review D **99**, 063529 (2019).
[138] N. Siemonsen, C. Mondino, D. Egana-Ugrinovic, J. Huang, M. Baryakhtar, and W. E. East, Phys. Rev. D **107**, 075025 (2023), arXiv:2212.09772 [astro-ph.HE].
[139] S. Morisaki, T. Fujita, Y. Michimura, H. Nakatsuka, and I. Obata, Phys. Rev. D **103**, L051702 (2021), arXiv:2011.03589 [hep-ph].
[140] S. F. Hassan and R. A. Rosen, JHEP **02**, 126 (2012), arXiv:1109.3515 [hep-th].
[141] A. Schmidt-May and M. von Strauss, J. Phys. A **49**, 183001 (2016), arXiv:1512.00021 [hep-th].
[142] L. Marzola, M. Raidal, and F. R. Urban, Phys. Rev. D **97**, 024010 (2018), arXiv:1708.04253 [hep-ph].
[143] J. M. Armaleo, D. López Nacir, and F. R. Urban, JCAP **09**, 031 (2020), arXiv:2005.03731 [astro-ph.CO].
[144] K. Aoki and K.-i. Maeda, Phys. Rev. D **97**, 044002 (2018), arXiv:1707.05003 [hep-th].
[145] E. Kun, Z. Keresztes, S. Das, and L. A. Gergely, Symmetry **10**, 520 (2018), arXiv:1905.04336 [astro-ph.CO].
[146] G. P. Centers *et al.*, Nature Commun. **12**, 7321 (2021), arXiv:1905.13650 [astro-ph.CO].
[147] Y. Manita, H. Takeda, K. Aoki, T. Fujita, and S. Mukohyama, Phys. Rev. D **109**, 095012 (2024), arXiv:2310.10646 [hep-ph].
[148] M. Tröbs and G. Heinzel, Measurement **39**, 120 (2006).
[149] G. Cowan, K. Cranmer, E. Gross, and O. Vitells, Eur. Phys. J. C **71**, 1554 (2011), [Erratum: Eur.Phys.J.C 73, 2501 (2013)], arXiv:1007.1727 [physics.data-an].
[150] H. Nakatsuka, S. Morisaki, T. Fujita, J. Kume, Y. Michimura, K. Nagano, and I. Obata, Phys. Rev. D **108**, 092010 (2023), arXiv:2205.02960 [astro-ph.CO].
[151] A. G. Abac *et al.* (KAGRA, LIGO Scientific, VIRGO), Phys. Rev. D **110**, 042001 (2024), arXiv:2403.03004 [astro-ph.CO].
[152] A. L. Miller, F. Badaracco, and C. Palomba (LIGO Scientific Collaboration, Virgo, KAGRA), Phys. Rev. D **105**, 103035 (2022), arXiv:2204.03814 [astro-ph.IM].
[153] N. Wiener *et al.*, *Extrapolation, interpolation, and smoothing of stationary time series: with engineering applications*, Vol. 8 (MIT press Cambridge, MA, 1964).
[154] R. Abbott *et al.* (LIGO Scientific Collaboration, Virgo, KAGRA), Phys. Rev. D **105**, 063030 (2022), arXiv:2105.13085 [astro-ph.CO].
[155] G. J. Feldman and R. D. Cousins, Phys. Rev. D **57**, 3873 (1998), arXiv:physics/9711021.
[156] L. Aiello, J. W. Richardson, S. M. Vermeulen, H. Grote, C. Hogan, O. Kwon, and C. Stoughton, Phys. Rev. Lett. **128**, 121101 (2022), arXiv:2108.04746 [gr-qc].
[157] S. Aharony, N. Akerman, R. Ozeri, G. Perez, I. Savoray, and R. Shaniv, Phys. Rev. D **103**, 075017 (2021), arXiv:1902.02788 [hep-ph].
[158] E. Savalle, A. Hees, F. Frank, E. Cantin, P.-E. Pottie, B. M. Roberts, L. Cros, B. T. Mcallister, and P. Wolf, Phys. Rev. Lett. **126**, 051301 (2021), arXiv:2006.07055 [gr-qc].
[159] C. J. Kennedy, E. Oelker, J. M. Robinson, T. Bothwell, D. Kedar, W. R. Milner, G. E. Marti, A. Derevianko, and J. Ye, Phys. Rev. Lett. **125**, 201302 (2020), arXiv:2008.08773 [physics.atom-ph].
[160] D. Antypas, O. Tretiak, A. Garcon, R. Ozeri, G. Perez, and D. Budker, Phys. Rev. Lett. **123**, 141102 (2019), arXiv:1905.02968 [physics.atom-ph].
[161] D. Antypas, O. Tretiak, K. Zhang, A. Garcon, G. Perez, M. G. Kozlov, S. Schiller, and D. Budker, Quantum Sci. Technol. **6**, 034001 (2021), arXiv:2012.01519 [physics.atom-ph].
[162] O. Tretiak, X. Zhang, N. L. Figueroa, D. Antypas, A. Brogna, A. Banerjee, G. Perez, and D. Budker, Phys. Rev. Lett. **129**, 031301 (2022), arXiv:2201.02042 [hep-ph].

[163] R. Oswald *et al.*, Phys. Rev. Lett. **129**, 031302 (2022), arXiv:2111.06883 [hep-ph].
[164] W. M. Campbell, B. T. McAllister, M. Goryachev, E. N. Ivanov, and M. E. Tobar, Phys. Rev. Lett. **126**, 071301 (2021), arXiv:2010.08107 [hep-ex].
[165] K. Beloy *et al.* (BACON), Nature **591**, 564 (2021), arXiv:2005.14694 [physics.atom-ph].
[166] X. Zhang, A. Banerjee, M. Leyser, G. Perez, S. Schiller, D. Budker, and D. Antypas, Phys. Rev. Lett. **130**, 251002 (2023), arXiv:2212.04413 [physics.atom-ph].
[167] K. Fukusumi, S. Morisaki, and T. Suyama, Phys. Rev. D **108**, 095054 (2023), arXiv:2303.13088 [hep-ph].
[168] N. Sherrill *et al.*, New J. Phys. **25**, 093012 (2023), arXiv:2302.04565 [physics.atom-ph].
[169] J. Bergé, M. Pernot-Borràs, J.-P. Uzan, P. Brax, R. Chhun, G. Métris, M. Rodrigues, and P. Touboul, Class. Quant. Grav. **39**, 204010 (2022), arXiv:2102.00022 [gr-qc].
[170] A. Hees, O. Minazzoli, E. Savalle, Y. V. Stadnik, and P. Wolf, Phys. Rev. D **98**, 064051 (2018), arXiv:1807.04512 [gr-qc].
[171] Y. Michimura, T. Fujita, S. Morisaki, H. Nakatsuka, and I. Obata, Phys. Rev. D **102**, 102001 (2020), arXiv:2008.02482 [hep-ph].
[172] K. Danzmann and L. S. Team, Advances in Space Research **32**, 1233 (2003).
[173] S. Babak, A. Petiteau, and M. Hewitson, (2021), arXiv:2108.01167 [astro-ph.IM].
[174] W.-R. Hu and Y.-L. Wu, Natl. Sci. Rev. **4**, 685 (2017).
[175] J. Luo *et al.* (TianQin), Class. Quant. Grav. **33**, 035010 (2016), arXiv:1512.02076 [astro-ph.IM].
[176] H. Kim, JCAP **12**, 018 (2023), arXiv:2306.13348 [hep-ph].
[177] M. Armano *et al.*, Phys. Rev. Lett. **116**, 231101 (2016).
[178] D. Vetrugno (LISA Pathfinder), (2017), 10.1142/S0218271817410231, [Erratum: Int.J.Mod.Phys.D 26, 1741023 (2017)].
[179] M. Armano *et al.*, Phys. Rev. Lett. **120**, 061101 (2018).
[180] A. L. Miller and L. Mendes, Phys. Rev. D **107**, 063015 (2023), arXiv:2301.08736 [gr-qc].
[181] J. Frerick, J. Jaeckel, F. Kahlhoefer, and K. Schmidt-Hoberg, Phys. Lett. B **848**, 138328 (2024), arXiv:2310.06017 [hep-ph].
[182] N. K. Porayko and K. A. Postnov, Phys. Rev. D **90**, 062008 (2014), arXiv:1408.4670 [astro-ph.CO].
[183] A. Hees, J. Guéna, M. Abgrall, S. Bize, and P. Wolf, Phys. Rev. Lett. **117**, 061301 (2016), arXiv:1604.08514 [gr-qc].
[184] T. Kumar Poddar, S. Mohanty, and S. Jana, Phys. Rev. D **100**, 123023 (2019), arXiv:1908.09732 [hep-ph].
[185] J. A. Dror, R. Laha, and T. Opferkuch, Phys. Rev. D **102**, 023005 (2020), arXiv:1909.12845 [hep-ph].
[186] X. Xue *et al.* (PPTA), Phys. Rev. Res. **4**, L012022 (2022), arXiv:2112.07687 [hep-ph].
[187] A. Kuntz and E. Barausse, Phys. Rev. D **109**, 124001 (2024), arXiv:2403.07980 [gr-qc].
[188] K. Nordtvedt, Phys. Rev. **169**, 1017 (1968).
[189] T. Damour and J. H. Taylor, Phys. Rev. D **45**, 1840 (1992).
[190] M. Kramer *et al.*, Science **314**, 97 (2006), arXiv:astro-ph/0609417.
[191] C. Smarra *et al.*, Phys. Rev. D **110**, 043033 (2024), arXiv:2405.01633 [astro-ph.HE].
[192] M. Fierz, Helv. Phys. Acta **29**, 128 (1956).
[193] P. Jordan, Z. Phys. **157**, 112 (1959).
[194] C. Brans and R. H. Dicke, Phys. Rev. **124**, 925 (1961).
[195] R. H. Dicke, Phys. Rev. **125**, 2163 (1962).
[196] T. Damour and G. Esposito-Farese, Class. Quant. Grav. **9**, 2093 (1992).
[197] T. Damour and G. Esposito-Farese, Phys. Rev. Lett. **70**, 2220 (1993).
[198] N. Aggarwal *et al.*, Living Rev. Rel. **24**, 4 (2021), arXiv:2011.12414 [gr-qc].
[199] K. K. Boddy, J. A. Dror, and A. Lam, (2025), arXiv:2502.15874 [hep-ph].
[200] Y. Du, V. S. H. Lee, Y. Wang, and K. M. Zurek, Phys. Rev. D **108**, 122003 (2023), arXiv:2306.13122 [astro-ph.CO].
[201] E. G. Adelberger, J. H. Gundlach, B. R. Heckel, S. Hoedl, and S. Schlamminger, Prog. Part. Nucl. Phys. **62**, 102 (2009).
[202] D. N. Spergel and P. J. Steinhardt, Phys. Rev. Lett. **84**, 3760 (2000), arXiv:astro-ph/9909386.
[203] D. Harvey, R. Massey, T. Kitching, A. Taylor, and E. Tittley, Science **347**, 1462 (2015), arXiv:1503.07675 [astro-ph.CO].
[204] S. W. Randall, M. Markevitch, D. Clowe, A. H. Gonzalez, and M. Bradac, Astrophys. J. **679**, 1173 (2008), arXiv:0704.0261 [astro-ph].
[205] M. Boylan-Kolchin, J. S. Bullock, and M. Kaplinghat, Mon. Not. Roy. Astron. Soc. **415**, L40 (2011), arXiv:1103.0007 [astro-ph.CO].
[206] P. R. Saulson, *Fundamentals of Interferometric Gravitational Wave Detectors*, 2nd ed. (World Scientific, 2017).
[207] M. I. Gresham, V. S. H. Lee, and K. M. Zurek, JCAP **02**, 048 (2023), arXiv:2209.03963 [astro-ph.HE].
[208] C.-H. Lee, R. Primulando, and M. Spinrath, Phys. Rev. D **107**, 035029 (2023), arXiv:2208.06232 [hep-ph].
[209] D. Baumann, H. S. Chia, and R. A. Porto, Phys. Rev. D **99**, 044001 (2019), arXiv:1804.03208 [gr-qc].
[210] M. Isi, L. Sun, R. Brito, and A. Melatos, Phys. Rev. D **99**, 084042 (2019), [Erratum: Phys.Rev.D 102, 049901 (2020)], arXiv:1810.03812 [gr-qc].
[211] R. Brito, S. Grillo, and P. Pani, Phys. Rev. Lett. **124**, 211101 (2020), arXiv:2002.04055 [gr-qc].
[212] A. Arvanitaki, M. Baryakhtar, and X. Huang, Phys. Rev. D **91**, 084011 (2015), arXiv:1411.2263 [hep-ph].
[213] S. J. Zhu, M. Baryakhtar, M. A. Papa, D. Tsuna, N. Kawanaka, and H.-B. Eggenstein, Phys. Rev. D **102**, 063020 (2020), arXiv:2003.03359 [gr-qc].
[214] C. Palomba *et al.*, Phys. Rev. Lett. **123**, 171101 (2019), arXiv:1909.08854 [astro-ph.HE].
[215] A. Arvanitaki, S. Dimopoulos, S. Dubovsky, N. Kaloper, and J. March-Russell, Phys. Rev. D **81**, 123530 (2010), arXiv:0905.4720 [hep-th].
[216] M. Baryakhtar, R. Lasenby, and M. Teo, Phys. Rev. D **96**, 035019 (2017), arXiv:1704.05081 [hep-ph].
[217] N. Siemonsen, T. May, and W. E. East, Phys. Rev. D **107**, 104003 (2023), arXiv:2211.03845 [gr-qc].
[218] D. Jones, L. Sun, N. Siemonsen, W. E. East, S. M. Scott, and K. Wette, Phys. Rev. D **108**, 064001 (2023), arXiv:2305.00401 [gr-qc].
[219] D. Jones, N. Siemonsen, L. Sun, W. E. East, A. L. Miller, K. Wette, and O. J. Piccinni, (2024), arXiv:2412.00320 [gr-qc].
[220] D. Brzeminski, A. Hook, J. Huang, and C. Ristow, (2024), arXiv:2407.18991 [hep-ph].
[221] R. Brito, S. Ghosh, E. Barausse, E. Berti, V. Cardoso,

I. Dvorkin, A. Klein, and P. Pani, Phys. Rev. D **96**, 064050 (2017), arXiv:1706.06311 [gr-qc].
[222] K. K. Y. Ng, M. Isi, C.-J. Haster, and S. Vitale, Phys. Rev. D **102**, 083020 (2020), arXiv:2007.12793 [gr-qc].
[223] H. Yoshino and H. Kodama, Prog. Theor. Phys. **128**, 153 (2012), arXiv:1203.5070 [gr-qc].
[224] H. Yoshino and H. Kodama, PTEP **2015**, 061E01 (2015), arXiv:1407.2030 [gr-qc].
[225] H. Yoshino and H. Kodama, Class. Quant. Grav. **32**, 214001 (2015), arXiv:1505.00714 [gr-qc].
[226] J. C. Aurrekoetxea, J. Marsden, K. Clough, and P. G. Ferreira, Phys. Rev. D **110**, 083011 (2024), arXiv:2409.01937 [gr-qc].
[227] T. Takahashi, H. Omiya, and T. Tanaka, Phys. Rev. D **110**, 104038 (2024), arXiv:2408.08349 [gr-qc].
[228] M. Baryakhtar, M. Galanis, R. Lasenby, and O. Simon, Phys. Rev. D **103**, 095019 (2021), arXiv:2011.11646 [hep-ph].
[229] S. Collaviti, L. Sun, M. Galanis, and M. Baryakhtar, Class. Quant. Grav. **42**, 025006 (2025), arXiv:2407.04304 [gr-qc].
[230] W. E. East and N. Siemonsen, Phys. Rev. D **108**, 124048 (2023), arXiv:2309.05096 [gr-qc].
[231] R. Abbott *et al.* (LIGO Scientific Collaboration, Virgo, KAGRA), Phys. Rev. D **105**, 102001 (2022), arXiv:2111.15507 [astro-ph.HE].
[232] T. May, W. E. East, and N. Siemonsen, (2024), arXiv:2410.21442 [gr-qc].
[233] N. Siemonsen and W. E. East, Phys. Rev. D **101**, 024019 (2020), arXiv:1910.09476 [gr-qc].
[234] H. Fukuda and K. Nakayama, JHEP **01**, 128 (2020), arXiv:1910.06308 [hep-ph].
[235] H. Omiya, T. Takahashi, T. Tanaka, and H. Yoshino, Phys. Rev. D **110**, 044002 (2024), arXiv:2404.16265 [gr-qc].
[236] E. A. Donley, N. R. Claussen, S. L. Cornish, J. L. Roberts, E. A. Cornell, and C. E. Wieman, Nature **412**, 295 (2001).
[237] A. Arvanitaki and S. Dubovsky, Phys. Rev. D **83**, 044026 (2011), arXiv:1004.3558 [hep-th].
[238] H. Omiya, T. Takahashi, T. Tanaka, and H. Yoshino, JCAP **06**, 016 (2023), arXiv:2211.01949 [gr-qc].
[239] W. E. East, Phys. Rev. Lett. **129**, 141103 (2022), arXiv:2205.03417 [hep-ph].
[240] W. E. East and J. Huang, JHEP **12**, 089 (2022), arXiv:2206.12432 [hep-ph].
[241] N. Xie and F. P. Huang, Sci. China Phys. Mech. Astron. **67**, 210411 (2024), arXiv:2207.11145 [hep-ph].
[242] D. Baumann, H. S. Chia, J. Stout, and L. ter Haar, JCAP **12**, 006 (2019), arXiv:1908.10370 [gr-qc].
[243] D. Baumann, H. S. Chia, R. A. Porto, and J. Stout, Phys. Rev. D **101**, 083019 (2020), arXiv:1912.04932 [gr-qc].
[244] A. Boudon, P. Brax, P. Valageas, and L. K. Wong, Phys. Rev. D **109**, 043504 (2024), arXiv:2305.18540 [astro-ph.CO].
[245] N. V. Krishnendu, K. G. Arun, and C. K. Mishra, Phys. Rev. Lett. **119**, 091101 (2017), arXiv:1701.06318 [gr-qc].
[246] R. O. Hansen, J. Math. Phys. **15**, 46 (1974).
[247] W. G. Laarakkers and E. Poisson, Astrophys. J. **512**, 282 (1999), arXiv:gr-qc/9709033.
[248] G. Pappas and T. A. Apostolatos, Phys. Rev. Lett. **108**, 231104 (2012), arXiv:1201.6067 [gr-qc].
[249] K. Chatziioannou, Gen. Rel. Grav. **52**, 109 (2020), arXiv:2006.03168 [gr-qc].
[250] E. Payne, L. Sun, K. Kremer, P. D. Lasky, and E. Thrane, Astrophys. J. **931**, 79 (2022), arXiv:2107.11730 [gr-qc].
[251] T. Takahashi, H. Omiya, and T. Tanaka, PTEP **2022**, 043E01 (2022), arXiv:2112.05774 [gr-qc].
[252] D. Baumann, G. Bertone, J. Stout, and G. M. Tomaselli, Phys. Rev. D **105**, 115036 (2022), arXiv:2112.14777 [gr-qc].
[253] D. Baumann, G. Bertone, J. Stout, and G. M. Tomaselli, Phys. Rev. Lett. **128**, 221102 (2022), arXiv:2206.01212 [gr-qc].
[254] G. M. Tomaselli, T. F. M. Spieksma, and G. Bertone, JCAP **07**, 070 (2023), arXiv:2305.15460 [gr-qc].
[255] G. M. Tomaselli, T. F. M. Spieksma, and G. Bertone, Phys. Rev. Lett. **133**, 121402 (2024), arXiv:2407.12908 [gr-qc].
[256] A. Arvanitaki, M. Baryakhtar, S. Dimopoulos, S. Dubovsky, and R. Lasenby, Phys. Rev. D **95**, 043001 (2017), arXiv:1604.03958 [hep-ph].
[257] V. Cardoso, O. J. C. Dias, G. S. Hartnett, M. Middleton, P. Pani, and J. E. Santos, JCAP **03**, 043 (2018), arXiv:1801.01420 [gr-qc].
[258] D. Ghosh and D. Sachdeva, Phys. Rev. D **103**, 095028 (2021), arXiv:2102.08857 [astro-ph.HE].
[259] K. K. Y. Ng, O. A. Hannuksela, S. Vitale, and T. G. F. Li, Phys. Rev. D **103**, 063010 (2021), arXiv:1908.02312 [gr-qc].
[260] R. Abbott *et al.* (LIGO Scientific Collaboration, Virgo), Phys. Rev. X **11**, 021053 (2021), arXiv:2010.14527 [gr-qc].
[261] K. K. Y. Ng, S. Vitale, O. A. Hannuksela, and T. G. F. Li, Phys. Rev. Lett. **126**, 151102 (2021), arXiv:2011.06010 [gr-qc].
[262] P. C. Peters, Phys. Rev. **136**, B1224 (1964).
[263] L.-q. Wen and J. R. Gair, Class. Quant. Grav. **22**, S445 (2005), arXiv:gr-qc/0502100.
[264] S. D'Antonio *et al.*, Phys. Rev. D **98**, 103017 (2018), arXiv:1809.07202 [gr-qc].
[265] B. G. Quinn and E. J. Hannan, *The estimation and tracking of frequency*, 9 (Cambridge University Press, 2001).
[266] L. Sun, R. Brito, and M. Isi, Phys. Rev. D **101**, 063020 (2020), [Erratum: Phys.Rev.D 102, 089902 (2020)], arXiv:1909.11267 [gr-qc].
[267] R. Abbott *et al.* (KAGRA, LIGO Scientific, VIRGO), Phys. Rev. D **106**, 042003 (2022), arXiv:2204.04523 [astro-ph.HE].
[268] V. Dergachev and M. A. Papa, Phys. Rev. Lett. **123**, 101101 (2019), arXiv:1902.05530 [gr-qc].
[269] O. D. Elbert, J. S. Bullock, and M. Kaplinghat, Mon. Not. Roy. Astron. Soc. **473**, 1186 (2018), arXiv:1703.02551 [astro-ph.GA].
[270] J. Ming, M. A. Papa, H.-B. Eggenstein, B. Beheshtipour, B. Machenschalk, R. Prix, B. Allen, and M. Bensch, Astrophys. J. **977**, 154 (2024), arXiv:2408.14573 [gr-qc].
[271] P. B. Covas, M. A. Papa, and R. Prix, (2024), arXiv:2409.16196 [gr-qc].
[272] F. Sauter, Z. Phys. **69**, 742 (1931).
[273] W. Heisenberg and H. Euler, Z. Phys. **98**, 714 (1936), arXiv:physics/0605038.
[274] J. S. Schwinger, Phys. Rev. **82**, 664 (1951).
[275] G. V. Dunne, H. Gies, and R. Schutzhold, Phys. Rev.

D **80**, 111301 (2009), arXiv:0908.0948 [hep-ph].
[276] A. Monin and M. B. Voloshin, Phys. Rev. D **81**, 085014 (2010), arXiv:1001.3354 [hep-th].
[277] R. N. Manchester, G. B. Hobbs, A. Teoh, and M. Hobbs, Astron. J. **129**, 1993 (2005), arXiv:astro-ph/0412641.
[278] L. Mirasola *et al.*, (2025), arXiv:2501.02052 [gr-qc].
[279] C. O'Hare, "cajohare/axionlimits: Axionlimits," `https://cajohare.github.io/AxionLimits/` (2020).
[280] A. Mirizzi, J. Redondo, and G. Sigl, JCAP **03**, 026 (2009), arXiv:0901.0014 [hep-ph].
[281] A. Caputo, H. Liu, S. Mishra-Sharma, and J. T. Ruderman, Phys. Rev. Lett. **125**, 221303 (2020), arXiv:2002.05165 [astro-ph.CO].
[282] F. McCarthy, D. Pirvu, J. C. Hill, J. Huang, M. C. Johnson, and K. K. Rogers, Phys. Rev. Lett. **133**, 141003 (2024), arXiv:2406.02546 [hep-ph].
[283] L. Tsukada, T. Callister, A. Matas, and P. Meyers, Phys. Rev. D **99**, 103015 (2019), arXiv:1812.09622 [astro-ph.HE].
[284] L. Tsukada, R. Brito, W. E. East, and N. Siemonsen, Phys. Rev. D **103**, 083005 (2021), arXiv:2011.06995 [astro-ph.HE].
[285] C. Yuan, Y. Jiang, and Q.-G. Huang, Phys. Rev. D **106**, 023020 (2022), arXiv:2204.03482 [astro-ph.CO].
[286] R.-Z. Guo, Y. Jiang, and Q.-G. Huang, JCAP **04**, 053 (2024), arXiv:2312.16435 [astro-ph.CO].
[287] S. Hoof, D. J. E. Marsh, J. Sisk-Reynés, J. H. Matthews, and C. Reynolds, (2024), arXiv:2406.10337 [hep-ph].
[288] Y. Guo, W. Zhong, Y. Ma, and D. Su, Phys. Rev. D **109**, 104046 (2024), arXiv:2309.07790 [gr-qc].
[289] L. Hui, J. P. Ostriker, S. Tremaine, and E. Witten, Phys. Rev. D **95**, 043541 (2017), arXiv:1610.08297 [astro-ph.CO].
[290] S.-J. Sin, Phys. Rev. D **50**, 3650 (1994), arXiv:hep-ph/9205208.
[291] H.-Y. Schive, T. Chiueh, and T. Broadhurst, Nature Phys. **10**, 496 (2014), arXiv:1406.6586 [astro-ph.GA].
[292] M. Aghaie, G. Armando, A. Dondarini, and P. Panci, Phys. Rev. D **109**, 103030 (2024), arXiv:2308.04590 [astro-ph.CO].
[293] R. K. Sachs and A. M. Wolfe, Astrophys. J. **147**, 73 (1967).
[294] N. Bartolo *et al.*, JCAP **12**, 026 (2016), arXiv:1610.06481 [astro-ph.CO].
[295] S. Babak, J. Gair, A. Sesana, E. Barausse, C. F. Sopuerta, C. P. L. Berry, E. Berti, P. Amaro-Seoane, A. Petiteau, and A. Klein, Phys. Rev. D **95**, 103012 (2017), arXiv:1703.09722 [gr-qc].
[296] K. Wang and Y. Zhong, Phys. Rev. D **108**, 123531 (2023), arXiv:2306.10732 [astro-ph.CO].
[297] P. Brax, P. Valageas, C. Burrage, and J. A. R. Cembranos, Phys. Rev. D **110**, 083515 (2024), arXiv:2402.04819 [astro-ph.CO].
[298] D. Blas, S. Gasparotto, and R. Vicente, (2024), arXiv:2410.07330 [hep-ph].
[299] K. Riles, Mod. Phys. Lett. **A32**, 1730035 (2017), arXiv:1712.05897 [gr-qc].
[300] G. Pagliaro, M. A. Papa, J. Ming, J. Lian, D. Tsuna, C. Maraston, and D. Thomas, Astrophys. J. **952**, 123 (2023), arXiv:2303.04714 [gr-qc].
[301] B. Bar-Or, J.-B. Fouvry, and S. Tremaine, Astrophys. J. **871**, 28 (2019), arXiv:1809.07673 [astro-ph.GA].
[302] S. Chen, A. Sesana, and C. J. Conselice, Mon. Not. Roy. Astron. Soc. **488**, 401 (2019), arXiv:1810.04184 [astro-ph.GA].
[303] J. Bramante, A. Delgado, and A. Martin, Phys. Rev. D **96**, 063002 (2017), arXiv:1703.04043 [hep-ph].
[304] N. F. Bell, G. Busoni, S. Robles, and M. Virgato, JCAP **03**, 086 (2021), arXiv:2010.13257 [hep-ph].
[305] B. Dasgupta, R. Laha, and A. Ray, Phys. Rev. Lett. **126**, 141105 (2021), arXiv:2009.01825 [astro-ph.HE].
[306] A. Ray, Phys. Rev. D **107**, 083012 (2023), arXiv:2301.03625 [hep-ph].
[307] S. Bhattacharya, B. Dasgupta, R. Laha, and A. Ray, Phys. Rev. Lett. **131**, 091401 (2023), arXiv:2302.07898 [hep-ph].
[308] S. Bhattacharya (2024) arXiv:2412.02453 [hep-ph].
[309] R. Abbott *et al.* (LIGO Scientific, VIRGO, KAGRA), Mon. Not. Roy. Astron. Soc. **524**, 5984 (2023), [Erratum: Mon.Not.Roy.Astron.Soc. 526, 6234 (2023)], arXiv:2212.01477 [astro-ph.HE].
[310] L. Goodenough and D. Hooper, (2009), arXiv:0910.2998 [hep-ph].
[311] D. Hooper and T. Linden, Phys. Rev. D **84**, 123005 (2011), arXiv:1110.0006 [astro-ph.HE].
[312] C. Gordon and O. Macias, Phys. Rev. D **88**, 083521 (2013), [Erratum: Phys.Rev.D 89, 049901 (2014)], arXiv:1306.5725 [astro-ph.HE].
[313] T. Daylan, D. P. Finkbeiner, D. Hooper, T. Linden, S. K. N. Portillo, N. L. Rodd, and T. R. Slatyer, Phys. Dark Univ. **12**, 1 (2016), arXiv:1402.6703 [astro-ph.HE].
[314] F. Calore, I. Cholis, C. McCabe, and C. Weniger, Phys. Rev. D **91**, 063003 (2015), arXiv:1411.4647 [hep-ph].
[315] K. N. Abazajian, N. Canac, S. Horiuchi, and M. Kaplinghat, Phys. Rev. D **90**, 023526 (2014), arXiv:1402.4090 [astro-ph.HE].
[316] K. N. Abazajian, JCAP **03**, 010 (2011), arXiv:1011.4275 [astro-ph.HE].
[317] F. Calore, I. Cholis, and C. Weniger, JCAP **03**, 038 (2015), arXiv:1409.0042 [astro-ph.CO].
[318] Q. Yuan and B. Zhang, JHEAp **3-4**, 1 (2014), arXiv:1404.2318 [astro-ph.HE].
[319] J. Petrović, P. D. Serpico, and G. Zaharijas, JCAP **02**, 023 (2015), arXiv:1411.2980 [astro-ph.HE].
[320] C. S. Ye and G. Fragione, Astrophys. J. **940**, 162 (2022), arXiv:2207.03504 [astro-ph.HE].
[321] B. Haskell, M. Priymak, A. Patruno, M. Oppenoorth, A. Melatos, and P. D. Lasky, Mon. Not. Roy. Astron. Soc. **450**, 2393 (2015), arXiv:1501.06039 [astro-ph.SR].
[322] S. K. Lander, N. Andersson, and K. Glampedakis, Mon. Not. Roy. Astron. Soc. **419**, 732 (2012), arXiv:1106.6322 [astro-ph.SR].
[323] A. Mastrano and A. Melatos, Mon. Not. Roy. Astron. Soc. **421**, 760 (2012), arXiv:1112.1542 [astro-ph.HE].
[324] S. K. Lander, Mon. Not. Roy. Astron. Soc. **437**, 424 (2014), arXiv:1307.7020 [astro-ph.HE].
[325] D. Hooper and T. Linden, JCAP **08**, 018 (2016), arXiv:1606.09250 [astro-ph.HE].
[326] H. Ploeg, C. Gordon, R. Crocker, and O. Macias, JCAP **12**, 035 (2020), [Erratum: JCAP 07, E01 (2021)], arXiv:2008.10821 [astro-ph.HE].
[327] J. T. Dinsmore and T. R. Slatyer, JCAP **06**, 025 (2022), arXiv:2112.09699 [astro-ph.HE].
[328] G. Woan, M. D. Pitkin, B. Haskell, D. I. Jones, and P. D. Lasky, Astrophys. J. Lett. **863**, L40 (2018), arXiv:1806.02822 [astro-ph.HE].
[329] R. Bartels, E. Storm, C. Weniger, and F. Calore, Na-

ture Astron. **2**, 819 (2018), arXiv:1711.04778 [astro-ph.HE].
[330] P. Gondolo and J. Silk, Phys. Rev. Lett. **83**, 1719 (1999), arXiv:astro-ph/9906391.
[331] D. Merritt, M. Milosavljevic, L. Verde, and R. Jimenez, Phys. Rev. Lett. **88**, 191301 (2002), arXiv:astro-ph/0201376.
[332] P. Ullio, H. Zhao, and M. Kamionkowski, Phys. Rev. D **64**, 043504 (2001), arXiv:astro-ph/0101481.
[333] D. Merritt, Phys. Rev. Lett. **92**, 201304 (2004), arXiv:astro-ph/0311594.
[334] G. Bertone and D. Merritt, Phys. Rev. D **72**, 103502 (2005), arXiv:astro-ph/0501555.
[335] M. Daniel, K. Pardo, and L. Sagunski, (2025), arXiv:2501.13601 [astro-ph.HE].
[336] H.-S. Zhao and J. Silk, Phys. Rev. Lett. **95**, 011301 (2005), arXiv:astro-ph/0501625.
[337] K. Kohri, T. Nakama, and T. Suyama, Phys. Rev. D **90**, 083514 (2014), arXiv:1405.5999 [astro-ph.CO].
[338] Y. N. Eroshenko, Astron. Lett. **42**, 347 (2016), arXiv:1607.00612 [astro-ph.HE].
[339] S. M. Boucenna, F. Kuhnel, T. Ohlsson, and L. Visinelli, JCAP **07**, 003 (2018), arXiv:1712.06383 [hep-ph].
[340] M. P. Hertzberg, E. D. Schiappacasse, and T. T. Yanagida, Phys. Lett. B **807**, 135566 (2020), arXiv:1910.10575 [astro-ph.CO].
[341] G. Bertone, A. R. A. C. Wierda, D. Gaggero, B. J. Kavanagh, M. Volonteri, and N. Yoshida, (2024), arXiv:2404.08731 [astro-ph.CO].
[342] F. Dosopoulou and J. Silk, (2025), arXiv:2502.15468 [astro-ph.HE].
[343] K. Eda, Y. Itoh, S. Kuroyanagi, and J. Silk, Phys. Rev. Lett. **110**, 221101 (2013), arXiv:1301.5971 [gr-qc].
[344] F. Duque, C. F. B. Macedo, R. Vicente, and V. Cardoso, Phys. Rev. Lett. **133**, 121404 (2024), arXiv:2312.06767 [gr-qc].
[345] S. Ghodla, (2024), arXiv:2410.15562 [astro-ph.CO].
[346] M. C. Miller, Class. Quant. Grav. **26**, 094031 (2009), arXiv:0812.3028 [astro-ph].
[347] K. Eda, Y. Itoh, S. Kuroyanagi, and J. Silk, Phys. Rev. D **91**, 044045 (2015), arXiv:1408.3534 [gr-qc].
[348] B. Carr, S. Clesse, J. Garcia-Bellido, M. Hawkins, and F. Kuhnel, Phys. Rept. **1054**, 1 (2024), arXiv:2306.03903 [astro-ph.CO].
[349] P. S. Cole, A. Coogan, B. J. Kavanagh, and G. Bertone, Phys. Rev. D **107**, 083006 (2023), arXiv:2207.07576 [astro-ph.CO].
[350] D. Tahelyani, A. Bhattacharyya, and A. S. Sengupta, (2024), arXiv:2411.14063 [gr-qc].
[351] M.-C. Chen, H.-Y. Liu, Q.-Y. Zhang, and J. Zhang, Phys. Rev. D **110**, 064018 (2024), arXiv:2405.11583 [gr-qc].
[352] P. S. Cole, G. Bertone, A. Coogan, D. Gaggero, T. Karydas, B. J. Kavanagh, T. F. M. Spieksma, and G. M. Tomaselli, Nature Astron. **7**, 943 (2023), arXiv:2211.01362 [gr-qc].
[353] X. Yuan, J.-d. Zhang, and J. Mei, (2024), arXiv:2412.00915 [gr-qc].
[354] L. Zwick, C. Tiede, A. A. Trani, A. Derdzinski, Z. Haiman, D. J. D'Orazio, and J. Samsing, Phys. Rev. D **110**, 103005 (2024), arXiv:2405.05698 [gr-qc].
[355] E. Wilcox, D. A. Nichols, and K. Yagi, Phys. Rev. D **110**, 124009 (2024), arXiv:2409.10846 [gr-qc].
[356] L. Sun and A. Melatos, Physical Review D **99**, 123003 (2019).
[357] A. Miller *et al.*, Phys. Rev. D **98**, 102004 (2018), arXiv:1810.09784 [astro-ph.IM].
[358] M. Oliver, D. Keitel, and A. M. Sintes, Physical Review D **99**, 104067 (2019).
[359] S. Banagiri, L. Sun, M. W. Coughlin, and A. Melatos, Phys. Rev. D **100**, 024034 (2019), arXiv:1903.02638 [astro-ph.IM].
[360] A. L. Miller *et al.*, Phys. Rev. D **100**, 062005 (2019), arXiv:1909.02262 [astro-ph.IM].
[361] H.-K. Guo and A. Miller, (2022), arXiv:2205.10359 [astro-ph.IM].
[362] M. Andrés-Carcasona, O. J. Piccinni, M. Martínez, and L.-M. Mir, PoS **EPS-HEP2023**, 067 (2023).
[363] G. Alestas, G. Morras, T. S. Yamamoto, J. Garcia-Bellido, S. Kuroyanagi, and S. Nesseris, Phys. Rev. D **109**, 123516 (2024), arXiv:2401.02314 [astro-ph.CO].
[364] A. L. Miller, N. Aggarwal, S. Clesse, F. De Lillo, S. Sachdev, P. Astone, C. Palomba, O. J. Piccinni, and L. Pierini, In press, Phys. Rev. D. (2024), arXiv:2407.17052 [astro-ph.IM].
[365] M. Andrés-Carcasona, O. J. Piccinni, M. Martínez, and L. M. Mir, (2024), arXiv:2411.04498 [gr-qc].
[366] J. C. Aurrekoetxea, K. Clough, J. Bamber, and P. G. Ferreira, Phys. Rev. Lett. **132**, 211401 (2024), arXiv:2311.18156 [gr-qc].
[367] B. J. Kavanagh, D. Gaggero, and G. Bertone, Phys. Rev. D **98**, 023536 (2018), arXiv:1805.09034 [astro-ph.CO].
[368] H. Koo, D. Bak, I. Park, S. E. Hong, and J.-W. Lee, Phys. Lett. B **856**, 138908 (2024), arXiv:2311.03412 [astro-ph.GA].
[369] A. Boudon, P. Brax, and P. Valageas, Phys. Rev. D **108**, 103517 (2023), arXiv:2307.15391 [astro-ph.CO].
[370] Z. Zhong, V. Cardoso, T. Ikeda, and M. Zilhão, Phys. Rev. D **108**, 084051 (2023), arXiv:2307.02548 [gr-qc].
[371] V. Cardoso, T. Ikeda, R. Vicente, and M. Zilhão, Phys. Rev. D **106**, L121302 (2022), arXiv:2207.09469 [gr-qc].
[372] V. Cardoso, T. Ikeda, Z. Zhong, and M. Zilhão, Phys. Rev. D **106**, 044030 (2022), arXiv:2206.00021 [gr-qc].
[373] R. Vicente and V. Cardoso, Phys. Rev. D **105**, 083008 (2022), arXiv:2201.08854 [gr-qc].
[374] L. Annulli, V. Cardoso, and R. Vicente, Phys. Rev. D **102**, 063022 (2020), arXiv:2009.00012 [gr-qc].
[375] L. Annulli, V. Cardoso, and R. Vicente, Phys. Lett. B **811**, 135944 (2020), arXiv:2007.03700 [astro-ph.HE].
[376] P. Brax, J. A. R. Cembranos, and P. Valageas, Phys. Rev. D **101**, 023521 (2020), arXiv:1909.02614 [astro-ph.CO].
[377] Y. Cao and Y. Tang, Phys. Rev. D **108**, 123017 (2023), arXiv:2307.05181 [gr-qc].
[378] D. Traykova, R. Vicente, K. Clough, T. Helfer, E. Berti, P. G. Ferreira, and L. Hui, Phys. Rev. D **108**, L121502 (2023), arXiv:2305.10492 [gr-qc].
[379] H. S. Chia, C. Doorman, A. Wernersson, T. Hinderer, and S. Nissanke, JCAP **04**, 018 (2023), arXiv:2212.11948 [gr-qc].
[380] T. Ikeda, L. Bernard, V. Cardoso, and M. Zilhão, Phys. Rev. D **103**, 024020 (2021), arXiv:2010.00008 [gr-qc].
[381] V. Cardoso, F. Duque, and T. Ikeda, Phys. Rev. D **101**, 064054 (2020), arXiv:2001.01729 [gr-qc].
[382] O. A. Hannuksela, K. W. K. Wong, R. Brito, E. Berti, and T. G. F. Li, Nature Astron. **3**, 447 (2019),

arXiv:1804.09659 [astro-ph.HE].
[383] J. Zhang and H. Yang, Phys. Rev. D **101**, 043020 (2020), arXiv:1907.13582 [gr-qc].
[384] T. Kumar Poddar, S. Mohanty, and S. Jana, Phys. Rev. D **101**, 083007 (2020), arXiv:1906.00666 [hep-ph].
[385] L. K. Wong, Phys. Rev. D **100**, 044051 (2019), arXiv:1905.08543 [hep-th].
[386] L. K. Wong, Phys. Rev. D **101**, 124049 (2020), arXiv:2004.03570 [hep-th].
[387] M. Kavic, S. L. Liebling, M. Lippert, and J. H. Simonetti, JCAP **08**, 005 (2020), arXiv:1910.06977 [astro-ph.HE].
[388] W. E. East, Phys. Rev. Lett. **121**, 131104 (2018), arXiv:1807.00043 [gr-qc].
[389] T. K. Poddar, A. Ghoshal, and G. Lambiase, Phys. Dark Univ. **46**, 101651 (2024), arXiv:2302.14513 [hep-ph].
[390] Y. Cao, Y.-Z. Cheng, G.-L. Li, and Y. Tang, (2024), arXiv:2411.17247 [gr-qc].
[391] A. Guo, J. Zhang, and H. Yang, Phys. Rev. D **110**, 023022 (2024), arXiv:2401.15003 [gr-qc].
[392] J. Bamber, J. C. Aurrekoetxea, K. Clough, and P. G. Ferreira, Phys. Rev. D **107**, 024035 (2023), arXiv:2210.09254 [gr-qc].
[393] G. Caneva Santoro, S. Roy, R. Vicente, M. Haney, O. J. Piccinni, W. Del Pozzo, and M. Martinez, Phys. Rev. Lett. **132**, 251401 (2024), arXiv:2309.05061 [gr-qc].
[394] A. Loeb, Astrophys. J. Lett. **819**, L21 (2016), arXiv:1602.04735 [astro-ph.HE].
[395] L. Sadeghian, F. Ferrer, and C. M. Will, Phys. Rev. D **88**, 063522 (2013), arXiv:1305.2619 [astro-ph.GA].
[396] B. J. Kavanagh, D. A. Nichols, G. Bertone, and D. Gaggero, Phys. Rev. D **102**, 083006 (2020), arXiv:2002.12811 [gr-qc].
[397] J. L. Feng, M. Kaplinghat, H. Tu, and H.-B. Yu, JCAP **07**, 004 (2009), arXiv:0905.3039 [hep-ph].
[398] D. E. Kaplan, G. Z. Krnjaic, K. R. Rehermann, and C. M. Wells, JCAP **05**, 021 (2010), arXiv:0909.0753 [hep-ph].
[399] M. R. Buckley and A. DiFranzo, Phys. Rev. Lett. **120**, 051102 (2018), arXiv:1707.03829 [hep-ph].
[400] S. Shandera, D. Jeong, and H. S. G. Gebhardt, Phys. Rev. Lett. **120**, 241102 (2018), arXiv:1802.08206 [astro-ph.CO].
[401] R. Abbott *et al.* (LIGO Scientific Collaboration, Virgo, KAGRA), Phys. Rev. Lett. **129**, 061104 (2022), arXiv:2109.12197 [astro-ph.CO].
[402] B. Abbott *et al.* (LIGO Scientific Collaboration, Virgo), Astrophys. J. Lett. **892**, L3 (2020), arXiv:2001.01761 [astro-ph.HE].
[403] S. Chandrasekhar, Astrophys. J. **74**, 81 (1931).
[404] R. Abbott *et al.* (LIGO Scientific Collaboration, Virgo), Astrophys. J. **896**, L44 (2020), arXiv:2006.12611 [astro-ph.HE].
[405] V. Bromm and R. B. Larson, Ann. Rev. Astron. Astrophys. **42**, 79 (2004), arXiv:astro-ph/0311019.
[406] R. A. Allsman *et al.* (Macho), Astrophys. J. Lett. **550**, L169 (2001), arXiv:astro-ph/0011506.
[407] H. Niikura, M. Takada, S. Yokoyama, T. Sumi, and S. Masaki, Phys. Rev. **D99**, 083503 (2019), arXiv:1901.07120 [astro-ph.CO].
[408] T. D. Brandt, Astrophys. J. Lett. **824**, L31 (2016), arXiv:1605.03665 [astro-ph.GA].
[409] S. M. Koushiappas and A. Loeb, Phys. Rev. Lett. **119**, 041102 (2017), arXiv:1704.01668 [astro-ph.GA].
[410] B. P. Abbott *et al.* (LIGO Scientific, Virgo), Phys. Rev. Lett. **123**, 161102 (2019), arXiv:1904.08976 [astro-ph.CO].
[411] D. Gaggero, G. Bertone, F. Calore, R. M. T. Connors, M. Lovell, S. Markoff, and E. Storm, Phys. Rev. Lett. **118**, 241101 (2017), arXiv:1612.00457 [astro-ph.HE].
[412] M. Raidal, V. Vaskonen, and H. Veermäe, JCAP **09**, 037 (2017), arXiv:1707.01480 [astro-ph.CO].
[413] M. Raidal, C. Spethmann, V. Vaskonen, and H. Veermäe, JCAP **02**, 018 (2019), arXiv:1812.01930 [astro-ph.CO].
[414] Y. Ali-Haimoud, E. D. Kovetz, and M. Kamionkowski, Phys. Rev. D **96**, 123523 (2017), arXiv:1709.06576 [astro-ph.CO].
[415] A. H. Nitz and Y.-F. Wang, The Astrophysical Journal **915**, 54 (2021), arXiv:2102.00868.
[416] K. S. Phukon, G. Baltus, S. Caudill, S. Clesse, A. Depasse, M. Fays, H. Fong, S. J. Kapadia, R. Magee, and A. J. Tanasijczuk, (2021), arXiv:2105.11449 [astro-ph.CO].
[417] A. L. Miller, N. Aggarwal, S. Clesse, and F. De Lillo, Phys. Rev. D **105**, 062008 (2022), arXiv:2110.06188 [gr-qc].
[418] A. H. Nitz and Y.-F. Wang, Phys. Rev. D **106**, 023024 (2022), arXiv:2202.11024 [astro-ph.HE].
[419] A. L. Miller, N. Aggarwal, S. Clesse, F. De Lillo, S. Sachdev, P. Astone, C. Palomba, O. J. Piccinni, and L. Pierini, Phys. Rev. Lett. **133**, 111401 (2024), arXiv:2402.19468 [gr-qc].
[420] N. C. M. Martens and D. Lehmkuhl, Stud. Hist. Phil. Sci. B **72**, 237 (2020), arXiv:2009.03890 [physics.hist-ph].
[421] S. Bird, I. Cholis, J. B. Muñoz, Y. Ali-Haïmoud, M. Kamionkowski, E. D. Kovetz, A. Raccanelli, and A. G. Riess, Phys. Rev. Lett. **116**, 201301 (2016).
[422] M. Sasaki, T. Suyama, T. Tanaka, and S. Yokoyama, Phys. Rev. Lett. **117**, 061101 (2016), [erratum: Phys. Rev. Lett.121,no.5,059901(2018)], arXiv:1603.08338 [astro-ph.CO].